PROBABILISTIC SOLUTIONS FOR SURVEY QUESTIONS IN "ARE WE OVERDESIGNING? – A SURVEY OF INTERNATIONAL PRACTICE"

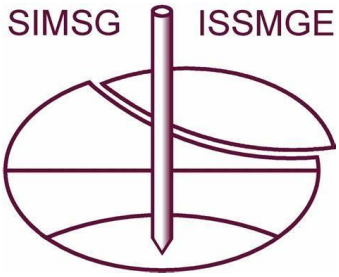

October 14, 2020

PREPARED BY
Technical Committee of Engineering Practice of Risk Assessment & Management (TC304)

EDITED BY
Jianye Ching (Chair of TC304, ISSMGE)
Jie Zhang (Secretary of TC304, ISSMGE)

Preface

In April 2019, the International Society for Soil Mechanics and Geotechnical Engineering (ISSMGE) launched a survey titled "Are We Overdesigning? – A Survey of International Practice". The survey is a joint initiative organized by the following groups/committees in ISSMGE:

Corporate Associates Presidential Group (CAPG),
Young Members Presidential Group (YMPG),
Technical Committee TC205 (Safety and Serviceability), and
Technical Committee TC304 (Risk)

This survey is intended to assess the consistency of calculation models and design methods for a variety of geotechnical structures and, where possible, to compare the results with full-scale tests and reliability analyses. TC304 is responsible to conduct reliability analyses.

The survey is based on two soil profiles, one in clay and the other in sand. Soil test results, typical of those one would find in a geotechnical investigation report, are provided for each soil profile. Ten specimen problems have been proposed, including concentrically and eccentrically loaded spread footings, axially and laterally loaded piles, slopes, and retaining structures. The idea is to keep the problems easy to analyze and representative of every-day geotechnical structures. The titles of the ten problems are summarized in Table 1. The details of these problems can be found at the following link:
https://www.issmge.org/news/are-we-overdesigning-a-survey-of-international-practice.

Table 1. Titles of the ten problems in the survey

1	Problem CLAY 1 – Vertically loaded spread footing
2	Problem CLAY 2 – Axially loaded pile
3	Problem CLAY 3 – Laterally loaded pile
4	Problem CLAY 4 – Slope design
5	Problem SAND 1 – Vertically loaded spread footing
6	Problem SAND 2 – Axially loaded pile
7	Problem SAND 3 – Design of spread footing with horizontal load
8	Problem SAND 4 – Slope design
9	Problem SAND 5 – Propped embedded retaining wall design
10	Problem SAND 6 – Soil nailed retaining wall design

In response to this survey, six working groups are established within TC304 to prepare *solutions* to these problems using probabilistic/reliability methods. Nine out of the ten problems are solved by TC304 working groups except the seventh problem in Table 1, as current knowledge about the model uncertainty for the design method of spread footing with horizontal

load is limited.

This report summarizes the detailed solutions to the nine problems in Table 1 prepared by the TC304 working groups. The purpose of this report is to illustrate how probabilistic methods can help solving practical geotechnical problems, to demonstrate the benefits of probabilistic methods, and to promote the use of probabilistic methods in geotechnical engineering.

We would like to acknowledge the tremendous efforts contributed by the working group members. Without their commitment and dedication, this report would not be possible.

Editors
Jianye Ching (Chair of TC304, ISSMGE)
Jie Zhang (Secretary of TC304, ISSMGE)

Contents

Probabilistic analysis of vertically loaded strip footing on clay

Zhiyong Yang, Jianfeng Xue, and Jianye Ching

1.1 Introduction

This section presents the probabilistic analysis results for the Problem CLAY 1 – vertically loaded strip footing. The geometry of the strip footing and the design problems are shown in Figure 1-1. The strip concrete footing has width of B = 2.0 m and height of H = 1.2 m. It is founded on a clay layer with an embedment depth of D_f = 0.75m. A concentric applied load P (not including the weight of the footing) is imposed on the footing. The problem requires the prediction of the performance of the strip footing: (1) predict the ultimate load capacity of the footing P_{ult} and (2) predict the load P_{25mm} that will cause the footing to settle by 25 mm in the long term. The weight of the concrete γ_c is not specified, and γ_c = 23 kN/m^3 is assumed in the following analysis. Section 1.2 introduces the prediction equations for P_{ult} and P_{25mm}, Section 1.3 presents the probabilistic characterization of the uncertain parameters involved in the problem, and Section 1.4 summarizes the prediction result.

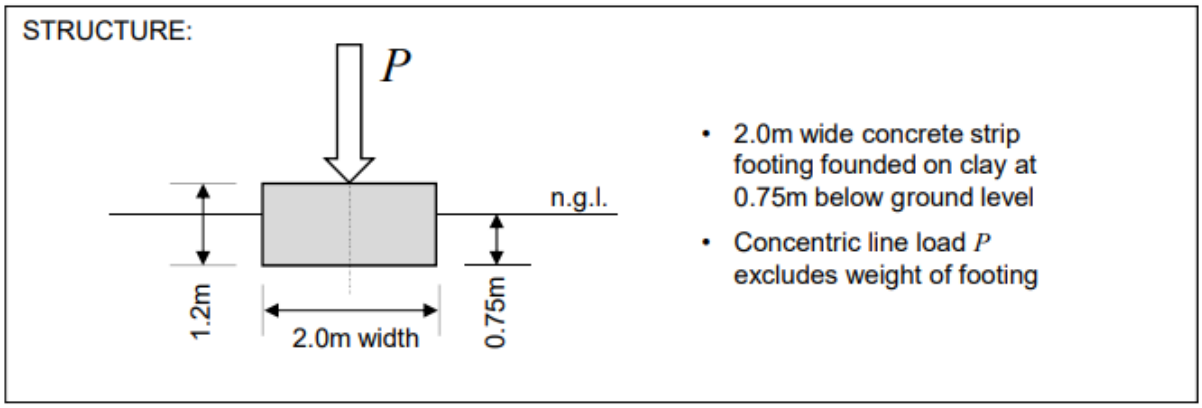

Figure 1-1 Schematic of the strip footing

1.2 Prediction equations for P_{ult} and P_{25mm}

1.2.1 Prediction equation for P_{ult}

The ultimate bearing capacity of the footing can be predicted by the formulae proposed by Eurocode 7 (EN 1997-1 2004):

$$q_{u,c1} = 5.14 \cdot s_{u,mob} s_c i_c + \gamma D_f \tag{1-1}$$

where $q_{u,c1}$ is the calculated ultimate bearing capacity; $s_{u,mob}$ is the mobilized undrained shear strength (to be elaborate later); the shape factors s_c = 1 for the strip footing; the inclination

factor $i_c = 1$ for concentric loading; $\gamma = 20$ kN/m^3 is the bulk unit weight for the clay.

The actual q_u and calculated $q_{u,c1}$ are different due to modeling errors. A database of 48 load test cases for footings in clays are compiled by Tang (2020). Among the 48 cases, the model factor (ε_{qu1}), defined as (actual q_u)/$q_{u,c1}$, for the 39 cases can be calcluated. The sample mean for the 39 model factors is 1.03, and the sample coefficient of variation (COV) is 29%. As a result, the relationship between the actual q_u (denoted by q_u) and calculated q_u (denoted by $q_{u,c1}$) is as follows:

$$q_u = q_{u,c1} \times \varepsilon_{qu1} \tag{1-2}$$

where ε_{qu1} is modeled as a lognormal random variable with mean = 1.03 and COV = 29%.

The total vertical load is equal to vertical load (P) + footing weight (W). As a result, P_{ult} can be computed as

$$P_{ult} = q_u B - W = q_{u,c1} \times \varepsilon_{qu1} \times B - W \tag{1-3}$$

where $W = \gamma_c \times 1.2 \times 2.0 = 55.2$ kN/m.

1.2.2 Prediction equation for P_{25mm}

The load P that causes the footing to settle by a certain amount can be predicted by the normalized load-settlement curve proposed by Akbas and Kulhawy (2009):

$$\frac{P+W}{q_u B} = \frac{(s/B)\times 100}{a(s/B)\times 100+b} \tag{1-4}$$

where s is the settlement; (a, b) are the fitting parameters (to be elaborated later). The P_{25mm} can be predicted by letting s = 0.025 m and $q_u = q_{u,c} \times \varepsilon_m$:

$$P_{25mm} = \frac{(0.025/B)\times 100}{a(0.025/B)\times 100+b} \times q_{u,c} \times \varepsilon_m \times B - W \tag{1-5}$$

Among the 48 footing load tests complied by Tang (2020), the (a, b) coefficients for 45 tests are calibrated based on the load-deformation data. The calibrated (a, b) data points are shown in Figure 1-2.

1.3 Probabilistic characterization of the uncertain parameters

1.3.1 Statistics of $s_{u,mob}$

The data points for the undrained shear strength (s_u) at the NGES-TAMU clay site are shown in Figure 1-3. The s_u data points have a sample mean of 111.3 kPa and a sample COV of 34.5%. Honjo and Otake (2013) indicated that for the ultimate bearing capacity of a footing, the mobilization zone is between the footing base and 0.7×B below the footing base. This suggests that the mobilization zone for the current footing problem is within the depth range of 0.75-

2.15 m. Akkaya and Vanmarcke (2003) adopted the single exponential auto-correlation model to analyze the NGES-TAMU clay site data and found that the vertical scale of fluctuation (SOF) is about 1.52 m. The spatially averaged s_u in the mobilization zone, denoted by $s_{u,mob}$, has a reduced COV due to spatial averaging (Vanmarcke 1977). This reduced COV is equal to the point COV (34.5%) multiplied by the COV reduction factor. For the single exponential model (Vanmarcke 1977), the COV reduction factor can be computed as $([2(D/SOF)-1+\exp[-2(D/SOF)]/[2(D/SOF)^2])^{0.5} = 0.77$, where $D = 0.7\times B = 1.4$ m is the size of the mobilization zone, and SOF = 1.52 m. As a result, the COV for $s_{u,mob}$ is $34.5\%\times 0.77 = 26.6\%$. Moreover, $s_{u,mob}$ is assumed to follow the lognormal distribution.

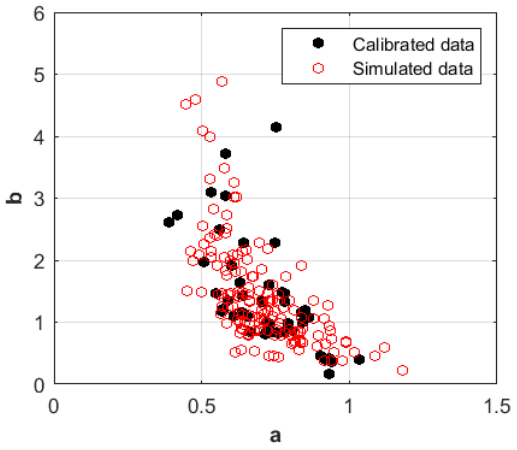

Figure 1-2 Scatter plot of a and b

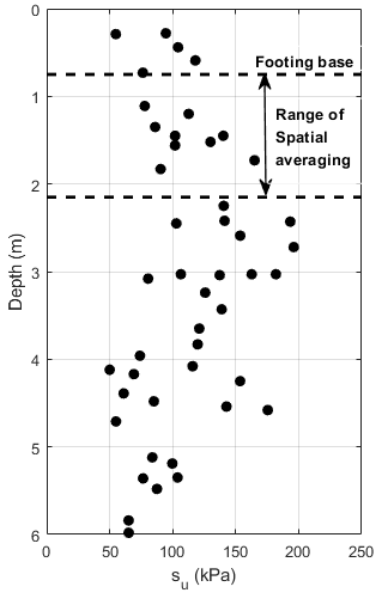

Figure 1-3 Undrained shear strength (s_u) for the NGES-TAMU clay site

1.3.2 Statistics of a and b

It is found that the (a, b) data in Figure 1-2 can be satisfactorily modeled by the lognormal distribution: the parameter a can be modeled as a lognormal distribution with mean = 0.71 and COV = 19.9% (p-value = 0.59), whereas the parameter b can be modeled as a lognormal distribution with mean = 1.44 and COV = 61.4% (p-value = 0.70). As a result, ln(a) is normal with mean = $\ln[0.71/(1+19.9\%^2)^{0.5}] = -0.361$ and standard deviation = $\ln(1+19.9\%^2)^{0.5} = 0.197$, and ln(b) is normal with mean = $\ln[1.44/(1+61.4\%^2)^{0.5}] = 0.201$ and standard deviation = $\ln(1+61.4\%^2)^{0.5} = 0.566$. The correlation coefficient (ρ) between (ln(a), ln(b)) is estimated by first estimating the Kendall correlation (r) between (a, b) and then implement the identity $\rho = \sin(\pi r/2)$. The resulting ρ estimate is -0.728. The dependency between (ln(a), ln(b)) is further modeled by a copula (Li et al. 2013). Four copulas are considered: Gaussian, Plackett, Frank, and No. 16 copulas. It is found that the Gaussian copula is optimal with the smallest AIC (Akaike 1974) and smallest BIC (Schwarz 1978). As a result, the Gaussian copula is adopted. The following procedure can be used to simulate (a, b) data from Gaussian copula:

1. Simulate the correlated standard normal vector $\underline{z}=[z_1\ z_2]$ with mean = [-0.361 0.201] and covariance matrix = $[0.197^2\ \rho\times0.197\times0.566;\rho\times0.197\times0.566\ 0.566^2]$;
2. Simulate the sample of a and b by $a = \exp(z_1)$ and $b = \exp(z_2)$.

The scatter plot for simulated (a, b) is shown in Figure 1-2.

There are in total four uncertain parameters ($s_{u,mob}$, ε_m, a, b) for predicting P_{ult} and P_{25mm}. The statistics of the four uncertain parameters are summarized in Table 1-1. All parameters are assumed to be mutually independent except for (a, b). The Gaussian copula is adopted to model the dependency between (a, b), and the correlation coefficient between (ln(a), ln(b)) is -0.728.

Table 1-1 Statistics of the random variables for the strip footing

Random variable	Mean	COV	Distribution
Mobilized undrained shear strength, $s_{u,mob}$	111.3 kPa	26.6%	Lognormal
Model factor for q_u, ε_{qu1}	1.03	29%	Lognormal
a	0.71	19.9%	Lognormal
b	1.44	61.4%	Lognormal

1.4 Prediction results

Monte Carlo simulation (MCS) with 1×10^7 samples are used to simulate the distribution of P_{ult} and P_{25mm} using Eqs. (1-3) and (1-5), respectively. The obtained histograms for P_{ult} and P_{25mm} are shown in Figure 1-4. The deterministic analysis results based on the mean values of the random variables are denoted as red lines in the figure. The statistics for P_{ult} and P_{25mm} are summarized in Table 1-2. For reference, the deterministic analysis results are also summarized in Table 1-2.

Table 1-2 Prediction results for P_{ult} and P_{25mm}

Predicted Loads	Mean	Median	Standard deviation	Deterministic analysis result
P_{ult}	1153.68 kN/m	1068.30 kN/m	479.08 kN/m	1153.57 kN
P_{25mm}	649.56 kN/m	586.28 kN/m	338.81 kN/m	595.03 kN

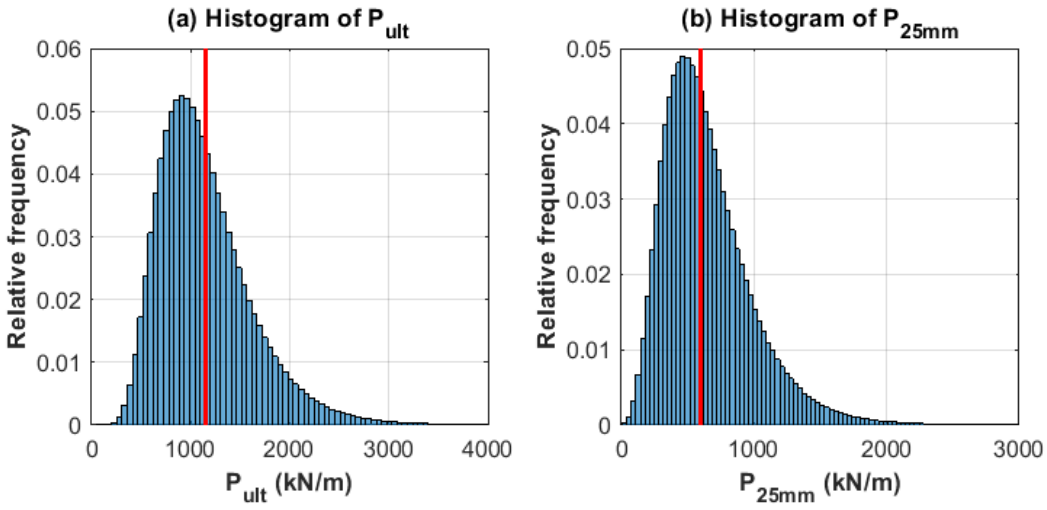

Figure 1-4 Histograms for P_{ult} and P_{25mm}

1.5 Methods based on CPT and PMT

1.5.1 Prediction equation for P_{ult} based on CPT

Tand et al. (1986) proposed an equation to predict q_u for footings in clay based on cone penetration test (CPT):

$$q_{u,c2} = \gamma D_f + R_k \left(q_{c,mob} - \gamma D_f \right) \tag{1-6}$$

where $q_{c,mob}$ is the mobilized cone tip resistance, defined as the mean q_c within B below the footing, and R_k is the bearing factor shown in Figure 1-5.

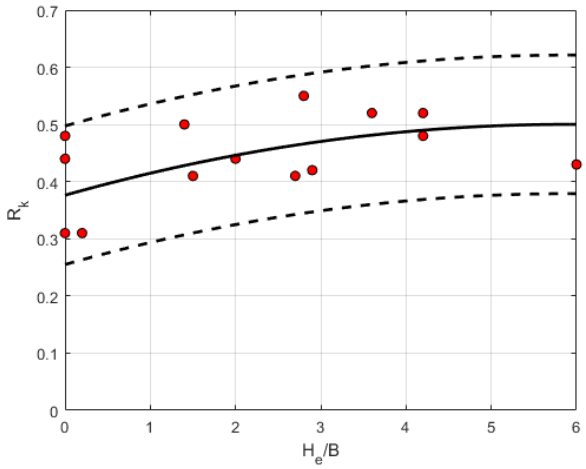

Figure 1-5 Bearing factor versus embedment ratio (data source: Tand, et al. 1986)

Tand et al. (1986) compiled 16 footing cases on clays. For each case, (H_e/B, R_k) are computed, where H_e is defined as the equivalent embedment depth:

$$H_e = \left(\int_0^{D_f} q_c(z)\,dz \right) \Big/ q_{c,mob} \tag{1-7}$$

The (H_e/B, R_k) data points for the 16 cases are shown in Figure 1-5. The following regression equation is obtained based on the 16 data points:

$$R_k = 0.376 + 0.042(H_e/B) - 0.00357(H_e/B)^2 + \varepsilon_{Rk} \qquad H_e/B \le 6 \tag{1-8}$$

where ε_{Rk} is the regression residual, modeled as a zero-mean normal random variable with standard deviation = 0.0606. The regression equation in Eq. (1-8) and its 95% confidence interval are plotted in Figure 1-5. Based on Eq. (1-7) and the q_c profile in Figure 1-6a, H_e for the current footing example is estimated to be 1.4 m. Because H_e/B = 0.7, R_k is a normal random variable with mean = $0.376+0.042\times0.7-0.00357\times0.7^2 = 0.404$ and standard deviation = 0.0606 (COV = 15%).

As a result, P_{ult} can be computed as

$$P_{ult} = q_u B - W = \left[\gamma D_f + R_k \left(q_{c,mob} - \gamma D_f \right) \right] \times B - W \tag{1-9}$$

Figure 1-6a shows the CPT test rests of the site. The sample mean of q_c within B = 2m below the footing base is 1.59 MPa and the sample COV is 12.2%. The COV reduction factor for the spatial averaging over the 2-m thick mobilization zone is $([2(2/1.52)-1+\exp[-2(2/1.52)]/[2(2/1.52)^2])^{0.5} = 0.70$. Therefore, the COV for $q_{c,mob}$ is equal to 12.2%×0.7 = 8.54%. It is further assumed that $q_{c,mob}$ is lognormally distributed.

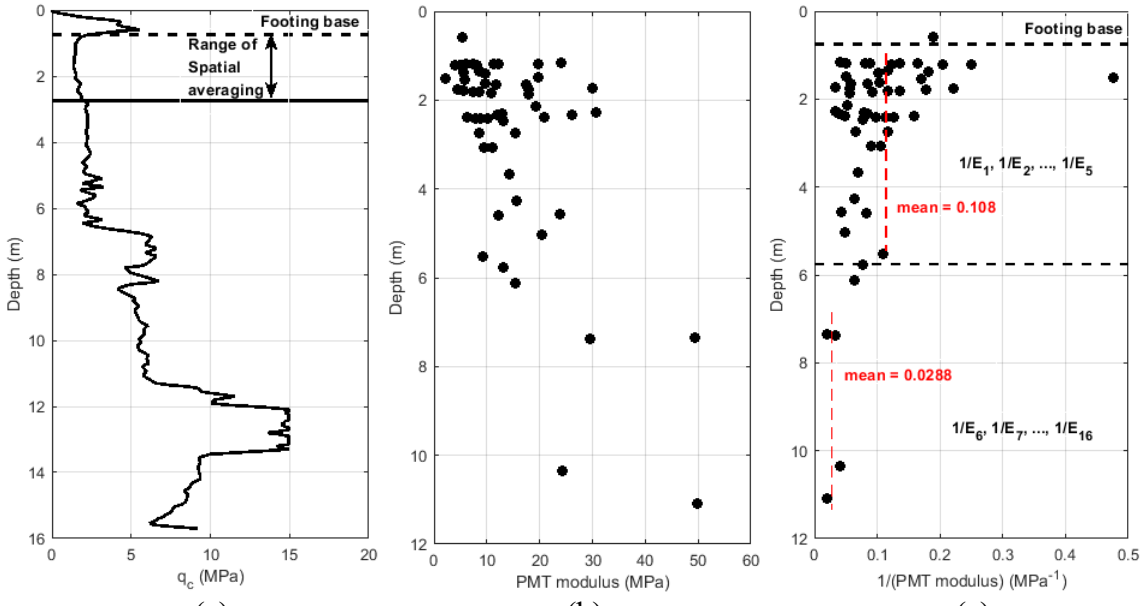

(a) (b) (c)

Figure 1-6 CPT and PMT test data at the NGES-TAMU clay site: (a) CPT tip resistence q_c; (b) PMT modulus; (c) 1/(PMT modulus)

1.5.2 Prediction equation for P_{25mm} based on PMT

Baguelin et al. (1978) proposed an equation to predict the settlement for a footing based on pressuremeter test (PMT) results. In this method, soils within 8B below the footing are divided in 16 layers with equal thickness (= 0.5B = 1m). The settlement can be calculated by

$$s_c = \frac{\alpha}{9E_{M,c}}(q-\gamma D_f)\lambda_c B + \frac{2}{9E_{M,d}}(q-\gamma D_f)B_0\left(\lambda_d \frac{B}{B_0}\right)^{\alpha} \tag{1-10}$$

where α is rheological factor; B_0 is equal to 0.6 m; λ_c and λ_d are factors depending on the footing dimension; q is the bearing stress on the footing face; $E_{M,c}$ is the PMT modulus for soils within 0.5B = 1m below the footing; $E_{M,d}$ is the weighted average PMT modulus for soils within 8B below the footing:

$$\frac{1}{E_{M,d}} = \frac{1}{4}\left(\frac{1}{E_1} + \frac{1}{0.85E_2} + \frac{1}{E_{3/5}} + \frac{1}{2.5E_{6/8}} + \frac{1}{2.5E_{9/16}}\right) \tag{1-11}$$

where E_n is the PMT modulus for the n-th soil layer (1st layer is right below the footing); $E_{m/n}$ (n > m) is the harmonic average for (E_m, E_{m+1}, …, E_n). Note that $E_{M,c} = E_1$. The actual settlement and calculated settlement are different due to modeling errors. A database of 9 load test cases for footings in clays are compiled by Baguelin et al. (1978). The model factor (ε_s), defined as (actual s)/s_c, for the 9 cases can be calcluated. The sample mean for the 9 model factors is 1.6, and the sample COV is 123%. As a result, the relationship between the actual settlement (denoted by s) and calculated settlement (denoted by s_c) is as follows:

$$s = s_c \times \varepsilon_s \tag{1-12}$$

where ε_s is modeled as a lognormal random variable with mean = 1.6 and COV = 123%. For the current NGES example, the footing is a strip footing on an overconsolidated clay. According to Baguelin et al. (1978), λ_c = 1.45 and λ_d = 2.4 for a strip footing, and α = 1 for overconsolidated clay. As a result,

$$s = \left(\frac{1.45}{9E_{M,c}} + \frac{4.8}{9E_{M,d}}\right)(q-\gamma D_f)B \times \varepsilon_s \tag{1-13}$$

The bearing stress corresponding to s = 25 mm can be calculated as

$$q_{25mm} = \left(\frac{0.025}{B \times \varepsilon_s}\right) \Bigg/ \left(\frac{1.45}{9E_{M,c}} + \frac{4.8}{9E_{M,d}}\right) + \gamma D_f \tag{1-14}$$

Hence, P_{25mm} can be computed as

$$\begin{aligned} P_{25mm} &= q_{25mm}B - W \\ &= \left(\frac{0.025}{\varepsilon_s}\right) \Bigg/ \left[\frac{1.45}{9E_1} + \frac{0.4}{3}\left(\frac{1}{E_1} + \frac{1}{0.85E_2} + \frac{1}{E_{3/5}} + \frac{1}{2.5E_{6/8}} + \frac{1}{2.5E_{9/16}}\right)\right] + \gamma D_f - W \end{aligned} \tag{1-15}$$

Figure 1-6b shows the PMT test rests of the site. According to the PMT test results, the statistics for (E_1, E_2, …, E_{16}) are summarized in Table 1-3. It is assumed that ($1/E_1$, $1/E_2$, …, $1/E_6$) have mean = 0.108MPa^{-1} and COV = 68%, and ($1/E_7$, $1/E_8$, …, $1/E_{16}$) have mean = 0.0288MPa^{-1} (see Figure 1-6c) and COV = 36%. The COV reduction factor for the spatial averaging for each 1-m soil layer is $([2(1/1.52)-1+\exp[-2(1/1.52)]/[2(1/1.52)^2])^{0.5}$ = 0.82. Therefore, the COV after spatial averaging in the table equals COV multiplied by 0.82. By definition, $1/E_{3/5}$ is the arithmetic average of $1/E_3$, $1/E_4$, and $1/E_5$. As a result, $1/E_{3/5}$ has mean = 0.108 and COV = 56%/sqrt(3) = 32% by assuming independence among ($1/E_3$, $1/E_4$, $1/E_5$). Similarly, $1/E_{6/8}$ has mean = 0.0288 and COV = 30%/sqrt(3) = 17%, and $1/E_{9/16}$ has mean = 0.0288 and COV = 30%/sqrt(8) = 11%. There are in total eight random variables ($q_{c,mob}$, ε_{qu2}, ε_s, $1/E_1$, $1/E_2$, $1/E_{3/5}$, $1/E_{6/8}$, $1/E_{9/16}$), and their statistics are shown in Table 1-4. All parameters are assumed to be mutually independent.

Table 1-3 Statistics for (E_1, E_2, …, and E_{16})

Layer	1/Modulus	Depth (m)	Mean (MPa^{-1})	COV	COV after spatial averaging
1	$1/E_1$	0.75-1.75	0.108	68%	56%
2	$1/E_2$	1.75-2.75			
3	$1/E_3$	2.75-3.75			
4	$1/E_4$	3.75-4.75			
5	$1/E_5$	4.75-5.75			
6	$1/E_6$	5.75-6.75	0.0288	36%	30%
7	$1/E_7$	6.75-7.75			
8	$1/E_8$	7.75-8.75			
9	$1/E_9$	8.75-9.75			
10	$1/E_{10}$	9.75-10.75			
11	$1/E_{11}$	10.75-11.75			
12	$1/E_{12}$	11.75-12.75			
13	$1/E_{13}$	12.75-13.75			
14	$1/E_{14}$	13.75-14.75			
15	$1/E_{15}$	14.75-15.75			
16	$1/E_{16}$	15.75-16.75			

Table 1-4 Statistics of the random variables for the strip footing (CPT & PMT methods)

Random variable	Mean	COV	Distribution
Mobilized cone tip resistance, $q_{c,mob}$	1.59 MPa	8.54%	Lognormal
Bearing factor, R_k	0.404	15%	Normal
Model factor for s, ε_s	1.6	123%	Lognormal
$1/E_1$	0.108MPa^{-1}	56%	Lognormal
$1/E_2$	0.108MPa^{-1}	56%	Lognormal
$1/E_{3/5}$	0.108MPa^{-1}	32%	Lognormal
$1/E_{6/8}$	0.0288MPa^{-1}	17%	Lognormal
$1/E_{9/16}$	0.0288MPa^{-1}	11%	Lognormal

1.5.3 Prediction results

Monte Carlo simulation (MCS) with 1×10^7 samples are used to simulate the distribution of P_{ult} and P_{25mm} using Eqs. (1-9) and (1-15), respectively. The obtained histograms for P_{ult} and P_{25mm} are shown in Figure 1-7. The deterministic analysis results based on the mean values of the random variables are denoted as red lines in the figure. The statistics for P_{ult} and P_{25mm} are summarized in Table 1-5. For reference, the deterministic analysis results are also summarized in Table 1-5.

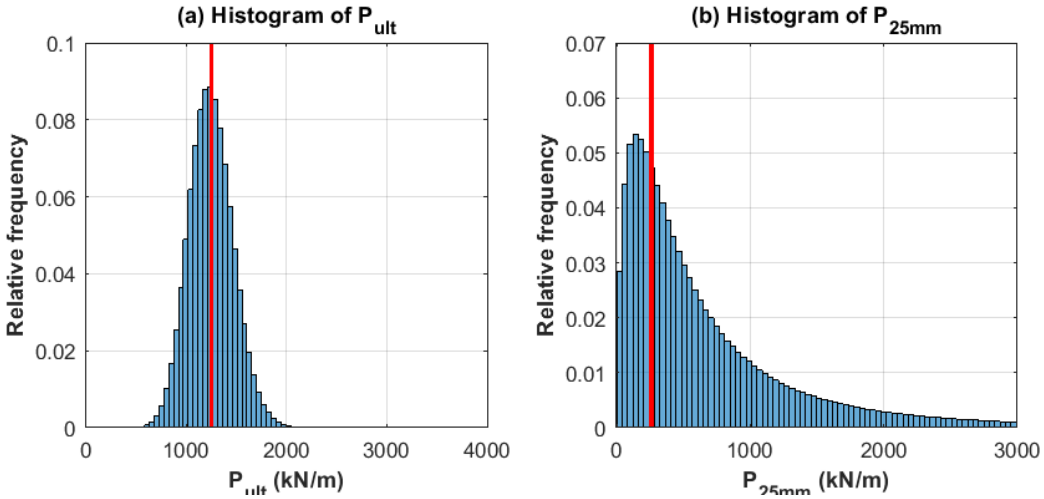

Figure 1-7 Histograms for P_{ult} and P_{25mm} (CPT & PMT methods)

Table 1-5 Prediction results for P_{ult} and P_{25mm} (CPT & PMT methods)

Predicted Loads	Mean	Median	Standard deviation	Deterministic analysis result
P_{ult}	1247.4 kN/m	1239.2 kN/m	220.7 kN/m	1247.4 kN/m
P_{25mm}	772.9 kN/m	455.8 kN/m	1054.2 kN/m	261.4 kN/m

References

Akaike, H. (1974). A new look at the statistical model identification. IEEE transactions on automatic control, 19(6), 716-723.

Akbas, S. O., and Kulhawy, F. H. (2009). Axial compression of footings in cohesionless soils. I: Load-settlement behavior. Journal of geotechnical and geoenvironmental engineering, 135(11), 1562-1574.

Akkaya, A. D., and Vanmarcke, E. H. (2003). Estimation of spatial correlation of soil parameters based on data from the Texas A&M University NGES. Probabilistic site characterization at the National Geotechnical Experimentation Sites (Eds G. A. Fenton and E. H. Vanmarcke), 29-40.

Baguelin F., Jézéquel J.F. and Shields D.H. 1978. The pressuremeter and foundation engineering. Series on Rock and Soil Mechanics.

Briaud, J. L. (2000). The National Geotechnical Experimentation Sites at Texas A&M University: Clay and Sand. A Summary. National Geotechnical Experimentation Sites: Geotechnical Special Publication, 93, 26–51.

EN 1997-1 (2004). Eurocode 7: Geotechnical design - Part 1: General rules [Authority: The European Union Per Regulation 305/2011, Directive 98/34/EC, Directive 2004/18/EC]

Honjo, Y., and Otake, Y. (2013). A simple method to assess the effects of soil spatial variability on the performance of a shallow foundation. In Foundation Engineering in the Face of Uncertainty: Honoring Fred H. Kulhawy (Eds. J. L. Withiam, K. K. Phoon, and M. Hussein), 385-404.

Li, D. Q., Tang, X. S., Phoon, K. K., Chen, Y. F., and Zhou, C. B. (2013). Bivariate simulation using copula and its application to probabilistic pile settlement analysis. International Journal for Numerical and Analytical Methods in Geomechanics, 37(6), 597-617.

Schwarz, G. (1978). Estimating the dimension of a model. The annals of statistics, 6(2), 461-464.

Tand, K.E., Funegard E.G., and Briaud J-L., 1986, "Bearing Capacity of Footings on Clays: CPT Method", Use of In-Situ Tests in Geotechnical Engineering, (GSP No. 6), ASCE, Reston, 1986, pp. 1017-1033.

Tang, C. (2020). Personal communication.

Vanmarcke, E. H. (1977). Probabilistic modeling of soil profiles. Journal of the geotechnical engineering division, 103(11), 1227-1246.

Probabilistic analysis of axially loaded pile in clay

Takayuki Shuku and Waldemar Hachich

2.1 Introduction

This manuscript describes reliability analysis for the Problem CLAY 2 (Problem 2) – Axially loaded pile. The schematic of the pile and target design problems are shown in Figure 2-1. The structure of this manuscript is as follows: in Section 2.2, deterministic design method for pile foundations based on a design code commonly used in Japan (JARA 2017) is outlined; in Section 2.3, a method of probabilistic analysis and uncertainty modeling are presented. Section 2.4 shows the results of probabilistic analysis and compares the probabilistic-based method and conventional factor-of-safety method in terms of target failure probability.

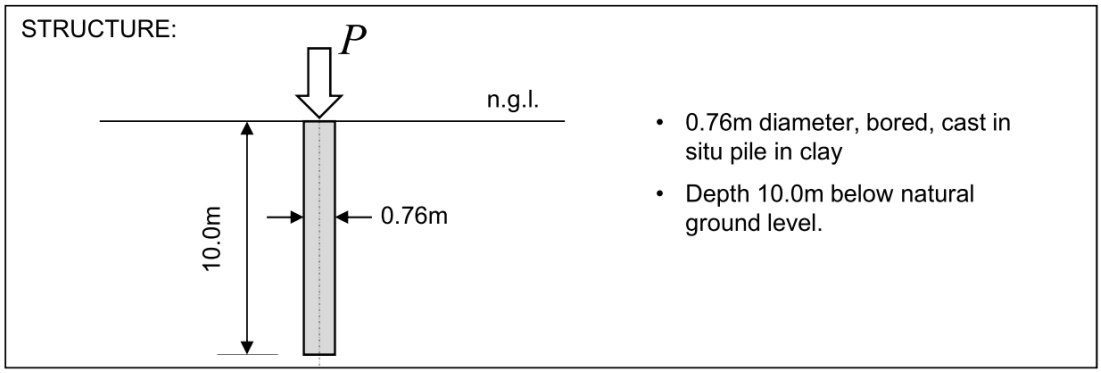

PROBLEM:

This problem requires the prediction of the performance of the pile.

1. Predict the ultimate load capacity of the pile P_{ult}.
2. If the method used separates shaft and base resistance, state $P_{ult\ (shaft)}$ and $P_{ult\ (base)}$.
3. Predict the load-settlement curve to failure.
4. Predict the expected performance of the pile based on the test results, not a conservative assessment as may be used in design calculations.

Figure 2-1 Schematic of the target structure and design problems

2.2 Pile design based on JARA (2017)

2.2.1 Ultimate bearing capacity

The ultimate bearing capacity P_{ult} of an axially loaded single pile is estimated by the model (equation) employed in JARA (2017). The equation consists of two terms, end-bearing

resistance $P_{ult(base)}$ and shaft friction resistance $P_{ult(shaft)}$, which are defined by:

$$P_{ult} = P_{ult(base)} + P_{ult(shaft)} = q_d A + U\sum L_i f_i \tag{2-1}$$

where q_d is the end-bearing resistance, A is the area of pile tip, U is the perimeter of pile, L_i is the thickness of ith layer for shaft friction, and f_i is a characteristic value of maximum friction force of ith layer. The q_d and f_i are calculated by the equations summarized in Tables 2-1 and 2-2. The q_d is estimated with SPT-N value (N_{SPT}) of the bearing layer, and f_i is calculated with cohesion c or N_{SPT}. All the equations summarized in Tables 2-1 and 2-2 were developed based on many load testing data (Nanazawa et al. 2018) and do not include any safety margins.

Table 2-1 End-bearing resistance q_d (JARA 2017).

Type of Pile	Type of Soil	q_d (kN/m^2)
Driven	Clay	$90N_{SPT}$ ($\leq$ 4,500)
	Sand	$130N_{SPT}$ ($\leq$ 6,500)
	Gravel	$130N_{SPT}$ ($\leq$ 6,500)
Cast-in-situ	Clay	$90N_{SPT}$ ($\leq$ 3,300)
	Sand	$110N_{SPT}$ ($\leq$ 3,300)
	Gravel	$160N_{SPT}$ ($\leq$ 8,000)
Pre-boring	Sand	$240N_{SPT}$ ($\leq$ 12,000)
	Gravel	$300N_{SPT}$ ($\leq$ 15,000)

Table 2-2 Shaft friction force f (JARA 2017).

Type of Pile	Type of Soil	f (kN/m^2)
Driven	Clay	c or $6N_{SPT}$ ($\leq$ 70)
	Sand	$5N_{SPT}$ ($\leq$ 100)
Cast-in-situ	Clay	c or $5N_{SPT}$ ($\leq$ 100)
	Sand	$5N_{SPT}$ ($\leq$ 120)
Pre-boring	Sand	c or $7N_{SPT}$ ($\leq$ 100)
	Gravel	$5N_{SPT}$ ($\leq$ 120)

2.2.2 Load-settlement curve

A bi-linear model (Figure 2-2) is used for estimating a load-settlement curve of axially loaded pile for simplicity. In the bi-linear model, the relation between load (P_j) and settlement (δ_j) is defined as:

$$P_j = K_V \delta_j \tag{2-2}$$

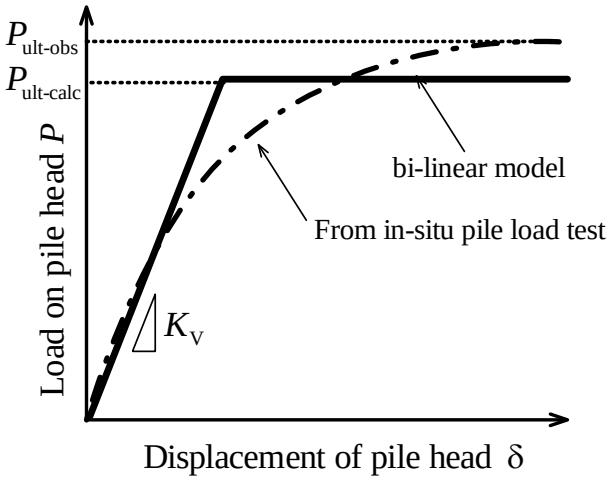

Figure 2-2 Schematic of load-displacement curve and bi-linear model

where the subscript j is load step number and K_V is vertical spring constant for single pile defined in JARA (2017) as:

$$K_V = \frac{1}{\frac{L}{2AE_p}(1+\lambda_{yu}\gamma_u-\zeta_e)+\zeta_d\frac{4\lambda_{yu}\gamma_u}{\pi D_p^2 k_V}} \tag{2-3}$$

where L is length of pile, A is pile tip area, E_p is elastic modulus of pile material, D_p is diameter of pile, the correction factors λ_{yu}, γ_e, and γ_d for K_V are summarized in Table 2-3, and the k_V and γ_u are defined as:

$$k_V = \frac{\alpha E_0}{0.3}\left(\frac{D_p}{0.3}\right)^{-3/4} \tag{2-4}$$

$$\gamma_u = \frac{P_{ult(base)}}{P_{ult}} \tag{2-5}$$

where E_0 and α are the elastic modulus of bearing layer and the transformation coefficient on E_0 which are summarized in Table 2-4.

Table 2-3 Correction factors

Pile Type	γ_{yu}	ζ_e	ζ_d
Driven	0.76	0.22	0.25
Cast-In-Situ	0.48	0.30	0.99
Pre-boring	0.58	0.04	0.16

Table 2-4 Transformation coefficient for E_0

E_0 estimated from	Transformation coefficient α	
	Consider earthquake	Not consider earthquake
Plate load test with 0.3m rigid plate	1	2
Pressure meter test	4	8
Uniaxial or triaxial compression test	4	8
SPT-N value ($E_0 = 2800N_{SPT}$)	1	2

2.3 Reliability analysis method

We simply estimate probability density functions (PDFs) of P_{ult}, $P_{ult(base)}$, $P_{ult(shaft)}$, K_V and δ using direct Monte Carlo simulation (MCS) considering variability of soil parameters (undrained strength c and N_{SPT} around the pile base) and model uncertainties.

The depth profiles of c and N_{SPT} are shown in Figure 2-3. Akkaya and Vanmarcke (2003) adopted the single exponential auto-correlation model to analyze the NGES-TAMU clay site data and found that the vertical scale of fluctuation (SOF) is about 1.52 m. For the shaft resistance, the size of mobilization zone in each soil layer is the length of the pile in the soil layer. The spatially averaged cohesion for shaft resistance in the mobilization zone has a reduced COV due to spatial averaging (Vanmarcke 1977). This reduced COV is equal to the point COV multiplied by the COV reduction factor. For the single exponential model (Vanmarcke 1977), the COV reduction factor can be computed as

$$([2(L_m/\mathrm{SOF})\text{-}1+\exp[-2(L_m/\mathrm{SOF})]]/[2(L_m/\mathrm{SOF})^2])^{0.5} \tag{2-6}$$

where L_m is the size of the mobilization zone. Let $\mathrm{COV}_{p,mob}$ denote the COV of the spatially averaged soil property. Using the above method, the values of L_m , COV reduction factor, and COV_{mob} for cohesion in different soil layers for estimation of the shaft resistance are calculated and summarized in Table 2-5. For the toe resistance, the mobilization zone size is 3.5 times of the diameter of the cross-section of the pile (Wang and Cao 2013). Using the same procedure, the size of the mobilized zone, the COV reduction factor and the COV of the averaged property for N_{SPT} are also calculated and shown in Table 2-5.

We assume that the variability of c and N_{SPT} follow log-normal distributions with the mean $\mu_{\ln p}$ and standard deviation $\sigma_{\ln p}$ given by:

$$\mu_{\ln p} = \ln \mu_p - \frac{1}{2}\sigma_{\ln p}^2 \tag{2-7}$$

$$\sigma_{\ln p} = \sqrt{\ln (1+\mathrm{COV}_p^2)} \tag{2-8}$$

where μ_p is the mean value and COV_p is coefficient of variation of parameter p, they are summarized in Table 2-5.

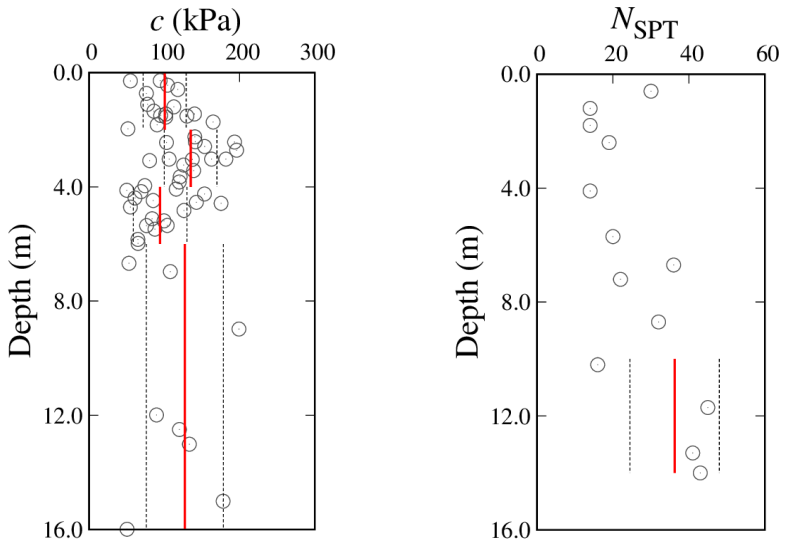

Figure 2-3 Depth profile of c and N_{SPT}

Table 2-5 Stochastic characteristics of geotechnical parameters

Parameter	μ_p	COV_p	L_m	COV reduction factor	COV_{mob}	$\mu_{\ln p}$	$\sigma_{\ln p}$
c_1	100.54	0.284	2	0.701	0.199	4.591	0.197
c_2	135.04	0.259	2	0.701	0.182	4.889	0.181
c_2	94.33	0.377	2	0.701	0.264	4.513	0.260
c_4	127.21	0.403	4	0.555	0.224	4.821	0.221
N_{SPT}	36.25	0.324	2.66	0.643	0.208	3.569	0.206

Nanazawa et al. (2018) investigated the accuracy of the Eqs. (2-1) and (2-3) by comparing the calculated $P_{ult(base)}^{cal}$, $P_{ult(shaft)}^{cal}$ and K_V^{cal} with their in-situ measured (referred to as "true") values. They defined a parameter M (= measured(true)/calculated) and evaluated the mean and standard deviations of that parameter (**Table 2-6**). Since the parameter M is always positive, we assumed that the parameter M follows log-normal distribution with the mean and standard deviation in **Table 2-6**. Finally, $P_{ult(base)}^{true}$, $P_{ult(shaft)}^{true}$ and K_V^{true} are given by

$$P_{ult(base)}^{true} = M_{ult(base)} \times P_{ult(base)}^{cal}, \quad M_{ult(base)} \sim LN(\mu_{\ln M_{ult(base)}}, \sigma_{\ln M_{ult(base)}}) \tag{2-9}$$

$$P_{ult(shaft)}^{true} = M_{ult(shaft)} \times P_{ult(shaft)}^{cal}, \quad M_{ult(shaft)} \sim LN(\mu_{\ln M_{ult(shaft)}}, \sigma_{\ln M_{ult(shaft)}}) \tag{2-10}$$

$$K_V^{true} = M_{K_V} \times K_V^{cal}, \quad M_{K_V} \sim LN(\mu_{\ln M_{K_V}}, \sigma_{\ln M_{K_V}}) \tag{2-11}$$

Table 2-6 Stochastic characteristics of model uncertainty

Parameter	μ_M	σ_M	$\mu_{\ln M}$	$\sigma_{\ln M}$	Reference
$P^{true}_{ult(base)}$ / $P^{cal}_{ult(base)}$	1.10	0.50	-0.016	0.472	Nanazawa et al. (2018)
$P^{true}_{ult(shaft)}$ / $P^{cal}_{ult(shaft)}$	1.08	0.68	-0.113	0.617	Nanazawa et al. (2018)
K^{true}_V / K^{cal}_V	0.92	0.43	-0.168	0.412	Nanazawa et al. (2018)

2.4 Results

2.4.1 Deterministic design method

The parameters used in the calculation of P_{ult}, $P_{ult(base)}$, $P_{ult(shaft)}$, K_V and δ_{limit} are summarized in Table 2-7. Cohesion c and Elastic modulus of soil E_0 around pile base are obtained from UU/CU compression test and pressure meter test. The arithmetic mean values of c and E_0 are used in the design. Since less data of N_{SPT} is available and there is no data just below the pile tip, the minimum value is employed in the deterministic design. The calculated P_{ult}, $P_{ult(base)}$, $P_{ult(shaft)}$, K_V and δ_{limit} are summarized in Table 2-8. Figure 2-4 shows the load-settlement curve to failure.

Table 2-7 Design parameters for deterministic analysis

Parameter		Tests	Description
c (kN/m^2)	110.43	UU and CU tests	arithmetic mean of the data
N_{SPT}	16.0	-	minimum value of the data
E_p (kN/m^2)	25,000,000	-	-
E_0 (kN/m^2)	37,100	Pressure meter test	arithmetic mean of the data

Table 2-8 Results of deterministic design

$P_{ult(base)}$, (q_dA)	798.42 kN
$P_{ult(shaft)}$ ($U\Sigma Lf$)	2387.61 kN
P_{ult} ($q_dA+U\Sigma L$)	3186.03 kN
K_V	700,649kN/m
δ_{limit}	4.55 mm

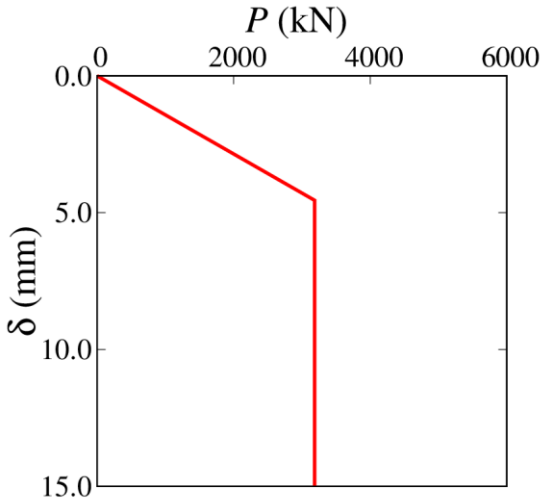

Figure 2-4 Load-settlement curve to failure

2.4.2 Probabilistic analysis

Probability distributions of the P_{ult}, $P_{ult(base)}$, $P_{ult(shaft)}$, K_V and δ_{limit} are shown in Figure 2-5, which are estimated using direct MCS with 100,000 samples. In order to discuss the advantage of probabilistic analysis, we compared the results by probabilistic and factor-of-safety methods in terms of the bearing capacity at serviceability limit state. In factor-of-safety method, allowable bearing capacity $P_{a(fos)}$, which corresponds to P_{sls}, is defined by

$$P_{a(fos)} = P_{ult} / n \tag{2-12}$$

where, n is factor of safety that is defined as 3 for static conditions and 2 for seismic conditions. Since the target problem is static, $P_{a(fos)}$ becomes 1,062.01kN. The target reliability index β_T for serviceability limit state is usually set as 1.5 (Otake and Honjo 2016), and it corresponds to failure probability p_f = 0.0679. We identified the bearing capacity P (P_{sls}) that satisfies p_f = 0.0679. Figure 2-6 shows the comparison between $P_{a(fos)}$ and P_{sls}. The identified P_{sls} is 1,195.34kN and the difference between two bearing capacity is about 133kN. Clearly, the probabilistic analysis considering soil variability and model uncertainty can contribute to more economical pile design than the conventional factor-of-safety method.

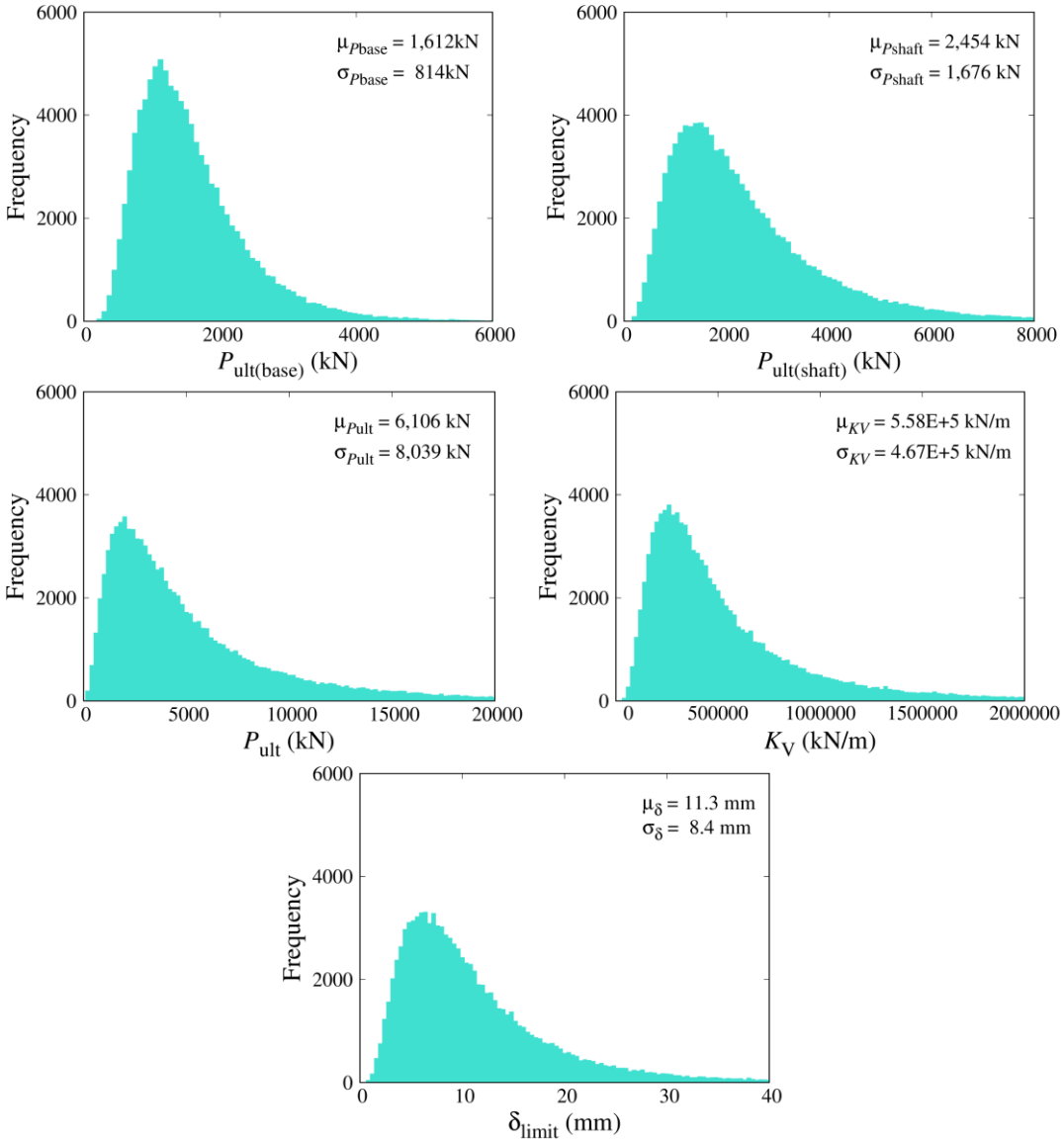

Figure 2-5 Probability distribution of P_{ult}, K_V and δ_{limit} with N_{MCS} = 100,000

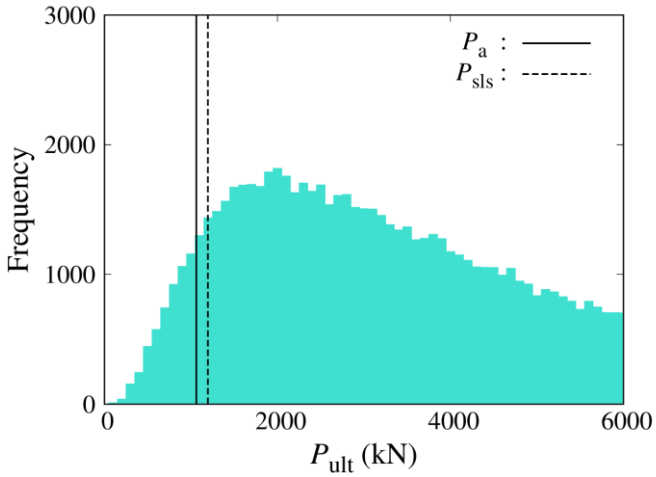

Figure 2-6 Comparison between P_a and P_{sls}

References

Akkaya, A. D., and Vanmarcke, E. H. (2003). Estimation of spatial correlation of soil parameters based on data from the Texas A&M University NGES. Probabilistic site characterization at the National Geotechnical Experimentation Sites (Eds G. A. Fenton and E. H. Vanmarcke), 29-40.

JARA (2017). Specifications for Highway Bridges IV, Japan Road Association (in Japanese).

Nanazawa, T., Kohno T., Miyahara, K. and Ohshiro, K. (2018). A study on a review for vertical bearing/deformation characteristics of piles and evaluation for the estimation accuracy, Technical Note of Public Work Research Institute, 4374, 104p (in Japanese).

Otake, Y. and Honjo, Y. (2016). Geotechnical reliability analysis and challenges in geotechnical design, Journal of JSCE C, Vol. 72, No. 4, pp.310 – 326. (in Japanese)

Vanmarcke, E. H. (1977). Probabilistic modeling of soil profiles. Journal of the geotechnical engineering division, 103(11), 1227-1246.

Wang, Y., and Cao, Z. (2013). Expanded reliability-based design of piles in spatially variable soil using efficient Monte Carlo simulations. Soils and Foundations, 53(6):820-834.

Probabilistic analysis of a laterally loaded pile in clay

Takayuki Shuku and Waldemar Hachich

3.1 Introduction

This paper presents results of deterministic and probabilistic analysis for the Problem CLAY 3 (Problem 3) – Laterally loaded pile. The schematic of the pile and target design problems are shown in Figure 3-1. This paper is structured as follows: in Section 3.2, a design method for a laterally loaded pile (Nakatani et al. 2009; JARA 2017) is outlined; in Section 3.3, a method of uncertainty modeling and probabilistic analysis are presented. The results by the deterministic and probabilistic methods are shown in Section 3.4.

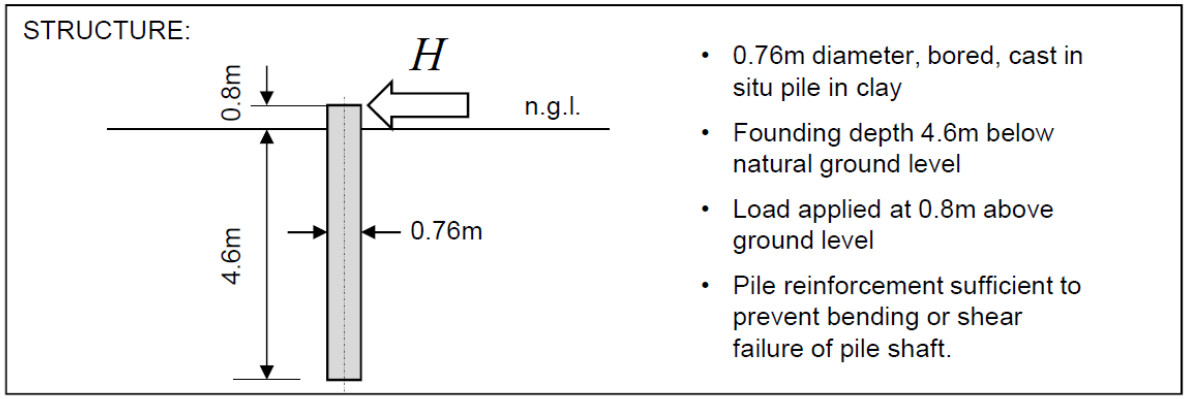

Figure 3-1 Schematic of the target structure and design problems

3.2 Deterministic design

3.2.1 Ultimate load capacity for laterally loaded single pile

The schematic of a simple model for calculating H_{ult} is shown in Figure 3-1 (Nakatani et al. 2009). Based on this model, H_{ult} is calculated by:

$$H_{\text{ult}} = a\alpha_P P_H D \tag{3-1}$$

where a is a correction factor for calculating the ultimate load capacity of single pile (= 0.8, Nakatani et al. 2009), α_P is the correction factor for lateral subgrade reaction of single pile (JARA 2002, summarized in Table 3-1), and D is the diameter of pile. The P_H is the passive earth pressure for 1/β (β is the characteristic value for pile) zone and calculated by:

$$P_H = \sum_i \left(\frac{p_{pui} + p_{pli}}{2} l_i \right) \tag{3-2}$$

where p_{pui} and p_{pli} are passive earth pressure shown in Figure 3-2, and l_i is the thickness of ith soil layer. The passive earth pressure at depth z (m) is given by:

$$P_{P(z)} = K_P \gamma z + 2c\sqrt{K_P} + K_P q \tag{3-3}$$

$$K_P = \frac{\cos^2 \phi}{\cos\delta \left(1 - \sqrt{\frac{\sin(\phi - \delta)\sin\phi}{\cos\delta}} \right)} \tag{3-4}$$

Table 3-1 Correction factor α_p

Type of Soil		α_p
Sand		3.0
Clay	$N_{\text{SPT}} > 2$	1.5
	$N_{\text{SPT}} \leq 2$	1.0

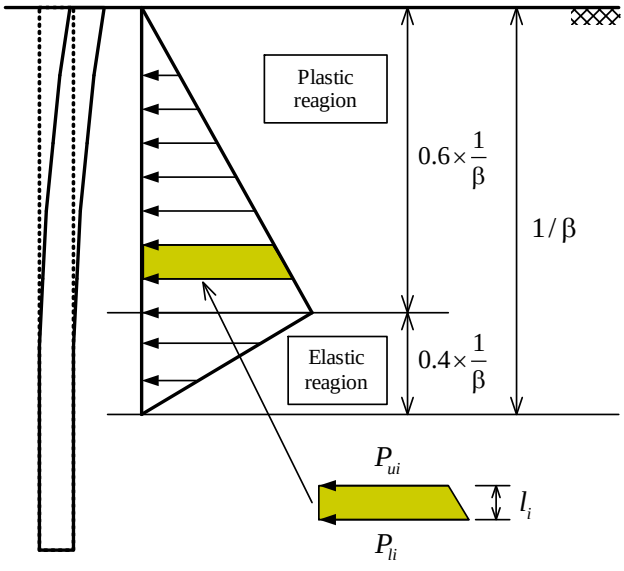

Figure 3-2 Calculation model for H_{ult}

where, c is cohesion (undrained strength), q is surcharge, K_P is the coefficient of passive earth pressure, ϕ is internal friction angle (degree) and δ is the friction angle between pile and soil. Finally, the passive earth pressure P_H is calculated based on a simple model (Nakatani et al. 2009) shown in Figure 3-2.

The parameter β is the characteristic value of pile which defines effective zone for subgrade reaction of pile and is taken as:

$$\beta = \sqrt[4]{\frac{k_H D}{4EI}} \tag{3-5}$$

$$k_H = \lambda k_0 (B'/0.3)^{-3/4} \tag{3-6}$$

$$k_0 = \alpha E_0 / 0.3 \tag{3-7}$$

$$B' = \sqrt{D/\beta} \tag{3-8}$$

where E_0 and α are the elastic modulus of bearing layer and the transformation coefficient on E_0 which are summarized in Table 3-2.

Table 3-2 Transformation coefficient for E_0

E_0 estimated from	Transformation coefficient α	
	Consider earthquake	Not consider earthquake
Plate load test with 0.3m rigid plate	1	2
Pressure meter test	4	8
Uniaxial or triaxial compression test	4	8
SPT-N value ($E_0 = 2800N_{SPT}$)	1	2

3.2.2 Deflection curve to failure

The deflection of laterally loaded single pile y is calculated based on the well-known beam-on-elastic-foundation model (e.g., Yamaguchi 1984) defined by:

$$\frac{d^4 y}{dz^4} = -\frac{k_H D}{EI} \tag{3-9}$$

where EI is the flexural stiffness of the pile, z is the depth in the soil, k_H is subgrade modulus, and D is diameter of pile. When $1.0 < \beta L_e \leq 3.0$ (L_e is the pile length), the deflection of pile head y_H is given by the following equation as a solution of Eq. (3-9):

$$y_{\mathrm{H}} = \frac{1}{2EI\beta^3}(C_1 + C_3) \tag{3-10}$$

$$C_1 = \frac{H}{\Delta}\left[-\cos 2\beta L_e e^{-2\beta L_e} - e^{-4\beta L_e}\right] + \frac{\beta M}{\Delta}\left[(\sin 2\beta L_e - \cos 2\beta L_e)e^{-2\beta L_e} - e^{-4\beta L_e}\right] \tag{3-11}$$

$$C_3 = \frac{H}{\Delta}\left[1 - \cos 2\beta L_e \cdot e^{-2\beta L_e}\right] + \frac{\beta M}{\Delta}\left[1 + (\cos 2\beta L_e + \sin 2\beta L_e)e^{-2\beta L_e}\right] \tag{3-12}$$

$$\Delta = 1 - 2(2 - \cos 2\beta L_e)e^{-2\beta L_e} + e^{-4\beta L_e} \tag{3-13}$$

where H is lateral force and M is the moment around pile head. We assumed that the deflection curve to failure can be modeled by a bi-linear model (shown in Figure 3-3). By substituting Eq. (3-1) into Eq. (3-6), the limit deflection of pile head δ_{ult} is obtained.

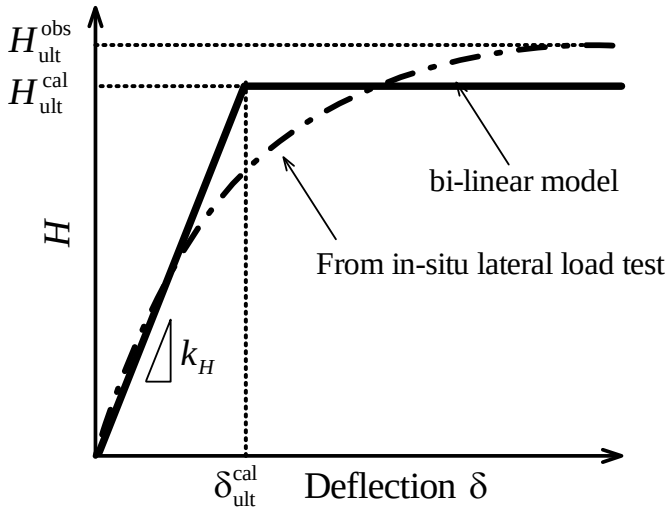

Figure 3-3 Bi-linear model for deflection curve to failure

2.3 Reliability analysis method

We estimate probability density function (PDF) of H_{ult} and δ_{limit} using direct Monte Carlo simulation (MCS) considering variability of soil parameters (unit weight of soil γ and cohesion c for 1/β region) and model uncertainties. The parameters k_H and β are the dominant factor in mechanical behavior of laterally loaded piles and should be estimated their probability distributions. In this example, however, those parameters are assumed to be constant values for simplicity.

The depth profile of c and γ are shown in Figure 3-4. Akkaya and Vanmarcke (2003) adopted the single exponential auto-correlation model to analyze the NGES-TAMU clay site data and found that the vertical scale of fluctuation (SOF) is about 1.52 m. For the lateral

resistance, the size of mobilization zone in each soil layer is assumed to be the length of the pile in the soil layer. The spatially averaged cohesion in the mobilization zone has a reduced COV due to spatial averaging (Vanmarcke 1977). This reduced COV is equal to the point COV multiplied by the COV reduction factor. For the single exponential model (Vanmarcke 1977), the COV reduction factor can be computed as

$$([2(L_m/\mathrm{SOF})-1+\exp[-2(L_m/\mathrm{SOF})]]/[2(L_m/\mathrm{SOF})^2])^{0.5} \tag{3-14}$$

where L_m is the size of the mobilization zone. Let $\mathrm{COV}_{\mathrm{mob}}$ denote the COV of the spatially averaged soil property. Using the above method, the values of L_m, COV reduction factor, and $\mathrm{COV}_{\mathrm{mob}}$ for different variables are calculated and summarized in Table 3-3.

We assume that the variabilities of the c and γ follow log-normal distribution with the mean $\mu_{\ln p}$ and standard deviation $\sigma_{\ln p}$ given by:

$$\mu_{\ln p} = \ln \mu_p - \frac{1}{2}\sigma_{\ln p}^2 \tag{3-15}$$

$$\sigma_{\ln p} = \sqrt{\ln (1+\mathrm{COV}_p^2)} \tag{3-16}$$

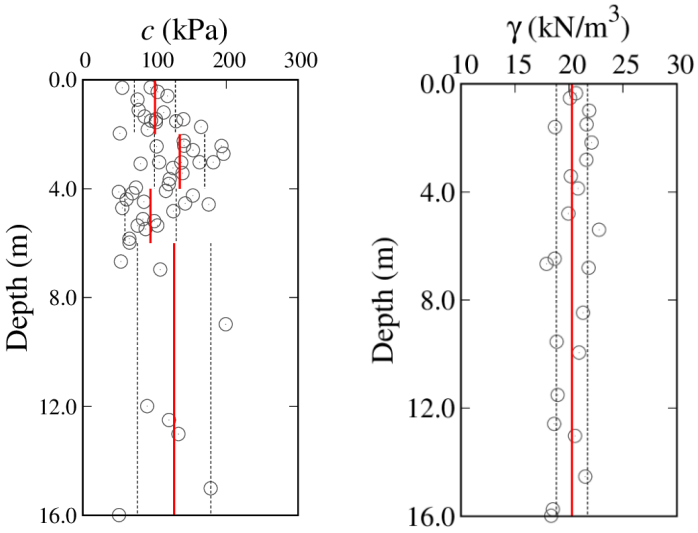

Figure 3-4 Depth profile of c and γ

where μ_p is the mean value and COV_p is coefficient of variation of parameter p which are summarized in Table 3-3.

Regarding the model uncertainty, Nakatani et al. (2009) investigated the accuracy Eq. (3-1) by comparing the calculated H_{ult} ($H_{\mathrm{ult}}^{\mathrm{cal}}$) with the measured H_{ult} ($H_{\mathrm{ult}}^{\mathrm{true}}$) obtained by pile load testing. They defined the parameter M = measured/calculated and evaluated the mean and standard deviations of M (Table 3-4). Since the M is not below zero, we assumed that the parameter M follows log-normal distribution with the mean and standard deviation in Table 3-

4. The ultimate load capacity of the pile to be estimated is given by

$$H_{\text{ult}}^{\text{true}} = M_{H_{\text{ult}}} \times H_{\text{ult}}^{\text{cal}}, \quad M_{H_{\text{ult}}} \sim N(\mu_{\ln M_{H_{\text{ult}}}}, \sigma_{\ln M_{H_{\text{ult}}}}) . \tag{3-17}$$

Table 3-3 Stochastic characteristics of geotechnical parameters

Parameter	μ_p	COV_p	L_m	COV reduction factor	COV_{mob}	$\mu_{\ln p}$	$\sigma_{\ln p}$
c_1	100.54	0.284	2	0.701	0.199	4.591	0.197
c_2	135.04	0.259	2	0.701	0.182	4.889	0.181
c_2	94.33	0.377	0.6	0.884	0.333	4.494	0.324
γ	20.284	0.071	4.6	0.525	0.037	3.009	0.037

Table 3-4 Model uncertainty

Parameter	μ_M	COV_M	$\mu_{\ln M}$	$\sigma_{\ln M}$	Reference
$H_{\text{ult}}^{\text{true}} / H_{\text{ult}}^{\text{cal}}$	1.041	0.446	-0.051	0.426	Nakatani et al. (2009)

3.4 Results

3.4.1 Deterministic design

The parameters used for H_{ult} and deflection curve are summarized in Table 3-5. Cohesion c and Elastic modulus of soil E_0 around pile base are obtained from UU/CU compression tests and pressure meter test. The arithmetic mean of c and E_0 are used in the design. The calculated H_{ult}, k_H, β and y_{ult} are summarized in Table 3-6. Figure 3-2 shows the deflection curve to failure of the pile.

Table 3-5 Design parameters

Parameter		Tests	How to calculate
c (kN/m^2)	93.14	UU and CU tests	arithmetic mean of data
E_{p} (kN/m^2)	25,000,000	-	-
E_0 (kN/m^2)	12,216	Pressure meter test	arithmetic mean of data

Table 3-6 Results of deterministic design

k_H	51574 kN/m^2
β	0.393328 m^{-1}
H_{ult}	251.8 kN
δ_{ult}	8.07 mm

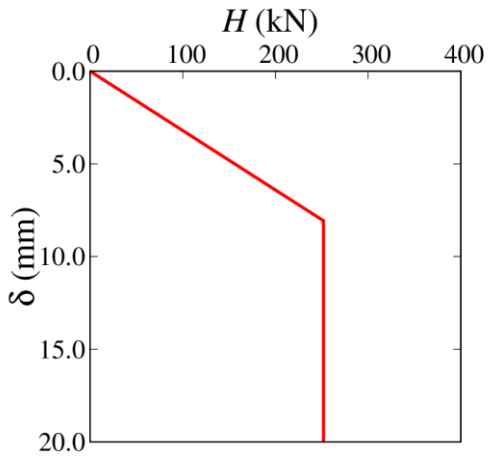

Figure 3-5 Load-settlement curve to failure

3.4.2 Probabilistic analysis

Probability distributions of H_{ult} and δ_{limit} are shown in Figure 3-6. The probability distributions are estimated with direct MCS with 100,000 samples. The sample mean μ and standard deviation σ are also presented. Since the model uncertainty is relatively high, it seems difficult to judge whether the presented distributions are reasonable or not.

There are following limitations of the deterministic/probabilistic analysis presented in this manuscript:

1) Although the model uncertainty is based on the database of pile loading tests, no data of cast-in-pile is included in the database.
2) The design method presented in this manuscript is based on the assumptions that the pile can be assumed to have semi-infinite length. Since the pile in Figure 3-1 is relatively short and has to be treated as finite-length pile.

Further research is necessary for reasonable design of laterally-loaded finite-length pile and cast-in-situ pile.

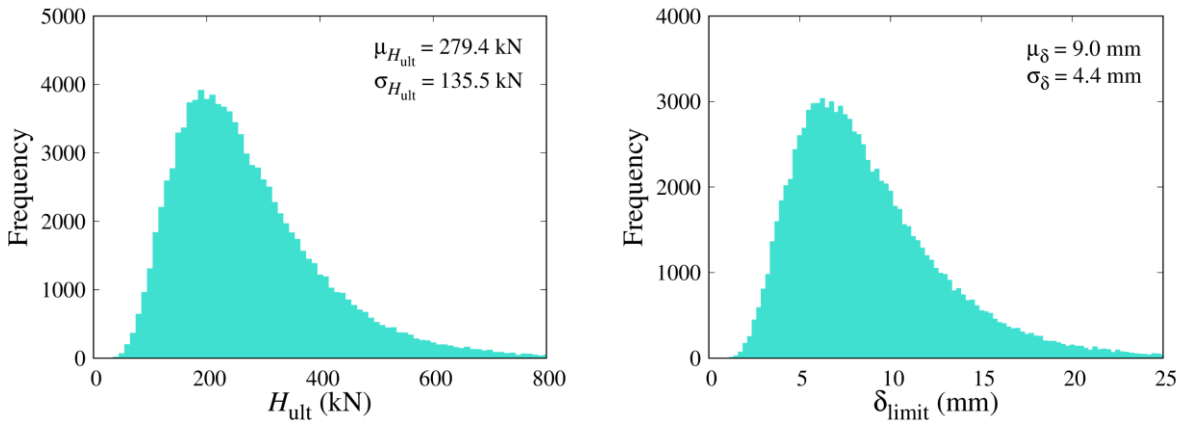

Figure 3-6 Probability distribution of H_{ult} and δ_{limit} with N_{MCS} = 100,000

References

Akkaya, A. D., and Vanmarcke, E. H. (2003). Estimation of spatial correlation of soil parameters based on data from the Texas A&M University NGES. Probabilistic site characterization at the National Geotechnical Experimentation Sites (Eds G. A. Fenton and E. H. Vanmarcke), 29-40.

JARA (2002). Specifications for Highway Bridges IV, Japan Road Association (in Japanese).

JARA (2017). Specifications for Highway Bridges IV, Japan Road Association (in Japanese).

Nakatani, S., Shirato, M., Khono, T. Iochi, H. and Kirikoshi, T. (2009). A study on limit states of laterally loaded pile, Technical Note of Public Work Research Institute, 4151, 83p (in Japanese).

Vanmarcke, E. H. (1977). Probabilistic modeling of soil profiles. Journal of the geotechnical engineering division, 103(11), 1227-1246.

Yamaguchi, H. (1984). *Soil Mechanics*, Gihodo Publishing Company, Ltd., pp.287- 291 (in Japanese).

Reliability-based design of spatially varying cohesive slope

Shui-Hua Jiang, Xian Liu, and Jianye Ching

4.1 Introduction

This section presents reliability-based design results for a cohesive slope. The geometry of the slope and the design problems are shown in Figure 4-1. A cohesive slope model with a foundation in Figure 4-2 is considered, which has a height of 6 m and an angle of β. The coordinate of the crest is (10+6/tanβ m, 9 m). The problem requires the design of a slope angle which ensures that a target probability of slope failure is not exceeded. Three different target probabilities of failure (0.0001, 0.001 and 0.01) are considered. The unit weight γ of the clay is determined based on the bulk density data. Section 4.2 presents the probabilistic characterization of the uncertain input parameters using laboratory and in-situ test data, respectively. Section 4.3 introduces stability analysis and reliability-based design of the cohesive slope using a limit equilibrium method (LEM) and an inverse first-order reliability method (FORM), respectively. Section 4.4 summarizes the reliability-based design results.

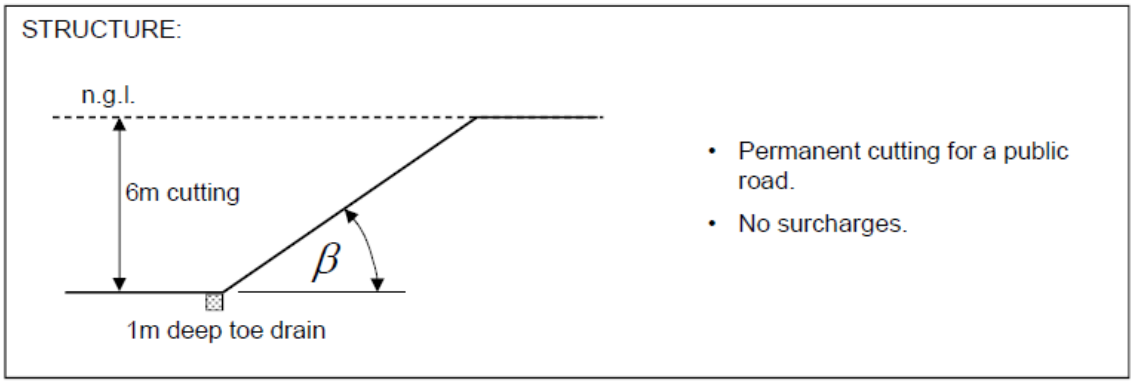

Figure 4-1 Schematic of a cohesive slope

4.2 Probabilistic characterization of the uncertain parameters

According to the slope structure as given in Reply sheet (see Figure 4-1), the slope geometry and random field mesh model, as shown in Figure 4-2, are used for reliability-based design of the slope angle in clay. To account for the inherent spatial variation of soil properties, the cohesive slope and foundation is discretized into 18 horizontal thin layers being homogeneous with a thickness of 0.5 m. In the cohesive soil layer, the short-term strength is characterized using the undrained shear strength (s_u). A single exponential autocorrelation function is adopted to characterize the spatial autocorrelation of s_u.

$$\rho\left(z_i, z_j\right) = \exp\left(-2\frac{\left|z_i - z_j\right|}{\delta_z}\right) \tag{4-1}$$

where δ_z is the vertical scale of fluctuation; z_i and z_j are the vertical coordinates of the centroids of the i-th and j-th soil layers, respectively. The Cholesky decomposition-based midpoint method is used to generate realizations of the random field of s_u (Li et al. 2015).

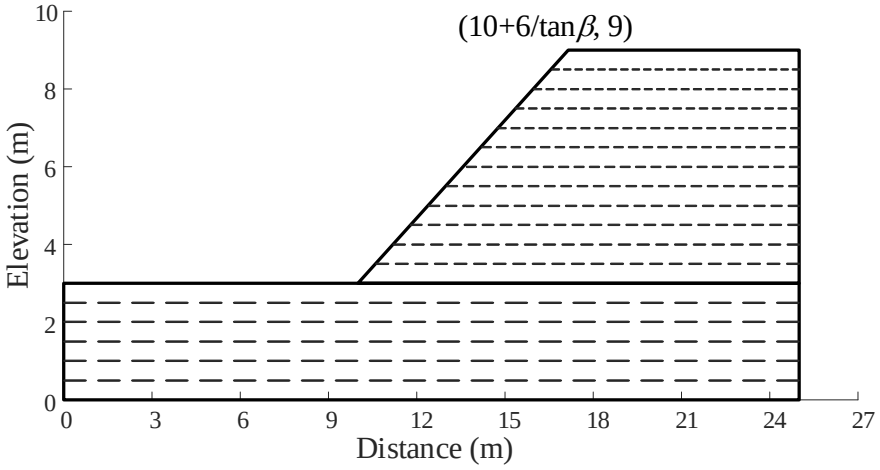

Figure 4-2 Slope geometry and random field mesh

4.2.1 Probabilistic characterization of s_u using laboratory test data

The soil samples obtained from the studied site are used to perform unconsolidated-undrained triaxial compression tests (UU) and unconfined compression tests (CU) for a direct laboratory measurement of s_u. Figure 4-3 shows the variations of the undrained shear strength obtained from the UU and CU data with the depth. The means (μ_{s_u}) and coefficients of variation (COV_{s_u}) of s_u are estimated by removing a constant trend using conventional statistical analyses, and listed in Table 1.

Akkaya and Vanmarcke (2003) adopted the single exponential autocorrelation model to analyze the Texas A&M University National Geotechnical Experimentation clay site data and found that the vertical scale of fluctuation (SOF) is about 1.52 m. Following Phoon and Kulhawy (1999), the coefficient of variation (COV) of the spatial average $s_{u,a}$ of undrained shear strength can be estimated as

$$\mathrm{COV}_{s_{u,a}} \approx \sqrt{\Gamma^2(L)\mathrm{COV}_w^2 + \mathrm{COV}_e^2} \tag{4-2}$$

where COV_w is the COV of inherent variability for the UU and CU tests; COV_e is the COV of the measurement error, which was estimated to be between 5 and 15% (Phoon and Kulhawy 1999), a value of COV_e = 15% is selected; $\Gamma(L)$ is the COV reduction factor, which can be computed as follows for the single exponential model (Vanmarcke 1977):

$$\Gamma(L) = \sqrt{\frac{\delta_z^2}{2L^2}\left[\frac{2L}{\delta_z} + \exp\left(-\frac{2L}{\delta_z}\right) - 1\right]} = 0.901 \tag{4-3}$$

where L = 0.5 m is the thickness of the horizontal thin layer, and δ_z = 1.52 m. Based on these, the values of $\mathrm{COV}_{s_{u,a}}$ can be estimated using Eq. (4-2), and summarized in Table 4-1. It is also assumed that the undrained shear strengths follow the lognormal distribution.

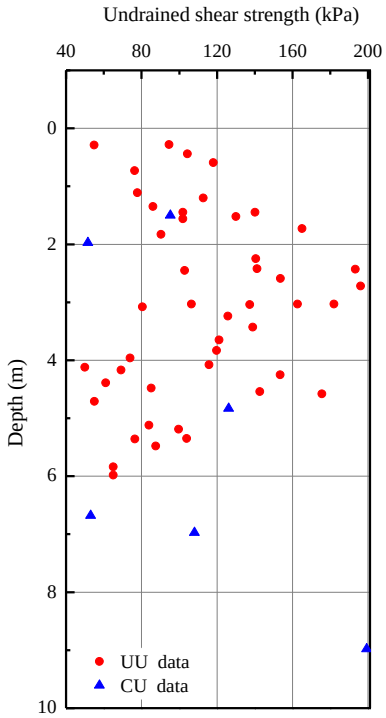

Figure 4-3 Variation of the undrained shear strength obtained from the UU and CU data with the depth

Table 4-1 Statistics of the uncertain input parameter obtained from the UU and CU data

Random variable	μ_{s_u}	COV_w	$\mathrm{COV}_{s_{u,a}}$	Distribution
s_u	110.637	0.361	0.358	Lognormal

4.2.2 Probabilistic characterization of s_u through correlation with corrected tip resistance

Besides, a set of cone tip resistance data acquired from Cone Penetration Test (CPT) at the studied site, as provided in Figure 4-4, are used to estimate s_u using the following transformation formula (Phoon and Kulhawy 1999):

$$\frac{s_u}{\sigma'_{v0}} = \frac{D_K(q_T - \sigma_{v0})}{\sigma'_{v0}} \tag{4-4}$$

where σ'_{v0} and σ_{v0} are the effective and total overburden stresses, respectively; D_K is the uncertain model slope; q_T is the corrected cone tip resistance (test measurement), which is defined as

$$q_T = q_c + (1-a)u_{bt} \tag{4-5}$$

where q_c is the cone tip resistance; a is the net area ratio; u_{bt} is the pore-water stress behind the cone tip, which is equal to zero for the studied site. As shown in Eq. (4-4), the value of D_K can significantly affect the estimation of s_u. In other words, to determine a reasonable value of D_K is quite crucial for the slope design. To this end, an extensive literature review is conducted. Table 4-2 summarizes the varying range of D_K as reported in geotechnical literature. To achieve a relatively conservative slope design scheme, the minimum value of $D_K = 0.0335$ is adopted here. Based on these, the undrained shear strengths for different depths can be estimated using Eq. (4-4) and shown in Figure 4-5. The corresponding means μ_{s_u} are evaluated using conventional statistical analyses, and listed in Table 4-3.

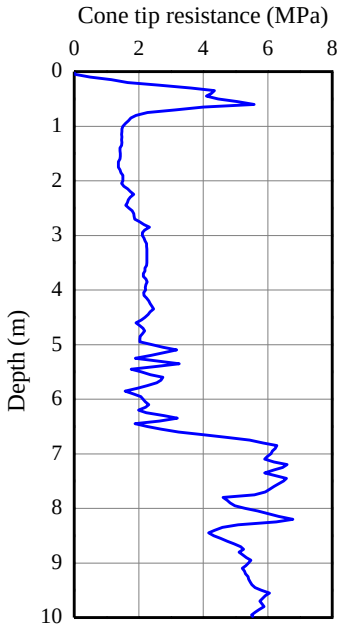

Figure 4-4 Variation of the cone tip resistance data with the depth

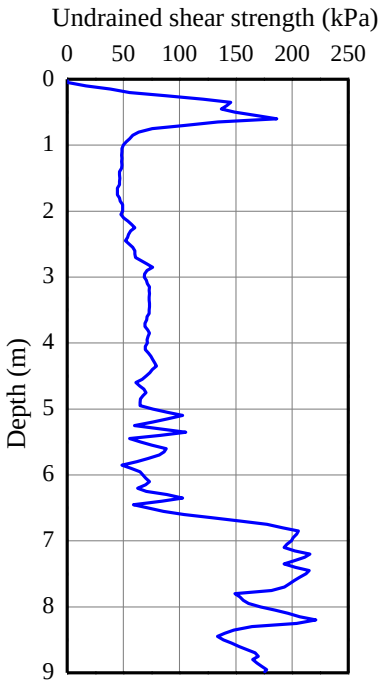

Figure 4-5 Variation of the undrained shear strength obtained from CPT data with the depth

Table 4-2 Summary of the values of D_K

Authors	Values of D_K
Aas et al. (1986)	0.0625~0.125
Rad and Lunne (1989)	0.0345~0.125
Powell and Quarterman (1988)	0.05~0.1
Karlsrud et al. (1996)	0.0667~0.167
Luune et al. (1997)	0.0541~0.0672
Rashwan et al. (2005)	0.0909
Larsson (2007)	0.0499~0.0746
Almeida et al. (2010)	0.0625~0.25
Hong et al. (2010)	0.05~0.143
Cai et al. (2010)	0.0667
Westerberg et al. (2015)	0.0335
Cao et al. (2016)	0.0789

Following Phoon and Kulhawy (1999), the COV of the spatial average $s_{u,a}$ of the undrained shear strength that is estimated from the CPT data using Eq. (4-4) can be evaluated as

$$\mathrm{COV}_{s_{u,a}} \approx \sqrt{\frac{\Gamma^2(L)\mathrm{COV}_w^2 + \mathrm{COV}_e^2}{(1-\sigma_{vm}/t)^2} + \mathrm{COV}_\varepsilon^2} \tag{4-6}$$

where COV_w denotes the COV of the corrected cone tip resistance (q_T) in clay; t is the mean value of q_T; COV_e is the COV of the measurement error, which was estimated to be between 5 and 15% (Phoon and Kulhawy 1999), a value of COV_e = 15% is selected; σ_{vm} is the average of total overburden stress; COV_ε is the transformation uncertainty, a value of $\mathrm{COV}_\varepsilon = 29\%$ is selected (Phoon and Kulhawy 1999); $\Gamma(L)$ is the COV reduction factor, which has been estimated using Eq. (4-3). Based on these, the values of $\mathrm{COV}_{s_{u,a}}$ for 18 soil layers can also be estimated using Eq. (4-6), and summarized in Table 4-3.

Table 4-3 Statistics of uncertain input parameters obtained from CPT data.

Random variable	Depth	μ_{s_u} (kPa)	COV_w	$\mathrm{COV}_{s_{u,a}}$	Distribution
$s_{u,1}$	0.25	81.235	0.749	0.751	Lognormal
$s_{u,2}$	0.75	94.896	0.535	0.585	Lognormal
$s_{u,3}$	1.25	48.009	0.017	0.328	Lognormal
$s_{u,4}$	1.75	46.895	0.039	0.330	Lognormal
$s_{u,5}$	2.25	54.086	0.065	0.334	Lognormal
$s_{u,6}$	2.75	66.085	0.088	0.339	Lognormal
$s_{u,7}$	3.25	72.626	0.014	0.329	Lognormal
$s_{u,8}$	3.75	71.212	0.017	0.329	Lognormal
$s_{u,9}$	4.25	73.850	0.046	0.332	Lognormal
$s_{u,10}$	4.75	66.916	0.059	0.335	Lognormal
$s_{u,11}$	5.25	80.737	0.199	0.379	Lognormal
$s_{u,12}$	5.75	70.325	0.172	0.369	Lognormal
$s_{u,13}$	6.25	75.208	0.165	0.366	Lognormal
$s_{u,14}$	6.75	161.397	0.276	0.416	Lognormal
$s_{u,15}$	7.25	203.963	0.041	0.330	Lognormal
$s_{u,16}$	7.75	178.049	0.125	0.348	Lognormal
$s_{u,17}$	8.25	173.754	0.172	0.366	Lognormal
$s_{u,18}$	8.75	165.507	0.058	0.334	Lognormal

4.3 Stability and reliability analyses of the slope

It is assumed that the groundwater table is far below the foundation, and thus does not pass through the slope toe. No tension cracks are considered in this study. The friction angle and the dilation angle are assumed to be zero, because the total stress analysis is adopted. The unit weight of the clay is derived based on the bulk density data, which also changes with the depth, as shown in Figure 4-6.

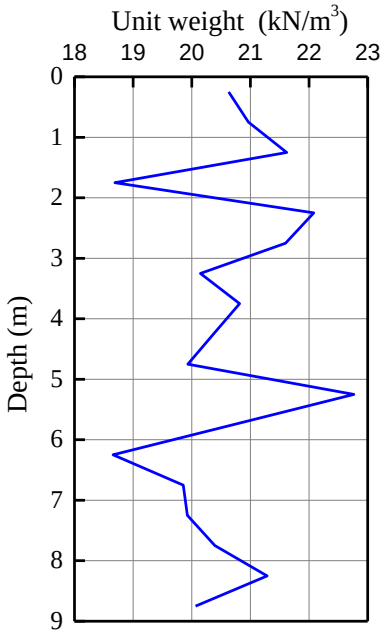

Figure 4-6 Variation of the unit weight of the clay with the depth.

The short-term stability of the slope under undrained conditions is also assessed using Bishop's simplified method. For a given β and one realization of random variables, the minimum factor of safety (FS_{min}) is evaluated and the corresponding critical slip surface is located among more than 2100 possible slip surfaces (see Figure 4-7). As a reference, the nominal value of FS_{min} based on the means of undrained shear strength in Table 4-3, and it is equal to 3.795. In addition, the critical slip surface is located and shown in Figure 4-7. Figure 4-8 presents the variations of the factors of safety with the slope angle based on two different sources of test data. It can be observed that the slope with a slope angle up to 90° will be stable when an allowable factor of safety of 1.5 is considered. Additionally, the factor of safety for the cohesive slope estimated based on the UU and CU data is significantly larger than that estimated based on the CPT data.

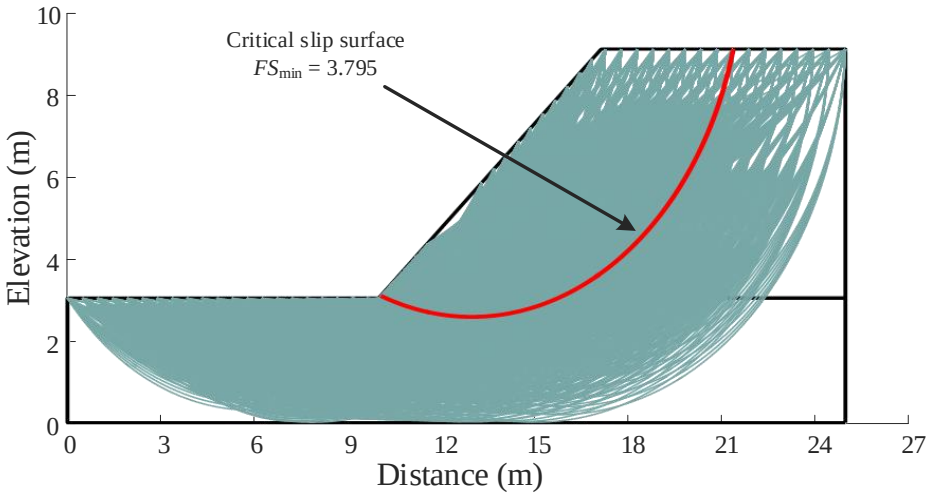

Figure 4-7 Slope with 2125 potential slip surfaces

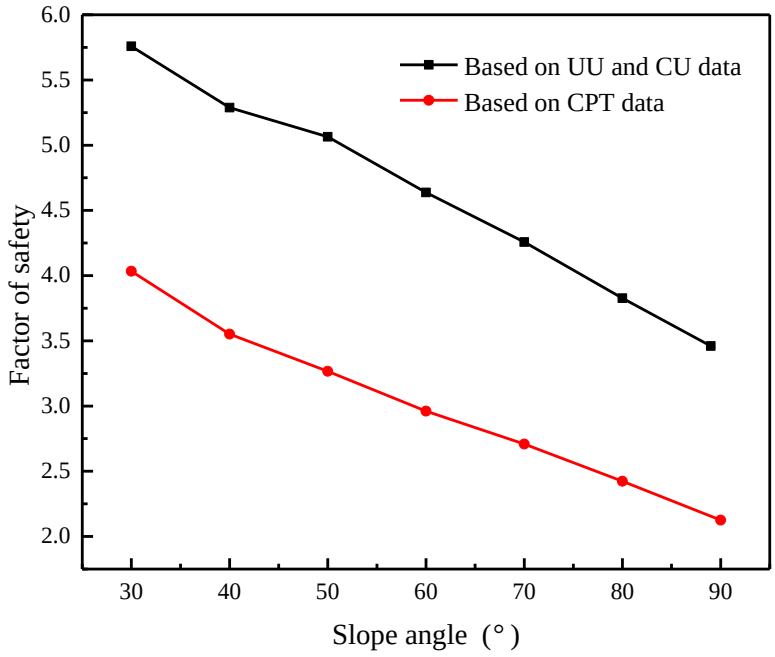

Figure 4-8 Variations of the factor of safety with the slope angle

Because of the model uncertainty of the Bishop's simplified method (Christian et al. 1994; Jiang et al. 2017), the following relationship between the actual factor of safety (FS_A) and the calculated $FS_{\min}$ is established (Bahsan et al. 2014):

$$FS_A = wFS_{\min}(\boldsymbol{s}_u) \tag{4-7}$$

where $\boldsymbol{s}_u = \left(s_{u,1}, s_{u,2}, ..., s_{u,18}\right)^{\mathrm{T}}$; w is the model factor, which is assumed to follow the lognormal distribution with mean= 1.066 and COV = 0.296 according to Bahsan et al. (2014). In this way, the limit state function can be expressed as

$$g(\boldsymbol{s}_u) = wFS_{\min}(\boldsymbol{s}_u) - 1.0 \tag{4-8}$$

4.4 Reliability-based design results

In this section, the slope angles for achieving the target probabilities of failure (0.0001, 0.001 and 0.01) are designed wherein the undrained shear strengths are determined from the UU and CU data and the CPT data, respectively. An inverse FORM formulated in x-space that is proposed by Ji et al. (2019) is employed to derive an optimized slope angle for the limit state function in Eq. (4-8). Figure 4-9 presents the iterative calculation process of the slope angles for different target probabilities of failure based on the CPT data. As seen from Figure 4-9, the slope angles β for achieving the target probabilities of failure (0.0001, 0.001 and 0.01) can be readily derived after 4 or 5 iterations. For a vertical scale of fluctuation of 1.52 m, the designed slope angles associated with the CPT data are 33.52°, 56.10° and 82.71°, respectively. In contrast, the designed slope angle for a target probability of slope failure of 0.0001 based on the UU and CU data is 85.21°. This is because the factor of safety is quite large and the probability of slope failure is sufficiently low in this case although a slope angle up to 90° is adopted. When a target probability of failure of 0.0001 is adopted that is acceptable for all slopes (U.S. Army Corps of Engineers 1997; Santamarina et al. 1992), the designed slope angles should be smaller than 33.52° at which the slope is to be cut. Additionally, the slope design results obtained from the probabilistic analysis are more conservative than those obtained from the deterministic analysis with a comparison of Figures 4-8 and 4-9.

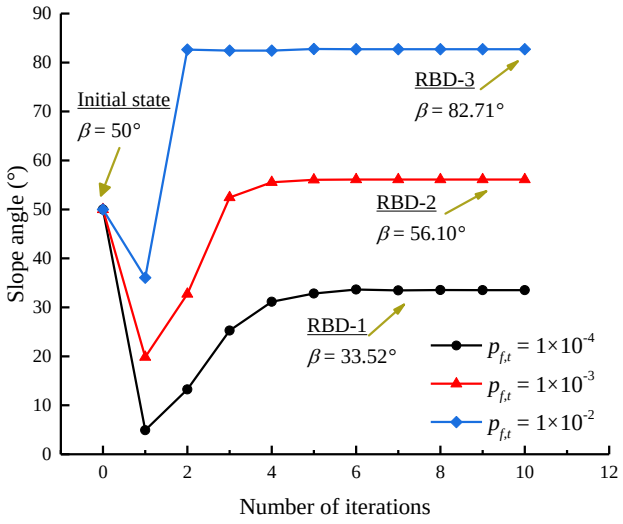

Figure 4-9 Variations of the designed slope angle for three scenarios based on the CPT data with the number of iterations

References

Aas, G., Lacasse, S., Lunne, T., Hoeg, K. (1986). Use of in situ tests for foundation design on clay. In Proc. of the ASCE Conference In-situ, 86: 1-30.

Akkaya, A.D., and Vanmarcke, E.H. (2003). Estimation of spatial correlation of soil parameters

based on data from the Texas A&M University NGES. Probabilistic site characterization at the National Geotechnical Experimentation Sites (Fenton G. A. andVanmarcke E. H., Eds), 29-40.

Almeida, M., Marques, M., Baroni, M. (2010). Geotechnical parameters of very soft clays from CPTu. In Proceedings of 2nd international symposium on cone penetration testing, CPT'10. pp. 2-46.

Bahsan, E., Liao, H.J., Ching, J., Lee, S.W. (2014). Statistics for the calculated safety factors of undrained failure slopes. Engineering Geology, 172: 85-94.

Cai, G.J., Liu, S.Y., Tong, L.Y., Du, G.Y. (2010). Field evaluation of undrained shear strength from piezocone penetration tests in soft marine clay. Marine Georesources and Geotechnology, 28(2): 143-153.

Cao, Z.J., Wang, Y., Li, D.Q. (2016). Site-specific characterization of soil properties using multiple measurements from different test procedures at different locations – A Bayesian sequential updating approach. Engineering Geology, 211, 150-161.

Christian, J.T., Ladd, C.C., Baecher, G.B. (1994). Reliability applied to slope stability analysis. Journal of Geotechnical Engineering, 120(12): 2180-207.

Hong, S., Lee, M., Kim, J., Lee, W. (2010). Evaluation of undrained shear strength of Busan clay using CPT. In Proceedings of 2nd international symposium on cone penetration testing, CPT'10. 2010, pp. 2-23.

Ji J., Zhang C., Gao Y, Gao Y.F., Kodikara, J. (2019). Reliability-based design for geotechnical engineering: An inverse FORM approach for practice. Computers and Geotechnics, 111: 22-29.

Jiang, S.H., Papaioannou, I., Li, C.G., Straub, D. 2017. Integrating LEM with FEM through model correction factor method in reliability analysis of spatially variable slopes. The 15th International Conference of the International Association for Computer Methods and Advances in Geomechanics, October 19-23, Wuhan, China. pp. 1-7.

Karlsrud, K., Lunne, T., Brattlieu, K. (1996). Improved CPTu correlations based on block samples. Reykjavik: Nordisk Geotekniker-mote.

Larsson, R. (2007). CPT-sondering. Statens geotekniska institut, SGI, Linköping.

Li, D.Q., Jiang, S.H., Cao, Z.J., Zhou, W., Zhou, C.B., Zhang, L.M. (2015). A multiple response-surface method for slope reliability analysis considering spatial variability of soil properties. Engineering Geology, 187: 60-72.

Lunne, T., Robertson, P.K., Powell, J.J.M. (1997). Cone penetration testing in geotechnical engineering practice. Blackie Academic and Professional, New York.

Phoon, K.K., Kulhawy, F.H. (1999). Evaluation of geotechnical property variability. Canadian Geotechnical Journal, 36(4), 625-639.

Powell, J.J.M., Quarterman, R.S.T. (1988). The interpretation of cone penetration tests in clays, with particular reference to rate effects. International Symposium on penetration testing;

Penetration Testing, 2, 903-909.

Rad, N.S., Lunne, T. (1989). Direct correlations between piezocone test results and undrained shear strength of clay. Publikasjon-Norges Geotekniske Institutt, 177: 1-7.

Rashwan, M.A., Koumoto, T., Park, J.H., Hino, T. (2005). Prediction of wet density and undrained shear strength of clays by electronic cone penetration testing. Transactions of the JSIDRE 236, 77-84.

Santamarina, J., Altschaeffl, A., Chameau, J. (1992). Reliability of slopes: Incorporating qualitative information. Transportation Research Record, 1343, 1-5.

U.S. Army Corps of Engineers. Engineering and design: introduction to probability and reliability methods for use in geotechnical engineering. Department of the Army, Washington, D.C. Engineer Technical Letter, 1110-2-547, 1997.

Vanmarcke, E. H. (1977). Probabilistic modeling of soil profiles. Journal of the Geotechnical Engineering Division, 103(11): 1227-1246.

Westerberg, B., Müller, R., Larsson, S. (2015). Evaluation of undrained shear strength of Swedish fine-grained sulphide soils. Engineering Geology, 188: 77-87.

Probabilistic analysis of vertically loaded square footing on sand

Zhiyong Yang and Jianye Ching

5.1 Introduction

This section presents the probabilistic analysis results for the Problem SAND 1 – vertically loaded square footing. The geometry of the square footing and the design problems are shown in Figure 5-1. The square concrete footing has width of B = 2.25 m and height of H = 1.2 m. It is founded on a sand layer with an embedment depth of D_f = 0.75m. A concentric applied load P (not including the weight of the footing) is imposed on the footing. The problem requires the prediction of the performance of the square footing: (1) predict the ultimate load capacity of the footing P_{ult} and (2) predict the load P_{25mm} that will cause the footing to settle by 25 mm in the long term. The weight of the concrete γ_c is not specified, and γ_c = 23 kN/m^3 is assumed in the following analysis. Section 5.2 introduces the prediction equations for P_{ult} and P_{25mm}, Section 5.3 presents the probabilistic characterization of the uncertain parameters involved in the problem, and Section 5.4 summarizes the prediction result.

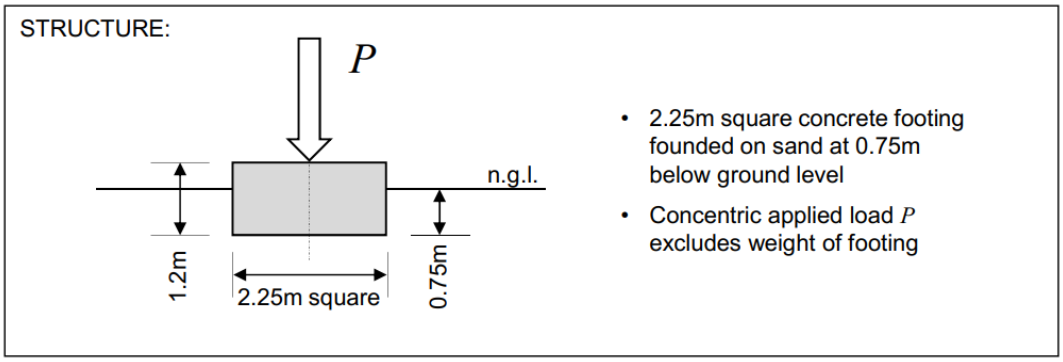

Figure 5-1 Schematic of the square footing

5.2 Prediction equations for P_{ult} and P_{25mm}

5.2.1 Prediction equation for P_{ult}

The ultimate bearing capacity of the footing can be predicted by the formulae proposed by Akbas and Kulhawy (2009b):

$$q_{u,c} = \begin{cases} 0.5\gamma B N_\gamma s_\gamma d_\gamma i_\gamma r_\gamma + \gamma D_f N_q s_q d_q i_q r_q & B > 1\text{m} \\ 0.5\gamma N_\gamma s_\gamma d_\gamma i_\gamma r_\gamma + \gamma D_f N_q s_q d_q i_q r_q & B \le 1\text{m} \end{cases} \tag{5-1}$$

where $q_{u,c}$ is the calculated ultimate bearing capacity;

$$N_q = e^{\pi \tan(\phi)} \tan^2\left(45^o + \phi_{mob}/2\right) \qquad N_\gamma = 2\left(N_q + 1\right)\tan\left(\phi_{mob}\right) \tag{5-2}$$

where ϕ_{mob} is the mobilized friction angle (to be elaborate later); the shape factors s_q and s_γ are

$$s_q = 1 + \tan(\phi_{mob}) \qquad s_\gamma = 0.6 \tag{5-3}$$

the depth factors d_q and d_γ are

$$d_q = 1 + 2\tan(\phi_{mob})\left[1 - \sin(\phi_{mob})\right]^2\left[(\pi/180)\tan^{-1}(D_f/B)\right] \qquad d_\gamma = 1 \tag{5-4}$$

$\tan^{-1}(D_f/B)$ is in degrees; the inclination factors $i_q = i_\gamma = 1$ because no horizontal load is imposed on the footing base; the soil compressibility factors r_q and r_γ are

$$r_q = r_\gamma = \begin{cases} 1 & \text{if } I_{rr} > I_{rc} \\ \exp\left[-3.8\tan(\phi_{mob}) + \dfrac{3.07\sin(\phi_{mob})\log_{10}(2I_{rr})}{1+\sin(\phi_{mob})}\right] & \text{if } I_{rr} < I_{rc} \end{cases} \tag{5-5}$$

$I_{rc} = 0.5\exp[2.85\cot(45° - \phi_{mob}/2)]$ is the critical rigidity index; $I_{rr} = I_r/(1+I_r\Delta)$ is the reduced rigidity index; $\Delta = 0.005[(45° - \phi_{mob})/20°][\gamma(D_f + 0.5B)]/P_a$ is the volumetric train; $I_r = G_{mob}/[\gamma(D_f + 0.5B)\tan(\phi_{mob})]$ is the rigidity index; G_{mob} is the mobilized shear modulus (to be elaborated later); $P_a = 101.3$ kPa is one atmosphere pressure.

The actual q_u and calculated $q_{u,c}$ are different due to modeling errors. A database of 106 load test cases for footings in cohesionless soils are compiled by Akbas and Kulhawy (2009b). The model factor (ε_m), defined as (actual q_u)/$q_{u,c}$, can be calcluated for each case. The sample mean for the 106 model factors is 1.04, and the sample coefficient of variation (COV) is 28%. As a result, the relationship between the actual q_u (denoted by q_u) and calculated q_u (denoted by $q_{u,c}$) is as follows:

$$q_u = q_{u,c} \times \varepsilon_m \tag{5-6}$$

where ε_m is modeled as a lognormal random variable with mean = 1.04 and COV = 28%.

The total vertical load is equal to vertical load (P) + footing weight (W). As a result, P_{ult} can be computed as

$$P_{ult} = q_u B^2 - W = q_{u,c} \times \varepsilon_m \times B^2 - W \tag{5-7}$$

5.2.2 Prediction equation for P_{25mm}

The load P that causes the footing to settle by a certain amount can be predicted by the normalized load-settlement curve proposed by Akbas and Kulhawy (2009a):

$$\frac{P+W}{q_u B^2} = \frac{(s/B)\times 100}{a(s/B)\times 100 + b} \tag{5-8}$$

where s is the settlement; (a, b) are the fitting parameters (to be elaborated later). The P_{25mm} can be predicted by letting s = 0.025 m and $q_u = q_{u,c} \times \varepsilon_m$:

$$P_{25mm} = \frac{(0.025/B)\times 100}{a(0.025/B)\times 100+b} \times q_{u,c} \times \varepsilon_m \times B^2 - W \quad (5\text{-}9)$$

Akbas and Kulhawy (2009a) calibrated the (a, b) parameters for 167 footing load tests conducted on cohesionless soils. The calibrated (a, b) data points are shown in Figure 5-2.

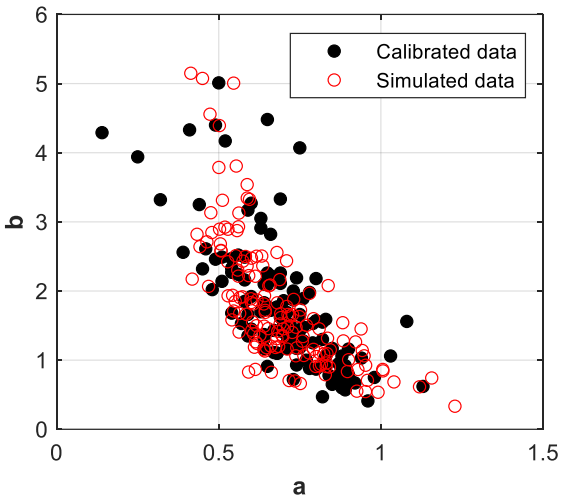

Figure 5-2 Scatter plot of a and b

5.3 Probabilistic characterization of the uncertain parameters

5.3.1 Statistics of ϕ_{mob} and G_{mob}

The data points for the effective stress friction angle (ϕ) at the NGES-TAMU sand site are shown in Figure 5-3a. The ϕ data points have a sample mean of 31.43° and a sample COV of 11%. Honjo and Otake (2013) indicated that for the ultimate bearing capacity of a footing, the mobilization zone is between the footing base and 0.7×B below the footing base. This suggests that the mobilization zone for the current footing problem is within the depth range of 0.75-2.33 m. Akkaya and Vanmarcke (2003) adopted the single exponential auto-correlation model to analyze the NGES-TAMU sand site data and found that the vertical scale of fluctuation (SOF) is about 1.75 m. The spatially averaged friction angle in the mobilization zone, denoted by ϕ_{mob}, has a reduced COV due to spatial averaging (Vanmarcke 1977). This reduced COV is equal to the point COV (11%) multiplied by the COV reduction factor. For the single exponential model (Vanmarcke 1977), the COV reduction factor can be computed as $([2(L/SOF)-1+\exp[-2(L/SOF)]/[2(L/SOF)^2])^{0.5} = 0.77$, where L = 0.7×B = 1.575 m is the size of the mobilization zone, and SOF = 1.75 m. As a result, the COV for ϕ_{mob} is 11%×0.77 = 8.8%. Moreover, ϕ_{mob} is assumed to follow the lognormal distribution.

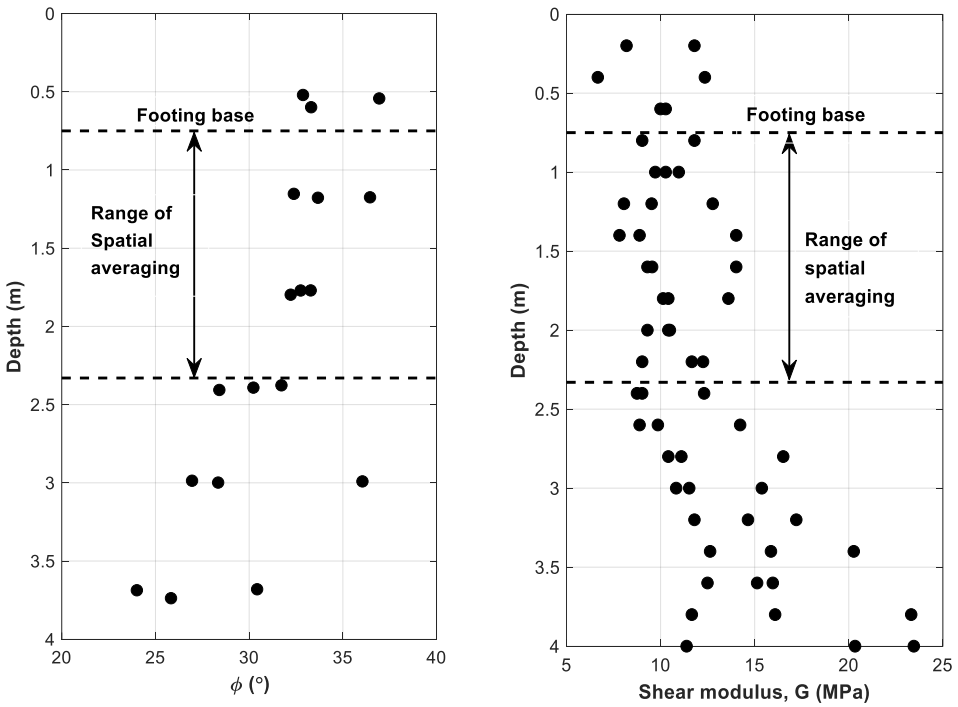

(a) Friction angle (b) Shear modulus

Figure 5-3 Friction angle (ϕ) and shear modulus (G) for the NGES-TAMU sand site (based on the data extracted from Briaud (2000))

The dilatometer test (DMT) was conducted at the NGES-TAMU sand site to measure the dilatometer modulus (E_D). This E_D can be converted to shear modulus (G) (Kulhawy and Mayne 1990):

$$G = E_D(1-\nu)/2 \tag{5-10}$$

where ν is the Poisson ratio of the silty sand, which is taken to be ν = 0.2. The resulting G data are shown in Figure 5-3b. The G data have a sample mean of 11.9 MPa and a sample COV of 26.9%. The COV for the spatially averaged G in the mobilization zone (i.e., G_{mob}) is therefore 26.9%×0.77 = 20.8%. Moreover, G_{mob} is also assumed to follow the lognormal distribution.

5.3.2 Statistics of a and b

It is found that the (a, b) data in Figure 5-2 can be satisfactorily modeled by the lognormal distribution: the parameter a can be modeled as a lognormal distribution with mean = 0.70 and COV = 22.2% (p-value = 0.08), whereas the parameter b can be modeled as a lognormal distribution with mean = 1.77 and COV = 53.5% (p-value = 0.99). As a result, ln(a) is normal with mean = $\ln[0.70/(1+22.2\%^2)^{0.5}]$ = -0.381 and standard deviation = $\ln(1+22.2\%^2)^{0.5}$ = 0.291, and ln(b) is normal with mean = $\ln[1.77/(1+53.5\%^2)^{0.5}]$ = 0.445 and standard deviation = $\ln(1+53.5\%^2)^{0.5}$ = 0.502. The correlation coefficient (ρ) between (ln(a), ln(b)) is estimated by first estimating the Kendall correlation (r) between (a, b) and then implement the identity ρ =

$\sin(\pi r/2)$. The resulting ρ estimate is -0.793. The dependency between (ln(a), ln(b)) is further modeled by a copula (Li et al. 2013). Four copulas are considered: Gaussian, Plackett, Frank, and No. 16 copulas. It is found that the Gaussian copula is optimal with the smallest AIC (Akaike 1974) and smallest BIC (Schwarz 1978). As a result, the Gaussian copula is adopted. The following procedure can be used to simulate (a, b) data from Gaussian copula:

3. Simulate the correlated standard normal vector $\underline{z}=[z_1\ z_2]$ with mean = [-0.381 0.445] and covariance matrix = $[0.291^2\ \rho\times0.291\times0.502;\rho\times0.291\times0.502\ 0.502^2]$;
4. Simulate the sample of a and b by $a = \exp(z_1)$ and $b = \exp(z_2)$.

The scatter plot for simulated (a, b) is shown in Figure 5-2.

There are in total five uncertain parameters (ϕ_{mob}, G_{mob}, ε_m, a, b) for predicting P_{ult} and P_{25mm}. The statistics of the five uncertain parameters are summarized in Table 5-1. All parameters are assumed to be mutually independent except for (a, b). The Gaussian copula is adopted to model the dependency between (a, b), and the correlation coefficient between (ln(a), ln(b)) is $\rho = -0.793$.

Table 5-1 Statistics of the random variables for the square footing

Random variable	Mean	COV	Distribution
Mobilized friction angle, ϕ_{mob}	31.43° (39.82°*)	8.8% (13.3%*)	Lognormal
Mobilized shear modulus, G_{mob}	11.9 MPa	20.8%	Lognormal
Model factor, ε_m	1.04	28%	Lognormal
a	0.70	22.2%	Lognormal
b	1.77	53.5%	Lognormal

* Statistics based on ϕ data transformed from SPT N data

5.4 Prediction results

5.4.1 Prediction results based on measured ϕ data

Monte Carlo simulation (MCS) with 1×10^7 samples are used to simulate the distribution of P_{ult} and P_{25mm} using Eqs. (5-7) and (5-9), respectively. The obtained histograms for P_{ult} and P_{25mm} are shown in Figure 5-4. Figure 5-4 also shows the deterministic analysis results with red lines. The deterministic analysis results are computed based on the mean values of the random variables. The statistics for P_{ult} and P_{25mm} are summarized in Table 5-2. For reference, the deterministic analysis results are also summarized in Table 5-2.

Table 5-2 Prediction results for P_{ult} and P_{25mm}

Predicted Loads	Mean	Median	Standard deviation	Deterministic analysis result
P_{ult}	5284.97 kN	4615.16 kN	2890.12 kN	4838.41 kN
P_{25mm}	2426.91 kN	2059.62 kN	1558.35 kN	2033.89 kN

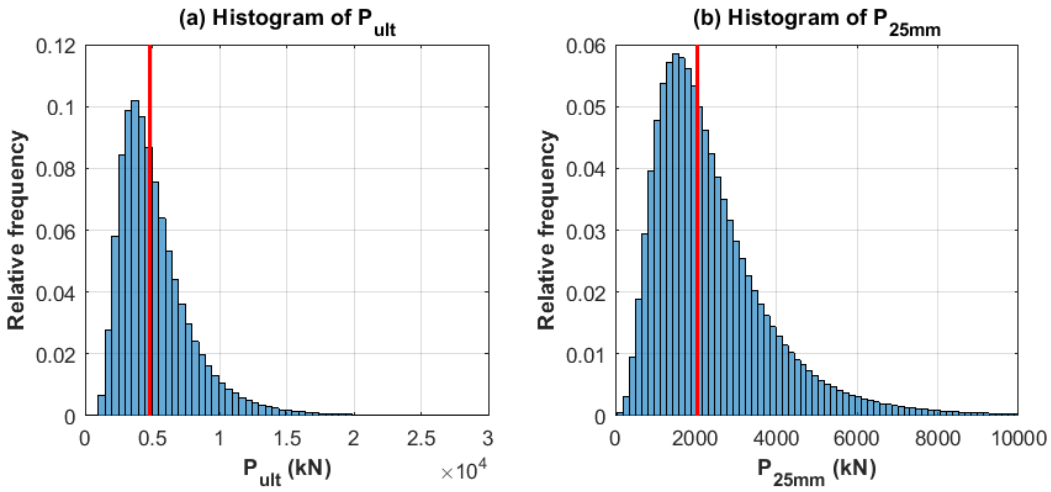

Figure 5-4 Histograms for P_{ult} and P_{25mm}.

5.4.2 Prediction results based on ϕ data transformed from SPT N data

The ϕ data in Figure 5-3a are quite low. The standard penetration test (SPT) was conducted at the NGES-TAMU sand site to measure the SPT blow count (N). This SPT N value can be converted to friction angle (ϕ) by the following transformation model (Mayne et al. 2001):

$$\phi \approx \sqrt{15.4\times(N_1)_{60}} + 20^{o} \qquad (N_1)_{60} = N_{60}/\left(\sigma'_{v0}/P_a\right)^{0.5} \tag{5-11}$$

where $(N_1)_{60}$ is the normalized SPT N value; N_{60} is the energy-corrected SPT N value; σ'_{v0} is the in-situ effective stress. The resulting ϕ data are shown in Figure 5-5. Also plotted in the figure are the ϕ profiles estimated by cone penetration tests (CPT). There is a general agreement between the ϕ data estimated by SPT N and the ϕ profiles estimated by CPT. The ϕ data has a sample mean of 39.82° and the sample COV of 11.4%. The reduced COV for ϕ_{mob} is 11.4%×0.77 = 8.8%. The transformation uncertainty for Eq. (5-11) is with a COV of about 10% (Ching et al. 2017). The total COV for ϕ_{mob} is approximately $[(8.8\%)^2+(10\%)^2]^{0.5}$ = 13.3%. These new statistics for ϕ_{mob} are shown in the parentheses in Table 5-1.

Based on the new statistics for ϕ_{mob}, MCS with 1×10^7 samples are used again to simulate the distribution of P_{ult} and P_{25mm}. The statistics for other uncertain parameters remain unchanged. The obtained histograms for P_{ult} and P_{25mm} are shown in Figure 5-6. Figure 5-6 also shows the deterministic analysis results with red lines. The deterministic analysis results are computed based on the mean values of the random variables. The statistics for P_{ult} and P_{25mm} are summarized in Table 5-3. For reference, the deterministic analysis results are also summarized in Table 5-3.

Table 5-3 Prediction results for P_{ult} and P_{25mm} (based on new statistics for ϕ_{mob})

Predicted Loads	Mean	Median	Standard deviation	Deterministic analysis result
P_{ult}	19915.22 kN	15558.69 kN	15467.17 kN	17096.59 kN
P_{25mm}	9349.08 kN	7020.97 kN	7939.50 kN	7386.21 kN

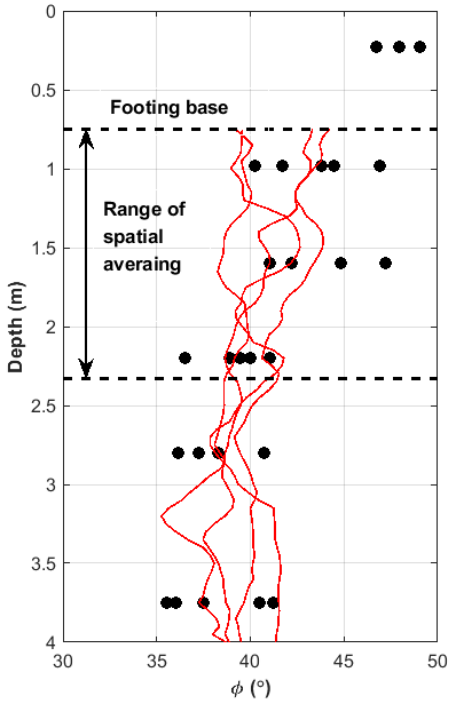

Figure 5-5 Friction angle (ϕ) transformed from SPT N values (based on the data extracted from Briaud (2000))

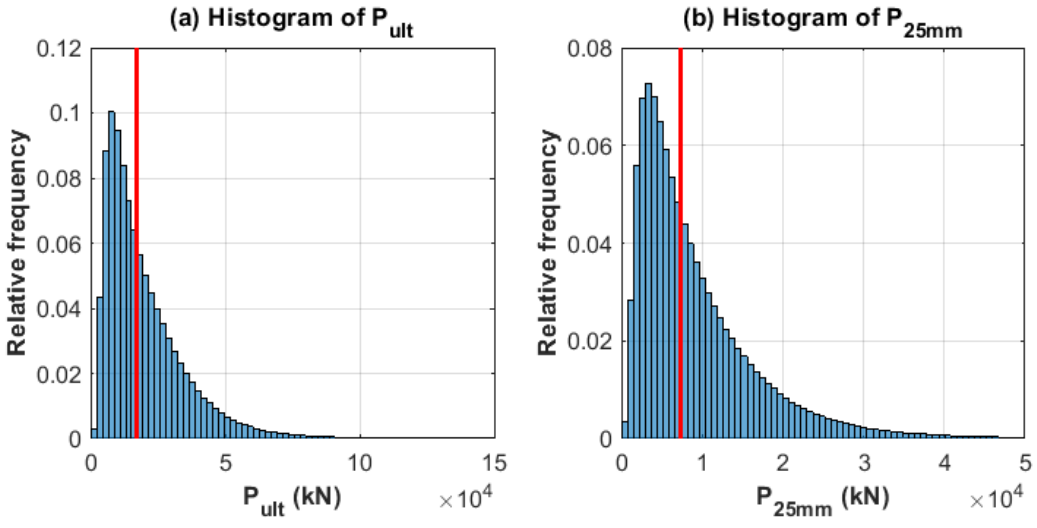

Figure 5-6 Histograms for P_{ult} and P_{25mm} (based on new statistics for ϕ_{mob})

References

Akaike, H. (1974). A new look at the statistical model identification. IEEE transactions on automatic control, 19(6), 716-723.

Akbas, S. O., and Kulhawy, F. H. (2009a). Axial compression of footings in cohesionless soils. I: Load-settlement behavior. Journal of geotechnical and geoenvironmental engineering, 135(11), 1562-1574.

Akbas, S. O., and Kulhawy, F. H. (2009b). Axial compression of footings in cohesionless soils. II: Bearing capacity. Journal of geotechnical and geoenvironmental engineering, 135(11), 1575-1582.

Akkaya, A. D., and Vanmarcke, E. H. (2003). Estimation of spatial correlation of soil parameters based on data from the Texas A&M University NGES. Probabilistic site characterization at the National Geotechnical Experimentation Sites (Eds G. A. Fenton and E. H. Vanmarcke), 29-40.

Briaud, J. L. (2000). The National Geotechnical Experimentation Sites at Texas A&M University: Clay and Sand. A Summary. National Geotechnical Experimentation Sites: Geotechnical Special Publication, 93, 26–51.

Ching, J., Lin, G. H., Chen, J. R., and Phoon, K. K. (2017). Transformation models for effective friction angle and relative density calibrated based on generic database of coarse-grained soils. Canadian Geotechnical Journal, 54(4), 481-501.

Honjo, Y., and Otake, Y. (2013). A simple method to assess the effects of soil spatial variability on the performance of a shallow foundation. In Foundation Engineering in the Face of Uncertainty: Honoring Fred H. Kulhawy (Eds. J. L. Withiam, K. K. Phoon, and M. Hussein), 385-404.

Kulhawy, F. H., and Mayne, P. W. (1990). Manual on estimating soil properties for foundation design, Report EL-6800. Electric Power Research Institute, Cornell University, Palo Alto.

Li, D. Q., Tang, X. S., Phoon, K. K., Chen, Y. F., and Zhou, C. B. (2013). Bivariate simulation using copula and its application to probabilistic pile settlement analysis. International Journal for Numerical and Analytical Methods in Geomechanics, 37(6), 597-617.

Mayne, P. W., Christopher, B. R., DeJong, J. (2001). Manual on Subsurface Investigations, National Highway Institute Publication No. FHWA NHI-01-031, Federal Highway Administration.

Schwarz, G. (1978). Estimating the dimension of a model. The annals of statistics, 6(2), 461-464.

Vanmarcke, E. H. (1977). Probabilistic modeling of soil profiles. Journal of the geotechnical engineering division, 103(11), 1227-1246.

Probabilistic analysis of axially loaded pile in sand

Takayuki Shuku and Waldemar Hachich

6.1 Introduction

This paper presents reliability analysis for the Problem SAND 2 (Problem 6) –Axially loaded pile. The schematic of the structure and the target design problems are shown in Figure 6-1. In this paper, only the results of the design problems 1, 2 and 3 are presented. This paper is structured as follows: in Section 6.2, deterministic design method for piles based on a design code commonly used in Japan (JARA 2017) is outlined; in Section 6.3, a method of probabilistic analysis and uncertainty modeling are presented. Then the results by the deterministic and probabilistic methods are shown in Section 6.4.

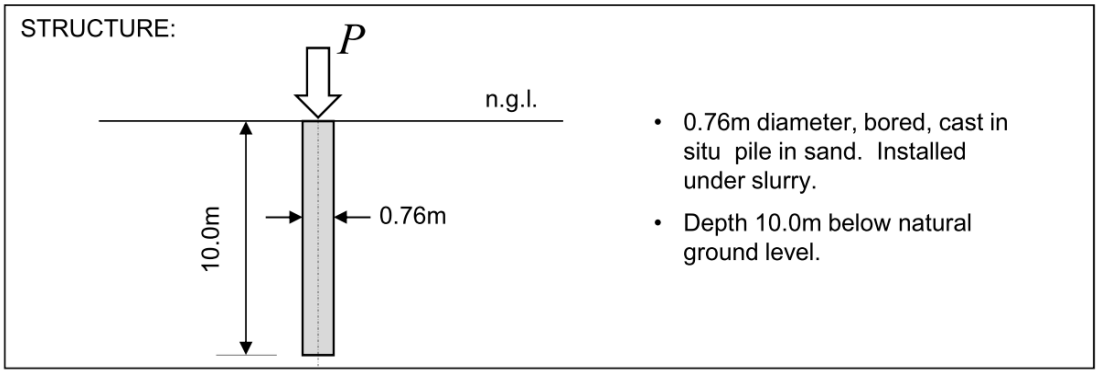

PROBLEM:

This problem requires the prediction of the performance of the pile.

1. Predict the ultimate load capacity of the pile P_{ult}.
2. If the method used separates shaft and base resistance, state $P_{ult\ (shaft)}$ and $P_{ult\ (base)}$.
3. Predict the load-settlement curve to failure.
4. Predict the expected performance of the pile based on the test results, not a conservative assessment as may be used in design calculations.

Figure 6-1 Schematic of the target structure and design problems

6.2 Design method based on JARA (2017)

6.2.1 Ultimate bearing capacity

The ultimate bearing capacity P_{ult} of an axially loaded single pile is estimated by the following model (JARA 2017) where the first term represents the end bearing resistance $P_{\mathrm{ult(base)}}$ and the

second term gives the shaft friction resistance $P_{ult(shaft)}$:

$$P_{ult} = P_{ult(base)} + P_{ult(shaft)} = q_d A + U\sum L_i f_i \tag{6-1}$$

where q_d is the characteristic value of end bearing resistance, A is the area of pile tip, U is the perimeter of pile, L_i is the thickness of ith layer for shaft friction, and f_i is a characteristic value of maximum friction force of ith layer. The q_d and f_i are calculated by the equations summarized in Tables 6-1 and 6-2. The q_d is estimated with SPT-N value (N_{SPT}) of the bearing layer, and f_i is calculated with cohesion c or N_{SPT}.

Table 6-1 End-bearing resistance q_d (JARA 2017)

Type of Pile	Type of Soil	q_d (kN/m^2)
Driven	Clay	$90N_{SPT}$ ($\leq$ 4,500)
	Sand	$130N_{SPT}$ ($\leq$ 6,500)
	Gravel	$130N_{SPT}$ ($\leq$ 6,500)
Cast-in-situ	Clay	$90N_{SPT}$ ($\leq$ 3,300)
	Sand	$110N_{SPT}$ ($\leq$ 3,300)
	Gravel	$160N_{SPT}$ ($\leq$ 8,000)
Pre-boring	Sand	$240N_{SPT}$ ($\leq$ 12,000)
	Gravel	$300N_{SPT}$ ($\leq$ 15,000)

Table 6-2 Shaft friction force f (JARA 2017)

Type of Pile	Type of Soil	f (kN/m^2)
Driven	Clay	c or $6N_{SPT}$ ($\leq$ 70)
	Sand	$5N_{SPT}$ ($\leq$ 100)
Cast-in-situ	Clay	c or $5N_{SPT}$ ($\leq$ 100)
	Sand	$5N_{SPT}$ ($\leq$ 120)
Pre-boring	Sand	c or $7N_{SPT}$ ($\leq$ 100)
	Gravel	$5N_{SPT}$ ($\leq$ 120)

2.2.2 Load-settlement curve

The bi-linear model (**Figure 6-2**) is used for estimating the load-settlement curve. In the bi-linear model, the load (P_j) and settlement (δ_j) relation is defined as:

$$P_j = K_V \delta_j \tag{6-2}$$

where subscript j is the step number and K_V is vertical spring constant for single pile defined in JARA (2017) as:

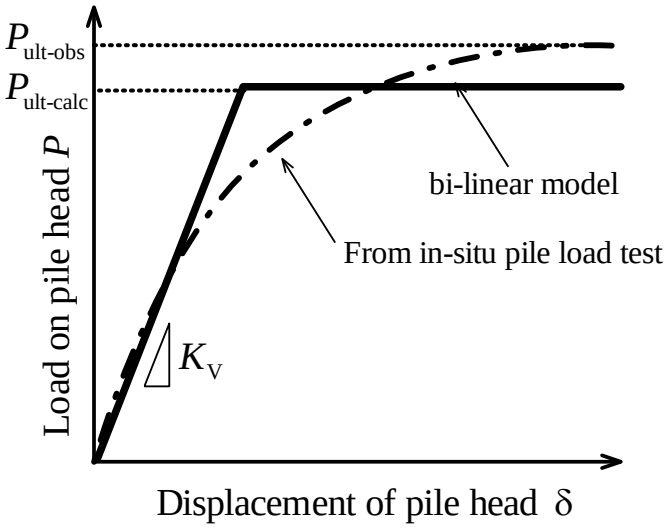

Figure 6-2 Schematic of load-displacement curve and bi-linear model

$$K_V = \frac{1}{\frac{L}{2AE_p}(1+\lambda_{yu}\gamma_u-\zeta_e)+\zeta_d\frac{4\lambda_{yu}\gamma_u}{\pi D_p^2 k_V}} \tag{6-3}$$

where L is length of pile, A is pile tip area, E_p is elastic modulus of pile material, D_p is diameter of pile, the correction factors λ_{yu}, γ_e, and γ_d for K_V are summarized in **Table 6-3**, and the k_V and γ_u are defined as:

$$k_V = \frac{\alpha E_0}{0.3}\left(\frac{D_p}{0.3}\right)^{-3/4} \tag{6-4}$$

$$\gamma_u = \frac{P_{ult(base)}}{P_{ult}} \tag{6-5}$$

where E_0 and α are the elastic modulus of bearing layer and the transformation coefficient on E_0 which are summarized in Table 6-4.

Table 6-3 Correction factors

Pile Type	γ_{yu}	ζ_e	ζ_d
Driven	0.76	0.22	0.25
Cast-In-Situ	0.48	0.30	0.99
Pre-boring	0.58	0.04	0.16

Table 6-4 Transformation coefficient for E_0

E_0 estimated from	Transformation coefficient α	
	Consider earthquake	Not consider earthquake
Plate load test with 0.3m rigid plate	1	2
Pressure meter test	4	8
Uniaxial or triaxial compression test	4	8
SPT-N value ($E_0 = 2800N_{SPT}$)	1	2

6.3 Reliability analysis method

We simply estimate probability density functions (PDFs) of P_{ult}, $P_{ult(base)}$, $P_{ult(shaft)}$, K_V and δ using direct Monte Carlo simulation (MCS) considering variability of SPT-N value (N_{SPT}) and model uncertainties.

The depth profile of N_{SPT} is shown in Figure 6-3. Akkaya and Vanmarcke (2003) adopted the single exponential auto-correlation model to analyze the NGES-TAMU sand site data and found that the vertical scale of fluctuation (SOF) is about 1.75 m. For the shaft resistance, the size of mobilization zone in each soil layer is the length of the pile in the soil layer. The spatially averaged N_{SPT} for shaft resistance calculation in the mobilization zone has a reduced COV due to spatial averaging (Vanmarcke 1977). This reduced COV is equal to the point COV multiplied by the COV reduction factor. For the single exponential model (Vanmarcke 1977), the COV reduction factor can be computed as

$$([2(L_m/\mathrm{SOF})\text{-}1+\exp[-2(L_m/\mathrm{SOF})]]/[2(L_m/\mathrm{SOF})^2])^{0.5} \tag{6-6}$$

where L_m is the size of the mobilization zone. Let COV_{mob} denote the COV of the spatially averaged soil property. Using the above method, the values of L_m, COV reduction factor, and COV_{mob} for N_{SPT} for estimating the shaft resistance are calculated and summarized in Table 6-5. For the toe resistance, the mobilization zone size is 3.5 times of the diameter of the cross-section of the pile (Wang and Cao 2013). Using the same procedure, the size of the mobilized zone, the COV reduction factor and the COV of the averaged property for N_{SPT} for estimating the toe resistance are also calculated and shown in Table 6-5.

We assume that the variability of N_{SPT} follows log-normal distribution with the mean $\mu_{\ln N}$ and standard deviation $\sigma_{\ln N}$ given by:

$$\mu_{\ln N} = \ln \mu_N - \frac{1}{2}\sigma^2_{\ln N} \tag{6-7}$$

$$\sigma_{\ln N} = \sqrt{\ln (1+\mathrm{COV}_N^2)} \tag{6-8}$$

where μ_N is the mean value and COV_N is coefficient of variation of N_{SPT}, they are summarized in Table 6-5.

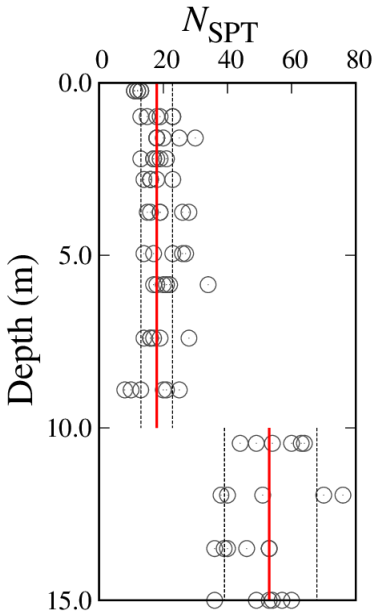

Figure 6-3 Depth profile of N_{SPT}

Table 6-5 Stochastic characteristics of N_{SPT}

Parameter	μ	COV	L_m	COV reduction factor	COV_{mob}	μ_{ln}	σ_{ln}
N_{SPT} for $P_{ult(shaft)}$	17.98	0.275	10	0.400	0.110	2.883	0.110
N_{SPT} for $P_{ult(base)}$	53.5	0.269	2.66	0.672	0.181	3.964	0.180

Nanazawa et al. (2018) investigated the accuracy of the Eqs. (6-1) and (6-3) by comparing the calculated $P_{ult(base)}^{cal}$, $P_{ult(shaft)}^{cal}$ and K_V^{cal} with their in-situ measured (referred to as "true") values. They defined the parameter M = measured(true)/calculated and evaluated the mean and standard deviations of M (Table 6-6). Since the M is not below zero, we assumed that the parameter M follows log-normal distribution with the mean and standard deviation in Table 6-6. The parameters to be estimated are given by:

$$P_{ult(base)}^{true} = M_{ult(base)} \times P_{ult(base)}^{cal}, \quad M_{ult(base)} \sim LN(\mu_{\ln M_{ult(base)}}, \sigma_{\ln M_{ult(base)}}) \tag{6-9}$$

$$P_{ult(shaft)}^{true} = M_{ult(shaft)} \times P_{ult(shaft)}^{cal}, \quad M_{ult(shaft)} \sim LN(\mu_{\ln M_{ult(shaft)}}, \sigma_{\ln M_{ult(shaft)}}) \tag{6-10}$$

$$K_V^{true} = M_{K_V} \times K_V^{cal}, \quad M_{K_V} \sim LN(\mu_{\ln M_{K_V}}, \sigma_{\ln M_{K_V}}) \tag{6-11}$$

Table 6-6 Stochastic characteristics of model uncertainty

Parameter	μ_M	COV_M	$\mu_{\ln M}$	$\sigma_{\ln M}$	Reference
$P^{true}_{ult(base)} / P^{cal}_{ult(base)}$	1.10	0.50	-0.016	0.472	Nanazawa et al. (2018)
$P^{true}_{ult(shaft)} / P^{cal}_{ult(shaft)}$	1.08	0.68	-0.113	0.617	Nanazawa et al. (2018)
K^{true}_V / K^{cal}_V	0.92	0.47	-0.183	0.447	Nanazawa et al. (2018)

6.4 Results

6.4.1 Deterministic design method (JARA 2017)

The parameters used for calculating P_{ult}, $P_{ult(base)}$, $P_{ult(shaft)}$, K_V and δ_{limit} are summarized in Table 6-7. The Elastic modulus of soil E_0 around pile base are obtained from pressure meter test. The arithmetic mean N_{SPT} and E_0 are used in the design. The calculated P_{ult}, $P_{ult(base)}$, $P_{ult(shaft)}$, K_V and δ_{limit} are summarized in Table 6-8. Figure 6-4 shows the load-settlement curve to failure.

Table 6-7 Design parameters for deterministic analysis.

Parameter		Tests	Description
N_{SPT} for base	53.50	-	arithmetic mean of the data
N_{SPT} for shaft	17.98	-	arithmetic mean of the data
E_p (kN/m^2)	25,000,000	-	-
E_0 (kN/m^2)	153,405	Pressure meter test	arithmetic mean of the data

Table 6-8 Results of deterministic design.

$P_{ult(base)}$, (q_dA)	1497.03 kN
$P_{ult(shaft)}$ ($U\Sigma Lf$)	2146.59 kN
P_{ult} ($q_dA+U\Sigma L$)	3643.62 kN
K_V	1,222,378 kN/m
δ_{limit}	2.98 mm

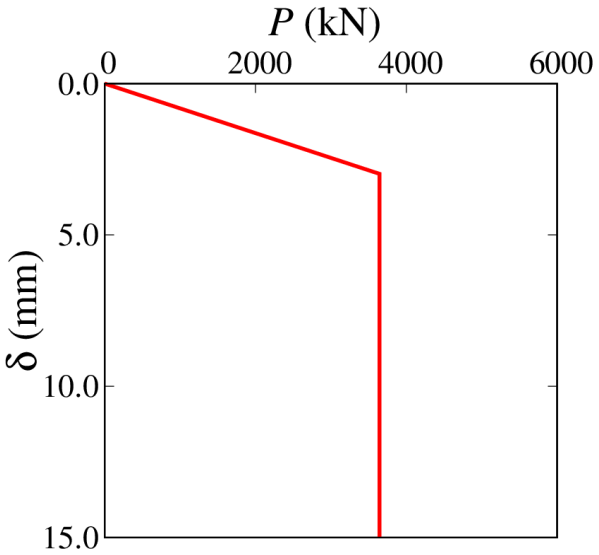

Figure 6-4 Load-settlement curve to failure

6.4.2 Probabilistic analysis

Probability distributions of the P_{ult}, $P_{ult(base)}$, $P_{ult(shaft)}$, K_V and δ_{limit} are shown in Figure 6-5, which are estimated with direct MCS with 100,000 samples. In order to discuss the advantage of probabilistic analysis, we compare the results by probabilistic and factor-of-safety methods in terms of the bearing capacity at serviceability limit state. In factor-of-safety method, allowable bearing capacity $P_{a(fos)}$, which corresponds to P_{sls}, is defined by

$$P_{a(fos)} = P_{ult} / n \tag{6-12}$$

where, n is factor of safety that is defined as 3 for static conditions and 2 for seismic conditions. Since the target problem is static, $P_{a(fos)}$ becomes 1,214.54kN. The target reliability index β_T for serviceability limit state is usually set as 1.5 (Otake and Honjo 2016), and it corresponds to failure probability p_f = 0.0679. We identified the bearing capacity P (P_{sls}) that satisfy p_f = 0.0679. Figure 6-6 shows the comparison between $P_{a(fos)}$ and P_{sls}. The identified P_{sls} is 1,964.54kN and the difference between two bearing capacity if about 750kN. Clearly, the probabilistic analysis considering soil variability and model uncertainty can contribute to more economical pile design than the conventional factor-of-safety method.

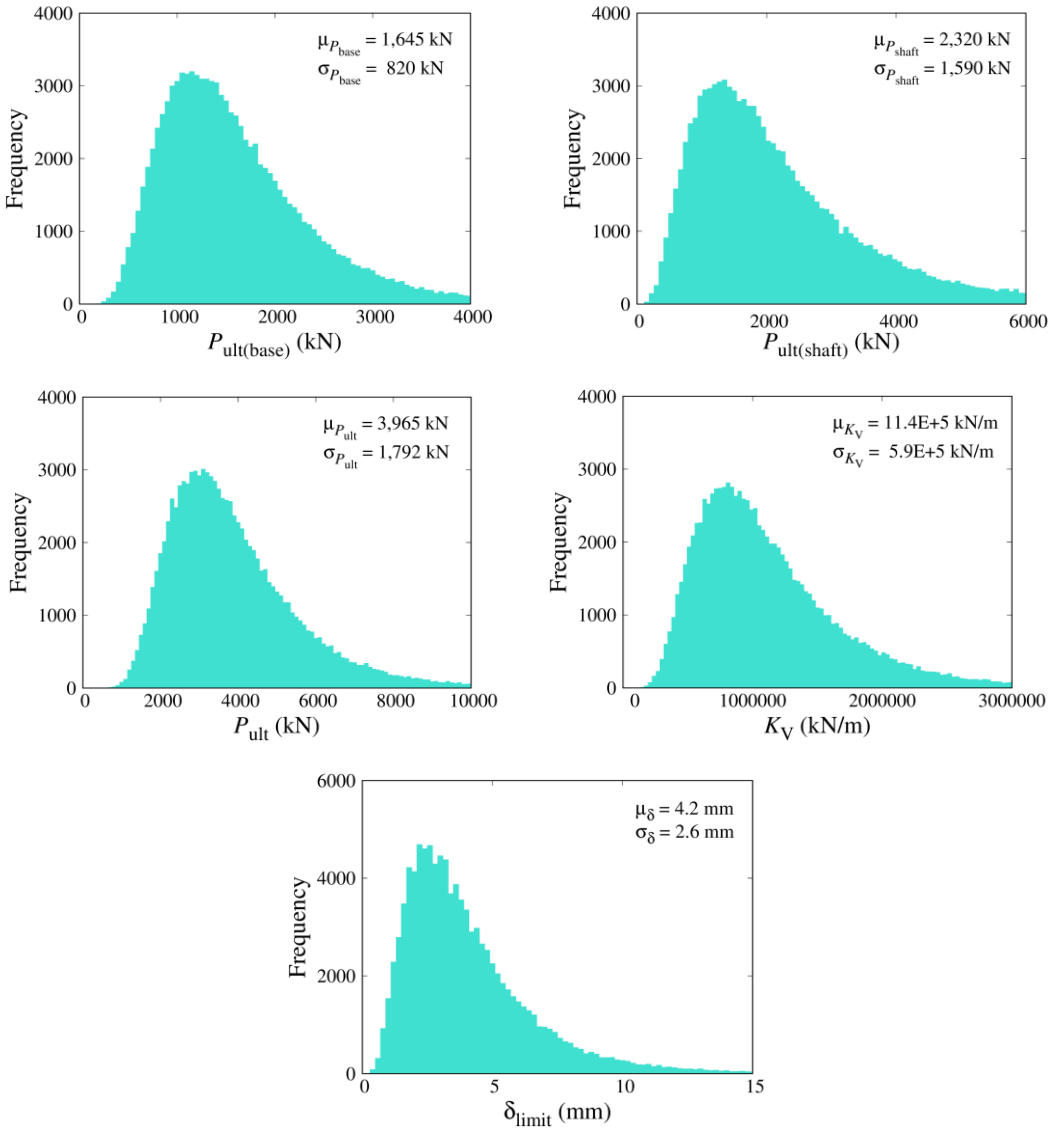

Figure 6-5 Probability distribution of P_{ult}, K_V and δ_{limit} with N_{MCS} = 100,000

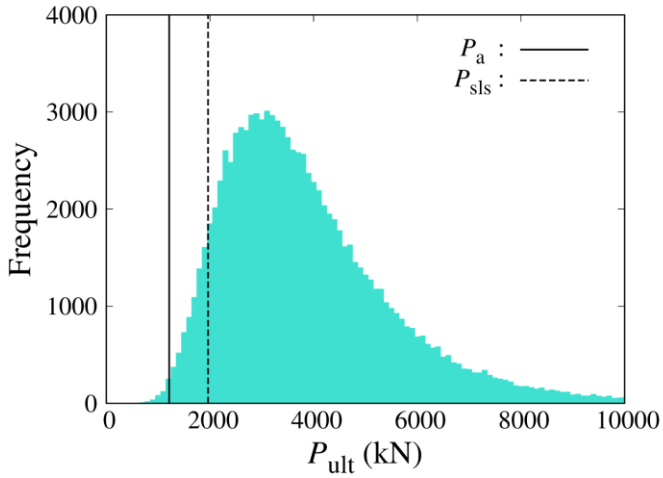

Figure 6-6 Comparison between P_a and P_{sls}

References

Akkaya, A. D., and Vanmarcke, E. H. (2003). Estimation of spatial correlation of soil parameters based on data from the Texas A&M University NGES. Probabilistic site characterization at the National Geotechnical Experimentation Sites (Eds G. A. Fenton and E. H. Vanmarcke), 29-40.

JARA (2017). Specifications for Highway Bridges IV, Japan Road Association (in Japanese).

Nanazawa, T., Kohno T., Miyahara, K. and Ohshiro, K. (2018). A study on a review for vertical bearing/deformation characteristics of piles and evaluation for the estimation accuracy, Technical Note of Public Work Research Institute, 4374, 104p (in Japanese).

Otake, Y. and Honjo, Y. (2016). Geotechnical reliability analysis and challenges in geotechnical design, Journal of JSCE C, Vol. 72, No. 4, pp.310 – 326 (in Japanese).

Vanmarcke, E. H. (1977). Probabilistic modeling of soil profiles. Journal of the geotechnical engineering division, 103(11), 1227-1246.

Reliability-based design of spatially varying sandy slope

Shui-Hua Jiang, Xian Liu, and Jianye Ching

7.1 Introduction

This section presents reliability-based design results for a sandy slope. The geometry of the slope and the design problems are shown in Figure 7-1. A sandy slope model in Figure 7-2 is considered because the failure circles are mostly shallow toe circles. The slope has a height of 6 m and an angle of β. The coordinates of the slope toe and crest are (0, 0) and (6/tanβ m, 6 m), respectively. The problem requires the design of a slope angle which ensures that a target probability of slope failure is not exceeded. Three different target probabilities of failure (0.0001, 0.001 and 0.01) are considered. The unit weight γ of the sand is not specified, and γ = 20 kN/m^3 is assumed in the following analysis. Section 7.2 presents the probabilistic characterization of uncertain input parameters involved in the problem. Section 7.3 introduces stability analysis and reliability-based design of the sandy slope using a limit equilibrium method (LEM) and an inverse first-order reliability method (FORM), respectively. Section 7.4 summarizes the reliability-based design results.

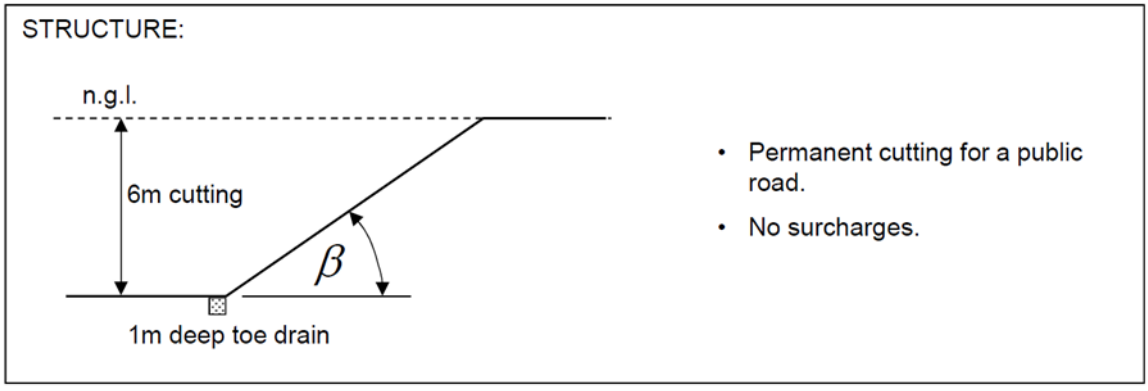

Figure 7-1 Schematic of a sandy slope

7.2 Probabilistic characterization of the uncertain parameters

To account for the inherent spatial variation of soil properties, the sandy slope is discretized into 12 horizontal thin layers being homogeneous with a thickness of 0.5 m. A single exponential autocorrelation function is adopted to characterize the spatial autocorrelation of the effective friction angle ϕ':

$$\rho\left(z_i, z_j\right) = \exp\left(-2\frac{\left|z_i - z_j\right|}{\delta_z}\right) \tag{7-1}$$

where δ_z is the vertical scale of fluctuation; z_i and z_j are the vertical coordinates of the

centroids of the *i*-th and *j*-th soil layers, respectively. Based on these, the Cholesky decomposition-based midpoint method is used to generate realizations of the random field of (Li et al. 2015).

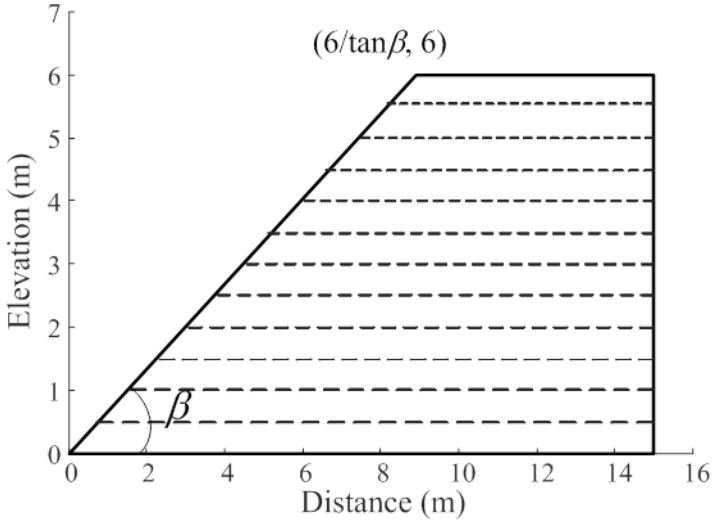

Figure 7-2 Slope geometry and discretization of soil layers

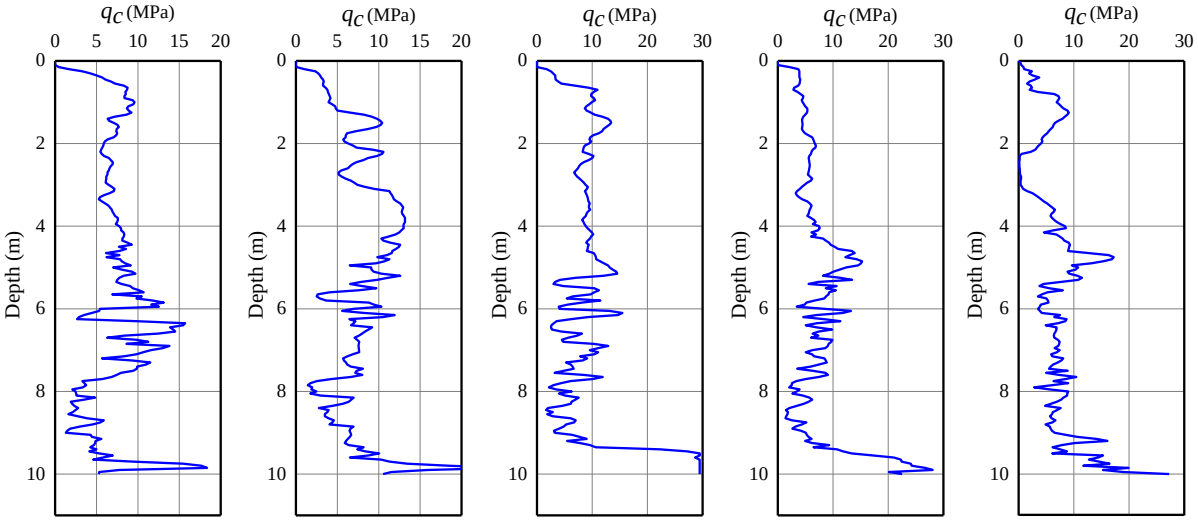

Figure 7-3 Variation of the cone tip resistance data with the depth

7.2.1 Probabilistic characterization of ϕ' using the cone penetration test data

Five sets of cone tip resistance data that are acquired from Cone Penetration Test (CPT) at the studied site, as provided in Figure 7-3, are adopted to estimate ϕ' using the following transformation formula (Kulhawy and Mayne 1990):

$$\phi' = 17.6 + 11.0 \log\left[(q_c / p_a) / (\sigma'_{v0} / p_a)^{0.5}\right] + \varepsilon \tag{7-2}$$

where q_c is the cone tip resistance; σ'_{v0} is the vertical effective stress, $\sigma'_{v0} = \gamma h$, in which γ and h are the unit weight and soil depth, respectively; p_a is one standard atmosphere pressure, p_a = 101.3 kPa; ε is the transformation error for the correlation in Eq. (7-2), which

is usually modeled as a normal random variable with zero mean and constant standard deviation. Figure 7-4 shows the variations of the estimated effective friction angles with the depth. The means $\mu_{\phi'}$ of the effective friction angles for different depths are evaluated using conventional statistical analyses, and listed in Table 7-1.

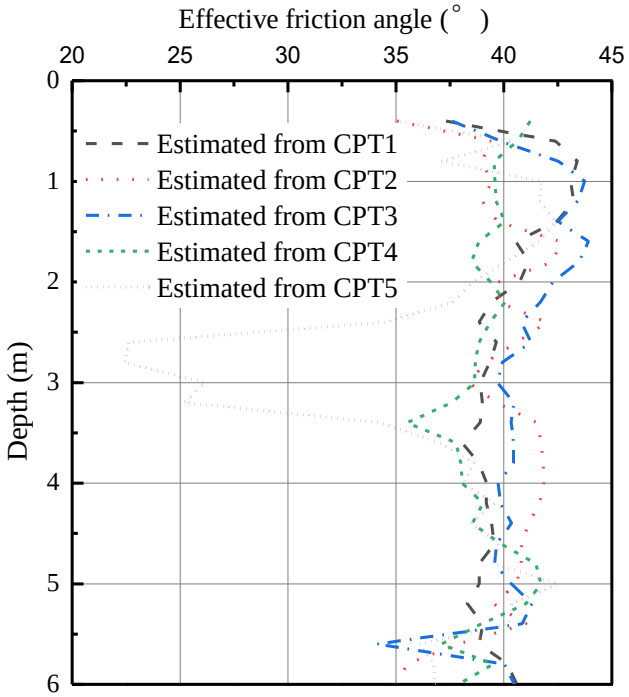

Figure 7-4 Variation of the effective friction angles estimated from the CPT data with the depth

Akkaya and Vanmarcke (2003) adopted the single exponential autocorrelation model to analyze the Texas A&M University National Geotechnical Experimentation sand site data and found that the vertical scale of fluctuation is about 1.75 m. Hence, a value of δ_z = 1.75 m is chosen in this study. Following Phoon and Kulhawy (1999), the coefficient of variation (COV) of the spatial average ϕ'_a of the effective friction angle that is transformed from q_c data using Eq. (7-2) can be estimated as

$$\mathrm{COV}_{\phi'_a} \approx \sqrt{\frac{22.8\left[\Gamma^2(L)\mathrm{COV}_w^2 + \mathrm{COV}_e^2\right] + \mathrm{SD}_\varepsilon^2}{\mu_{\phi'}^2}} \tag{7-3}$$

where SD_ε is the standard deviation of the transformation error ε in Eq. (7-2), SD_ε = 2.8°; COV_e is the COV of the measurement error for q_c, which can be assumed to be comparable to that produced by the electric cone penetration test and estimated to be between 5 and 15%, a value of COV_e = 15% is selected; COV_w is the COV of the inherent variability for q_c in sand, which is estimated using the five sets of q_c data in Figure 7-3; $\mu_{\phi'}$ is the mean of ϕ'; $\Gamma(L)$ is the COV reduction factor, which can be computed as follows for the single exponential autocorrelation model (Vanmarcke 1977):

$$\Gamma(L)=\sqrt{\frac{\delta_z^2}{2L^2}\left[\frac{2L}{\delta_z}+\exp\left(-\frac{2L}{\delta_z}\right)-1\right]}=0.913 \tag{7-4}$$

where L = 0.5 m is the thickness of the horizontal thin layer, and δ_z = 1.75 m. Based on these, the values of $\mathrm{COV}_{\phi'_a}$ for 12 layers can be estimated using Eq. (7-3), and summarized in Table 7-1. Additionally, it is assumed that the effective friction angles follow lognormal distributions since the lognormal distribution is particularly suited for soil parameters that cannot take on negative values.

Table 7-1 Statistics of uncertain input parameters obtained from the CPT data

Friction angle	Depth	$\mu_{\phi'}$ (°)	COV_w	$\mathrm{COV}_{\phi'_a}$	Distribution
ϕ'_1	0.25	37.228	0.391	0.090	Lognormal
ϕ'_2	0.75	40.791	0.463	0.086	Lognormal
ϕ'_3	1.25	41.405	0.310	0.077	Lognormal
ϕ'_4	1.75	40.918	0.335	0.079	Lognormal
ϕ'_5	2.25	39.412	0.469	0.090	Lognormal
ϕ'_6	2.75	36.287	0.501	0.100	Lognormal
ϕ'_7	3.25	37.248	0.472	0.095	Lognormal
ϕ'_8	3.75	39.315	0.306	0.081	Lognormal
ϕ'_9	4.25	39.727	0.203	0.076	Lognormal
ϕ'_{10}	4.75	40.262	0.252	0.077	Lognormal
ϕ'_{11}	5.25	40.059	0.309	0.080	Lognormal
ϕ'_{12}	5.75	37.787	0.420	0.091	Lognormal

7.2.2 Probabilistic characterization of ϕ' using the standard penetration test data

Besides, six sets of the SPT N data are acquired from the standard penetration test at the studied site. This SPT N data can also be used to estimate ϕ' using the following transformation formula (Mayne et al. 2001):

$$\phi'=\approx\sqrt{15.4\times(N_1)_{60}}+20^\circ \qquad (N_1)_{60}=N_{60}/(\sigma'_{v0}/p_a)^{0.5} \tag{7-5}$$

where $(N_1)_{60}$ is the normalized SPT N value; N_{60} is the energy-corrected SPT N value; σ'_{v0} is the in-situ effective stress.

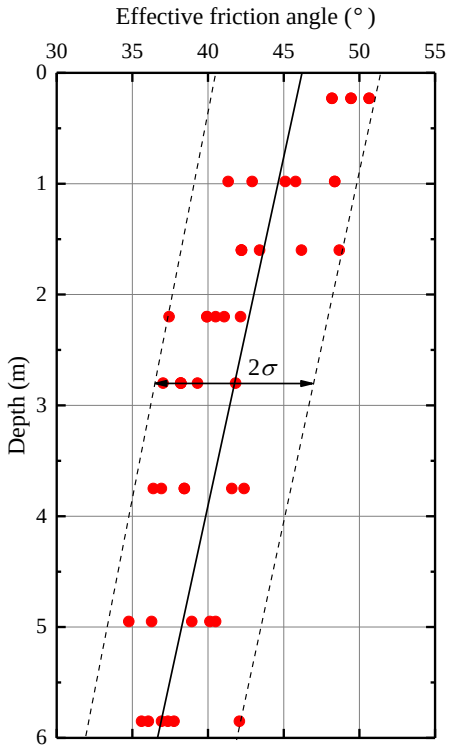

Figure 7-5 Variation of the effective friction angle estimated from the SPT *N* data with the depth

Figure 7-5 shows the variation of the effective friction angle estimated from the SPT *N* data with the depth. The ϕ' data obtained using Eq. (7-5) has a sample COV of 0.124. Therefore, the reduced COV for ϕ' is 0.124×0.913 = 0.113. The transformation uncertainty for Eq. (7-5) is with a COV of about 0.1 (Ching et al., 2017). The total COV for ϕ' is approximately $[(0.113)^2+(0.1)^2]^{0.5}$ = 0.151. Based on these, the statistics of the uncertain input parameters obtained from the SPT data are summarized in Table 7-2.

7.3 Stability and reliability analyses of the slope

It is also assumed that the groundwater table is far below the slope, and thus does not pass through the slope toe. No tension cracks are considered in this study. As reported in the literature (e.g., Steward et al., 2011; Li et al. 2015), the failure of the sandy slope mostly occurs along the shallow toe circles. For a given β and one realization of random variables, the short-term stability of the slope is assessed using Bishop's simplified method, and the corresponding critical slip surface is located among more than 1600 possible slip surfaces (see Figure 7-6). As a reference, the minimum factor of safety (FS_{min}) is evaluated based on the means of effective friction angles in Table 7-1, it is equal to 1.204, and the critical slip surface is located and shown in Figure 7-6. Furthermore, Figure 7-7 presents the variations of the factors of safety estimated based on the CPT and SPT data with the slope angle. It can be observed that the slope will be stable as long as the designed slope angle is smaller than 28° when an allowable factor of safety of 1.5 is considered.

Table 7-2 Statistics of uncertain input parameters obtained from the SPT data

Friction angle	Depth	$\mu_{\phi'}$ (°)	$COV_{\phi'_a}$	Distribution
ϕ'_1	0.25	45.802	0.151	Lognormal
ϕ'_2	0.75	45.006	0.151	Lognormal
ϕ'_3	1.25	44.210	0.151	Lognormal
ϕ'_4	1.75	43.414	0.151	Lognormal
ϕ'_5	2.25	42.619	0.151	Lognormal
ϕ'_6	2.75	41.823	0.151	Lognormal
ϕ'_7	3.25	41.027	0.151	Lognormal
ϕ'_8	3.75	40.231	0.151	Lognormal
ϕ'_9	4.25	39.435	0.151	Lognormal
ϕ'_{10}	4.75	38.639	0.151	Lognormal
ϕ'_{11}	5.25	37.844	0.151	Lognormal
ϕ'_{12}	5.75	37.048	0.151	Lognormal

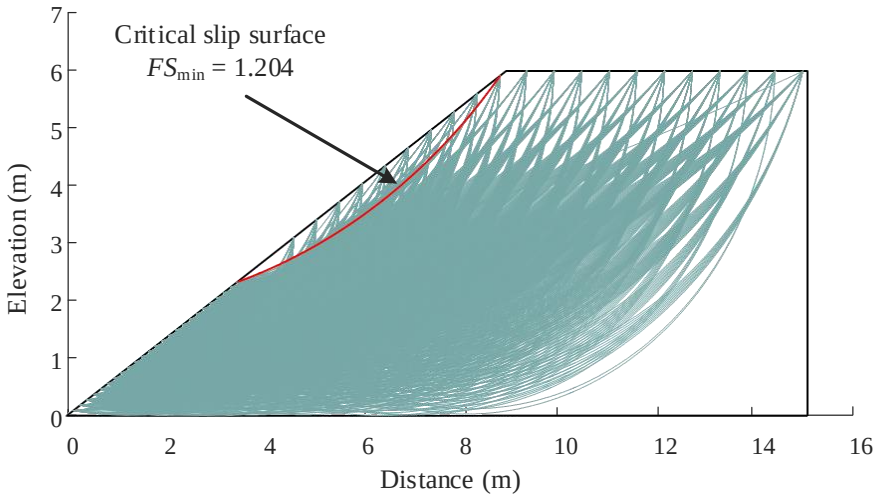

Figure 7-6 Slope with 1636 potential slip surfaces

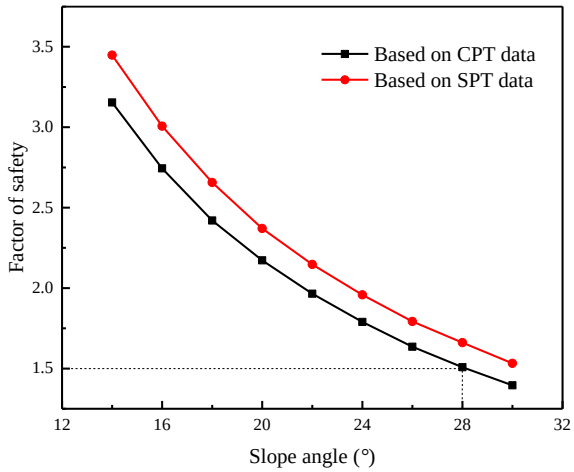

Figure 7-7 Variation of the safety factor with the slope angle

Because of the model uncertainty of the Bishop's simplified method (Christian et al. 1994; Jiang et al. 2017), the following relationship between the actual factor of safety (FS_A) and the calculated FS_{min} is established (Bahsan et al. 2014):

$$FS_A = wFS_{\min}(\boldsymbol{\phi}') \tag{7-6}$$

where $\boldsymbol{\phi}' = (\phi_1', \phi_2', ..., \phi_{12}')^T$; w is the model factor, which is assumed to follow the lognormal distribution with mean= 1.066 and COV = 0.296 according to Bahsan et al. (2014). In this way, the limit state function can be written as

$$g(\boldsymbol{\phi}') = wFS_{\min}(\boldsymbol{\phi}') - 1.0 \tag{7-7}$$

7.4 Reliability-based design results

In this section, the slope angles for achieving the target probabilities of failure (0.0001, 0.001 and 0.01) are designed wherein the effective friction angles are estimated from the CPT data and SPT data, respectively. An inverse FORM formulated in x-space that is proposed by Ji et al. (2019) is employed to estimate the probabilities of slope failure for the limit state function in Eq. (7-7). Figures 7-8 and 7-9 present the iterative calculation processes of the slope angles for different target probabilities of failure based on the CPT and SPT data, respectively. It is evident that the probability of slope failure increases significantly as the slope angle increases. The slope angles β for achieving the target probabilities of failure (0.0001, 0.001 and 0.01) can be readily derived after 4 or 5 iterations.

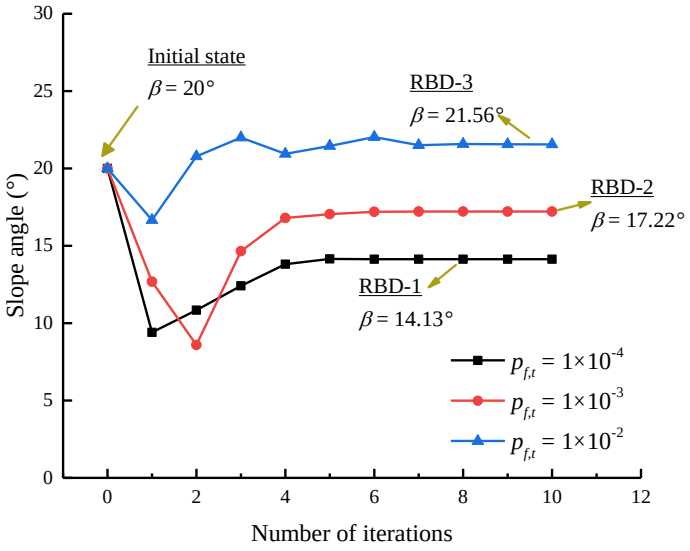

Figure 7-8 Variations of the designed slope angle for three scenarios based on the CPT data with the number of iterations

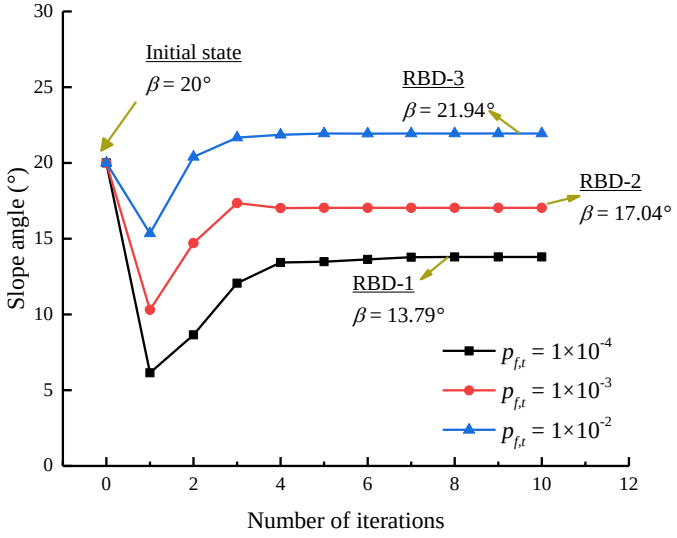

Figure 7-9 Variations of the designed slope angle for three scenarios based on the SPT data with the number of iterations

For a vertical scale of fluctuation of 1.75 m, the designed slope angles associated with the CPT data are 14.13°, 17.22° and 21.56°, respectively. In contrast, the designed slope angles associated with the SPT data are 13.79°, 17.04° and 21.94°, respectively. It is interesting to note that the sandy slope is more stable when the SPT data is used for slope design from the perspective of deterministic analysis (see Figure 4-7). However, the designed slope angles associated with the SPT data are smaller than those associated with the CPT data from the perspective of probabilistic analysis. This is because the variability of the SPT data is larger than that of the CPT data. Additionally, when a target probability of failure of 0.0001 is adopted that is acceptable for all slopes (U.S. Army Corps of Engineers 1997; Santamarina et al. 1992),

the designed slope angle should be less than 13.79° at which the slope is to be cut. The slope design results obtained from the probabilistic analysis are more conservative than those obtained from the deterministic analysis.

References

Akkaya, A.D., Vanmarcke, E.H. (2003). Estimation of spatial correlation of soil parameters based on data from the Texas A&M University NGES. Probabilistic site characterization at the National Geotechnical Experimentation Sites (Eds G. A. Fenton and E. H. Vanmarcke), 29-40.

Bahsan, E., Liao, H.J., Ching, J., Lee, S.W. (2014). Statistics for the calculated safety factors of undrained failure slopes. Engineering Geology, 172: 85-94.

Ching, J., Lin, G. H., Chen, J. R., and Phoon, K. K. (2017). Transformation models for effective friction angle and relative density calibrated based on generic database of coarse-grained soils. Canadian Geotechnical Journal, 54(4), 481-501.

Christian, J.T., Ladd, C.C., Baecher, G.B. (1994). Reliability applied to slope stability analysis. Journal of Geotechnical Engineering, 120(12): 2180-207.

Ji J., Zhang C., Gao Y, Gao Y.F., Kodikara, J. (2019). Reliability-based design for geotechnical engineering: An inverse FORM approach for practice. Computers and Geotechnics, 111: 22-29.

Jiang, S.H., Papaioannou, I., Li, C.G., Straub, D. (2017). Integrating LEM with FEM through model correction factor method in reliability analysis of spatially variable slopes. The 15th International Conference of the International Association for Computer Methods and Advances in Geomechanics, October 19-23, Wuhan, China. pp. 1-7.

Kulhawy, F.H., Mayne, P.W. (1990). Manual on estimating soil properties for foundation design. Report EL 6800, Electric Power Research Inst., Palo Alto.

Li, D.Q., Jiang, S.H., Cao, Z.J., Zhou, W., Zhou, C.B., Zhang, L.M. (2015). A multiple response-surface method for slope reliability analysis considering spatial variability of soil properties. Engineering Geology, 187: 60-72.

Mayne, P. W., Christopher, B. R., DeJong, J. (2001). Manual on Subsurface Investigations, National Highway Institute Publication No. FHWA NHI-01-031, Federal Highway Administration.

Phoon, K.K., Kulhawy, F.H. (1999). Evaluation of geotechnical property variability. Canadian Geotechnical Journal, 36(4), 625-639.

Santamarina, J., Altschaeffl, A., Chameau, J. (1992). Reliability of slopes: Incorporating qualitative information. Transportation Research Record, 1343, 1-5.

Steward, T., Sivakugan, N., Shukla, S.K., Das, B. M. (2011). Taylor's slope stability charts revisited. International Journal of Geomechanics, 11(4): 348-352.

U.S. Army Corps of Engineers. (1997). Engineering and design: introduction to probability and

reliability methods for use in geotechnical engineering. Department of the Army, Washington, D.C. Engineer Technical Letter, 1110-2-547.

Vanmarcke, E.H. (1977). Probabilistic modeling of soil profiles. Journal of the Geotechnical Engineering Division, 103(11): 1227-1246.

Probabilistic analysis of propped embedded retaining wall

Takayuki Shuku, Zijun Cao, Timo Schweckendiek, and Marco Redaelli

8.1 Introduction

This paper presents reliability analysis for the Problem SAND 5 (Problem 9) – Propped embedded retaining wall. The schematic of the structure and target design problems are shown in Figure 8-1. The design problem 3, Specify the minimum yield moment of wall element M_{yield}, is difficult to answer because the material of the wall is not specified. Only the results for the design problems 1 and 2 are presented. This paper is structured as follows: in Section 8.2, LRFD method for the permanent retaining wall structure based on a design code commonly used in Japan (JRA 1999; JPHA 2018) is outlined; in Section 8.3, a method of probabilistic analysis and uncertainty modeling are presented. Then the results by the LRFD and the probabilistic analysis are shown in Section 8.4, and finally a summary of the results are presented in Section 8.5.

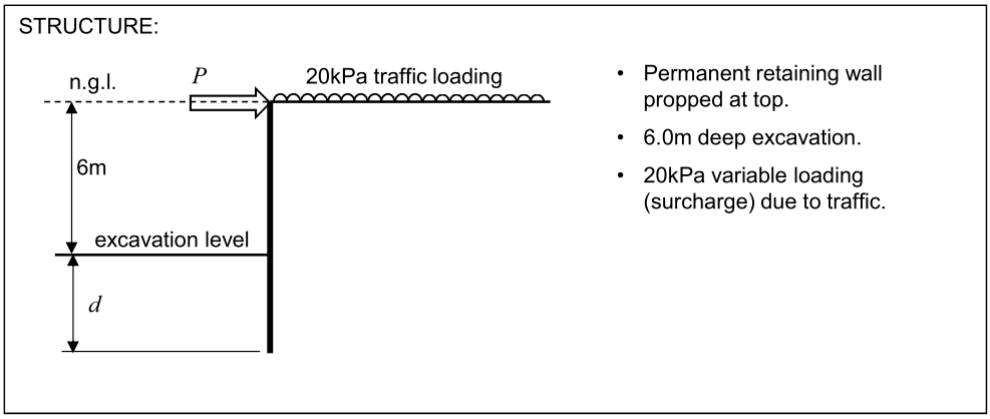

PROBLEM:

This is a design problem requiring the specification of the geometry of the wall, the propping force and the strength of the wall in bending.

1. Specify the required depth of embedment d (m).
2. Specify the propping force P (kN/m).
3. Specify the minimum yield moment of wall element M_{yield} (kNm/m).

Design to be based on the stability of the wall without considering serviceability requirements.

Figure 8-1 Schematic of the target structure and design problems

8.2 Design method based on JPHA (2018)

8.2.1 Free earth support method

The required depth of embedment d (m) is calculated using the free earth support method (JRA 1999; JPHA 2018), that is commonly used in design practice in Japan. The schematic of the method is shown in Figure 8-2a. In this method, depth of embedment d (m) satisfying the following equation is identified:

$$\frac{\gamma_S S}{\gamma_R R} \leq 1.0 \tag{8-1}$$

where, S is the characteristic value of load, R is the characteristic value of resistance, and γ_S and γ_R are the partial factor for S and R respectively. Specifically, the S and R are the moment defined as:

$$R = P_p \times \ell_p \tag{8-2}$$

$$S = P_a \times \ell_a \tag{8-3}$$

where, P indicates earth pressure, ℓ indicates the arm length for the moment, the subscripts "p" and "a" indicate "passive" and "active" respectively. The coefficients for active and passive earth pressure are taken as:

$$K_p = \frac{\cos^2(\phi)}{\cos(\delta)\left[1-\sqrt{\frac{\sin(\phi-\delta)\sin(\phi)}{\cos(\delta)}}\right]^2} \tag{8-4}$$

$$K_a = \frac{\cos^2(\phi)}{\cos(\delta)\left[1+\sqrt{\frac{\sin(\phi+\delta)\sin(\phi)}{\cos(\delta)}}\right]^2} \tag{8-5}$$

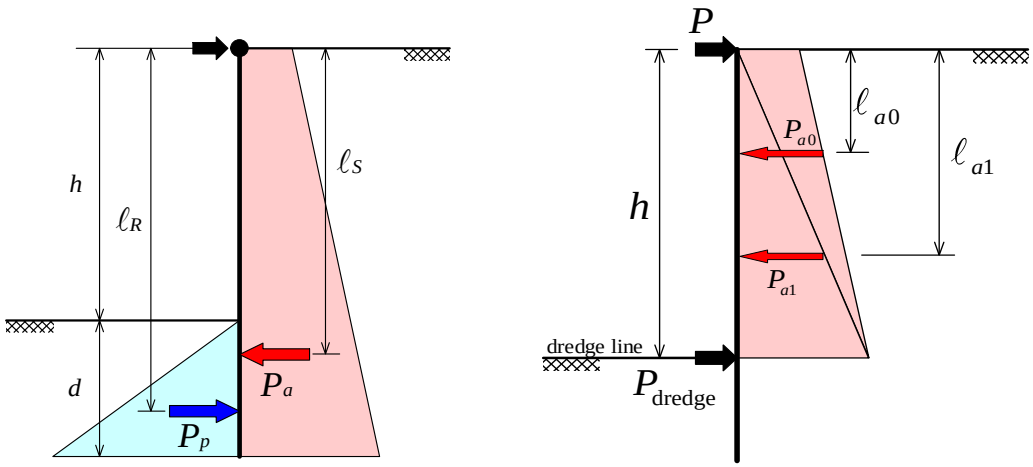

(a) (b)

Figure 8-2 Schematic of (a) free earth support method and (b) virtual beam method

where ϕ is internal friction angle, δ is the friction angle between wall and soil and is taken as $\phi/3$. Since the internal friction angle of the soil is not specified, we use the transformation model that is defined as the following equations (Mayne et al. 2001):

$$\phi = \sqrt{15.4(N_1)_{60}} + 20^\circ \tag{8-6}$$

$$(N_1)_{60} = (p_a / \sigma'_v)^{0.5}(E_f / 60)N_{SPT} \tag{8-7}$$

where p_a is atmospheric pressure, E_f is SPT system efficiency, N_{SPT} is the SPT-N value and σ'_v is the effective overburden pressure. As defined in Eq. (8-7), internal friction angle depends on the overburden pressure σ'_v and depth z to be focused. However, we assumed that ϕ is independent with depth z and used the single σ'_v calculated with the mean value of depth for simplicity. The uncertainty associated with N_{SPT} and transformation uncertainty associated with Eq. (8-6) will be introduced later.

8.2.2 Virtual beam method

The propping force P is calculated using the virtual beam method (JPHA 2018). In the method, the propping force P is calculated based on the simple beam model supported by the P and the dredge line (Figure 8-2b):

$$P = P_{a0} + P_{a1} - \frac{P_{a0}\ell_{a2} + P_{a1}\ell_{a1}}{h} \tag{8-8}$$

where P_a is active earth pressure, ℓ is the arm length for the moment around the top of the wall.

8.3 Reliability analysis method

8.3.1 Required depth of embedment

We give the minimum value of required embedment depth satisfying a s failure probability p_f. To estimate failure probability, we use direct Monte Carlo simulation (MCS) considering uncertainties in design, and the p_f is given as:

$$p_f = \frac{1}{N_{MCS}} \sum_{k=1}^{N_{MCS}} I(G(\mathbf{x}) < 0) = \frac{\text{no. of failure samples}}{\text{total no. of samples}} \tag{8-9}$$

where, $\mathbf{x}$ is the design parameter vector and G is the performance function defined by:

$$G(\mathbf{x}) = R(\mathbf{x}) - S(\mathbf{x}) \tag{8-10}$$

To calculate R and S, we use the free earth support method.

In the analysis, variability of N_{SPT} and the uncertainty associated with the transformation model between SPT-N value and internal friction angle. The depth profile of N_{SPT} is shown in Figure 8-3. Akkaya and Vanmarcke (2003) adopted the single exponential auto-correlation model to analyze the NGES-TAMU sand site data and found that the vertical scale of

fluctuation (SOF) is about 1.75 m. For the active earth pressure in free earth support method and the virtual beam method, the size of mobilization zone is assumed to be the depth of excavation, which should be a conservative estimation of the size of the mobilization zone. The spatially averaged variables for active earth pressure calculation in the mobilization zone have a reduced COV due to spatial averaging (Vanmarcke 1977). This reduced COV is equal to the point COV multiplied by the COV reduction factor. For the single exponential model (Vanmarcke 1977), the COV reduction factor can be computed as

$$([2(L_m/\mathrm{SOF})\text{-}1+\exp[-2(L_m/\mathrm{SOF})]]/[2(L_m/\mathrm{SOF})^2])^{0.5} \tag{8-11}$$

where L_m is the size of the mobilization zone. Let $\mathrm{COV}_{\mathrm{mob}}$ denote the COV of the spatially averaged soil property. Using the above method, the values of L_m, COV reduction factor, and $\mathrm{COV}_{\mathrm{mob}}$ for different random variables are calculated and summarized in Table 8-1. For the passive earth pressure, the size of the mobilization zone is assumed to be zero, which is also on the conservative side. Based on such an assumption, the COV reduction factor for the estimating the passive earth pressure is 1.0.

We divided the soil layer into two, top (0 ~ 10m) and bottom (10 ~ 15m) layers, and estimated trend models and the standard deviation. The model of N_{SPT} used in the analysis is defined as:

$$N_{\mathrm{SPT}}(z)=\begin{cases}17.98+\varepsilon_{N1} & (0\le z<10)\\ 53.50+\varepsilon_{N2} & (10\le z<15)\end{cases} \tag{8-12}$$

where ε_N is the variability of N_{SPT} following log-normal distribution with the mean $\mu_{\ln N}$ and standard deviation $\sigma_{\ln N}$ as follows:

$$\mu_{\ln N}=\ln\mu_N-\frac{1}{2}\sigma^2_{\ln N} \tag{8-13}$$

$$\sigma_{\ln N}=\sqrt{\ln(1+\mathrm{COV}_N^2)} \tag{8-14}$$

where μ_N is the mean value and COV_N is coefficient of variation of N_{SPT} data.

The transformation model taken as:

$$\phi=\sqrt{15.4(N_1)_{60}}+20^\circ+\varepsilon_\phi \tag{8-15}$$

where ε_ϕ is the uncertainty associated with the transformation model following normal distribution with a zero mean and a standard deviation σ_ϕ of 2.22°.

8.3.2 Propping force

We simply apply the direct MCS based on the virtual beam method (shown in section 8.2.2) considering the variability of SPT-*N* value and the model error associated with the transformation model to the estimation for probability density function (PDF) of the propping

force.

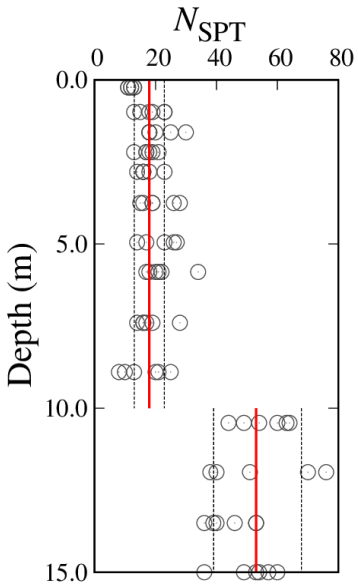

Figure 8-3 Depth profile of N_{SPT} and trend models

8.4 Results

8.4.1 LRFD method for permanent retaining wall structures

The parameters used for calculating R and S are summarized in Table 8-1. We identified the minimum depth satisfying Eq. (8.1) with trial and error using the method outlined in Section 5.2. In the Eq. (8.1), the partial factors γ_R and γ_R are defined as 0.72 and 1.09 in the JPHA (2018) and correspond to the target failure probability P_{ft} of 2.0×10^{-2} (Matsubara et al. 2017). Finally, the required depth of embedment and propping force are obtained as 3.3 m and 41.36 kN/m respectively.

Table 8-1 Design parameters

Design problem	R or S	γ_t (kN/m^3)	N_{SPT}	L_m	COV reduction factor	σ_v (kN/m^2)	ϕ (degree)	c (kN/m^2)	K_p, K_a
1	R (P_p)	19.0	17.98	0	1.000	50.0	38.7	0.0	2.806
	S (P_a)			6	0.499	86.5	36.3	0.0	0.238
2	S (P_a)			6	0.499	57.0	38.1	0.0	0.220

8.4.2 Reliability analysis

We specified the target failure probability P_{ft} as 2.0×10^{-2}, and the embedment depth satisfying

the probability was estimated as 2.6 m. The convergent property of MC is shown in Figure 8-4. The results by 20 runs are shown to investigate the effect of the random seeds on P_f. It seems at least 5,000 samples are necessary to get reliable P_f. The distribution of MC samples of R and S is shown in Figure 8-5. The required depth by the MC-based reliability analysis is shorter than that by the LRFD.

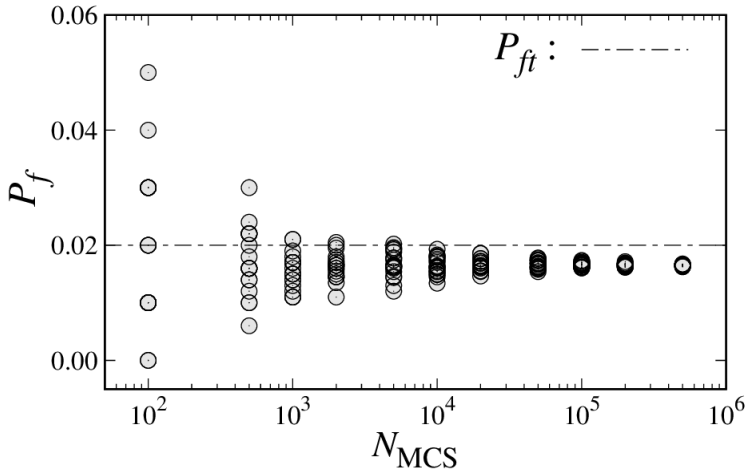

Figure 8-4 Convergent of P_f (20 runs with different random seeds), $P_{ft} = 2.0\times10^{-2}$

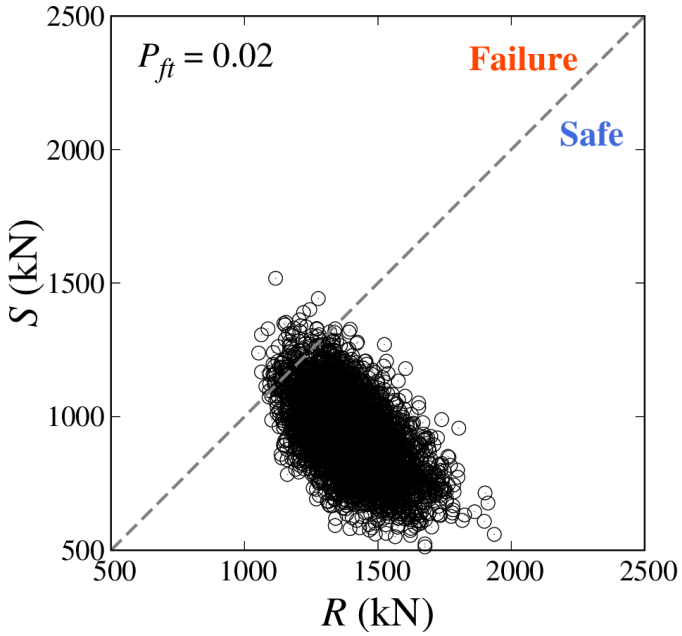

Figure 8-5 MC samples of R and S with N_{MCS} = 500,000), $P_{ft} = 2.0\times10^{-2}$

We also show the results of reliability analysis with the target failure probability P_{ft} = 1.0×10^{-4} (corresponds to the target reliability index = 3.7) in Figures 8-6 and 8-7. Since the P_{ft}

is small, at least 500,000 MC samples should be used to get reliable P_f. The required depth of embedment is estimated as 3.1m.

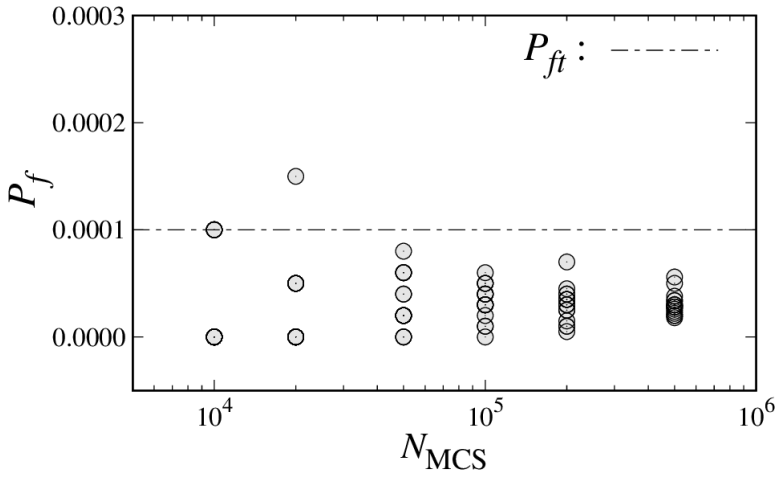

Figure 8-6 Convergent of P_f (20 runs with different random seeds), $P_{ft} = 1.0\times10^{-4}$

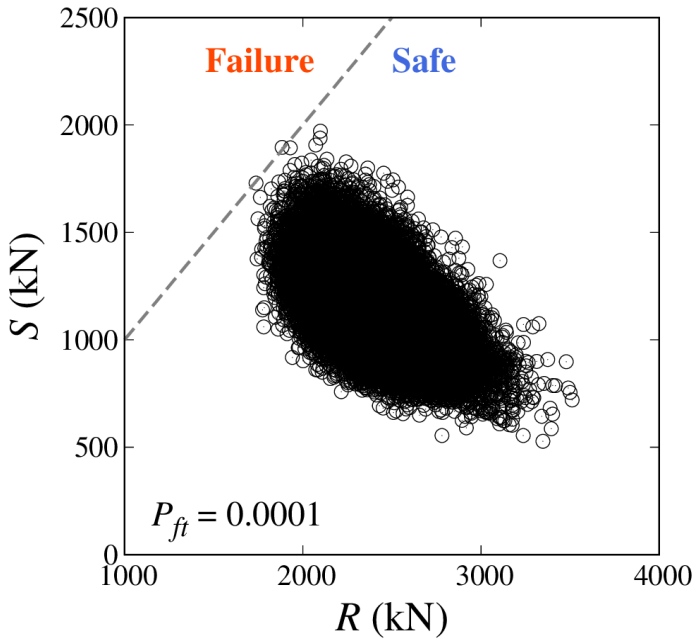

Figure 8-7 MC samples of R and S with N_{MCS} = 500,000), $P_{ft} = 1.0\times10^{-4}$

Probability distribution of the propping force P is shown in Figure 8-8. The distribution seems to follow Gaussian distribution, and mean value μ_P and the standard deviation σ_P are

estimated as 34.10kN and 3.77kN respectively. The deterministic P estimated based on the virtual beam method (shown in *8.2.2*) is 38.28 kN and is larger than μ_P. This is because the different transformation models on ϕ are used in the earth pressure calculation.

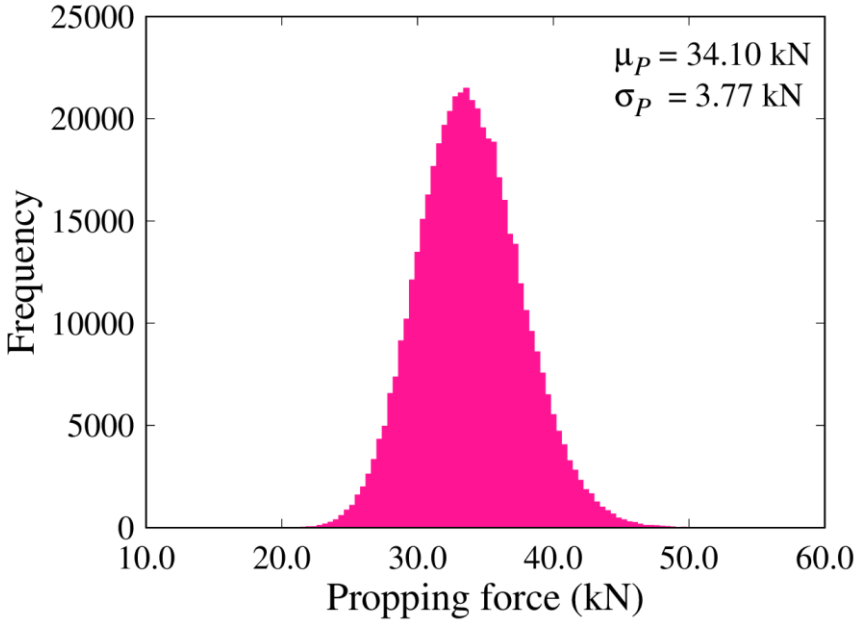

Figure 8-8 Probability distribution of P with N_{MCS} = 500,000.

8.4 Comparison

Table 8-2 summarizes the final design results on required depth of embedment using the LRFD method and RBD. The results imply that more economical design for the retaining wall can be achieved by using reliability analysis than LRFD based on JPHA (2018).

Table 8-2 Final design results

Design methods	p_{ft}	d (m)
LRFD (JPHA 2018)	2.0×10^{-2}	3.1
MCS	2.0×10^{-2}	2.6
	1.0×10^{-4}	3.3

References

Akkaya, A. D., and Vanmarcke, E. H. (2003). Estimation of spatial correlation of soil

parameters based on data from the Texas A&M University NGES. Probabilistic site characterization at the National Geotechnical Experimentation Sites (Eds G. A. Fenton and E. H. Vanmarcke), 29-40.

JARA (1999). Design Guideline for Temporal Structures, Japan Road Association, (in Japanese).

JARA (2017). Specifications for Highway Bridges IV, Japan Road Association (in Japanese).

JPHA (2018). Technical Standards for Port and Harbor Facilities, Japan Port and Harbor Association (in Japanese).

Mayne, P. W., Christopher, B. R., DeJong, J. (2001). Manual on Subsurface Investigations, National Highway Institute Publication No. FHWA NHI-01-031, Federal Highway Administration.

Vanmarcke, E. H. (1977). Probabilistic modeling of soil profiles. Journal of the geotechnical engineering division, 103(11), 1227-1246.

Probability-based analysis and design of soil nail wall

Zi-Jun Cao, Guo-Hui Gao, Takayuki Shuku, Timo Schweckendiek, and Marco Redaelli

9.1 Introduction

This chapter presents deterministic design results and reliability-based design (RBD) results of Problem Sand 6 (i.e., soil nail wall) based on JGJ 120-2012 (2012) in China. The problem is shown in Figure 9-1. This chapter is organized as follows: In Section 9.2, deterministic design method of soil nail capacity based on JGJ 120-2012 in China is outlined, and the design results are provided as well; In Section 9.3, the Android App of BEST (Bayesian Equivalent Sample Toolkit) is applied to probabilistic characterization of soil internal friction angle based on standard penetration test (SPT) data; In Section 9.4, Monte Carlo simulation-based full probabilistic design approach is employed to perform RBD of the sand problem.

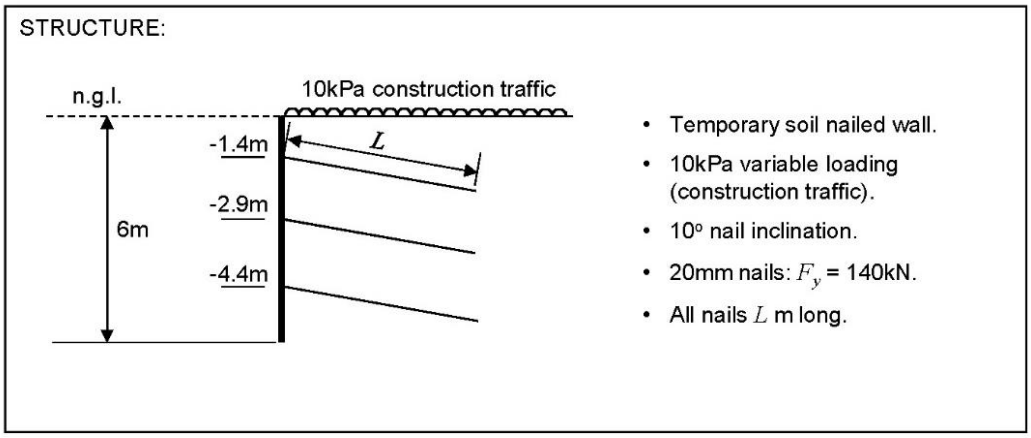

PROBLEM:

This is a design problem requiring the specification of the length of the soil nails and their horizontal spacing.

1. Specify the required length of the soil nails (L).
2. Specify horizontal spacing (S_H).

Design to be based on the stability of the wall without considering serviceability requirements.

Figure 9-1 Schematic of the target structure and design problems

9.2 Deterministic design of the soil nail wall based on JGJ 120-2012 in China

9.2.1 Calculation of soil nail capacity

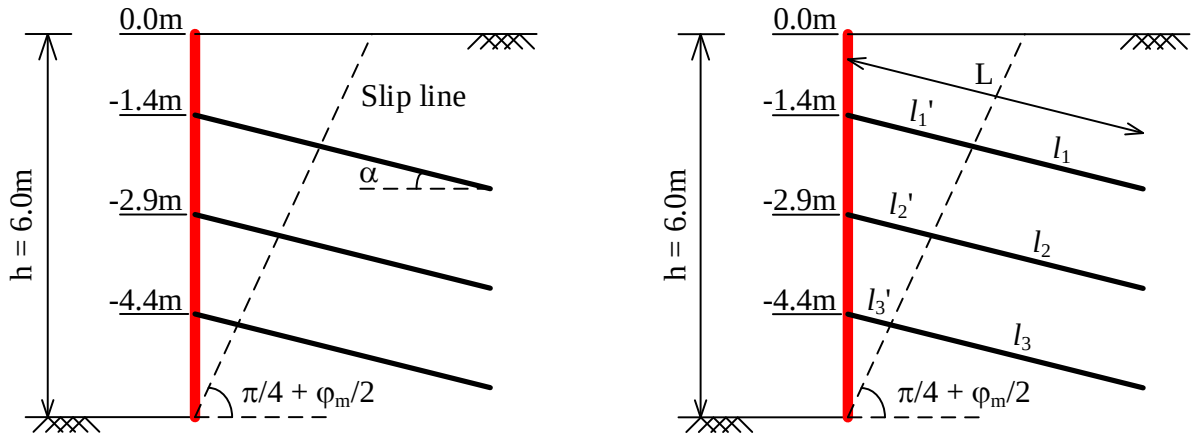

Figure 9-2 Illustration of the soil nail wall system

The safety factor of pullout capacity of single soil nail (as shown in Figure 9-2) is calculated as:

$$FS_{t,j} = \frac{R_{k,j}}{N_{k,j}} \tag{9-1}$$

in which $FS_{t,j}$ is the safety factor of soil nail pullout capacity in the j-th row; $N_{k,j}$ and $R_{k,j}$ are the standard value of axial tensile force and the standard value of ultimate pullout resistance for the soil nails in the j-th row, respectively, and they are calculated as:

$$N_{k,j} = \frac{1}{\cos\alpha_j}\zeta\eta_j p_{ak,j} S_V S_H \tag{9-2}$$

$$R_{k,j} = \min\left[R_{k,j}^{'}, N_j\right] \tag{9-3}$$

in which α_j is the inclination angle of the soil nails in the j-th row and is equal to 10 degrees in this design problem; ζ is the reduction factor of the active earth pressure; η_j is the adjustment factor of axial tension for the soil nail in the j-th row; $p_{ak,j}$ is the standard value of active earth pressure strength on the soil nails in j-th row; S_V and S_H is vertical and horizontal spacing, respectively. The S_H is suggested ranging from 1.0 to 2.0m in JGJ 120-2012, and S_V is fixed at 1.5m in this design. $R_{k,j}^{'}$ is the standard value of ultimate pullout resistance, which originates from the cohesive force between soil and nail in the j-th row; N_j is the design value of tensile capacity of the j-th row soil nail. ζ is calculated using the following equation:

$$\zeta = \tan\frac{\beta-\varphi_m}{2}\left(\frac{1}{\tan\frac{\beta+\varphi_m}{2}} - \frac{1}{\tan\beta}\right) \Big/ \tan^2\left(\frac{\pi}{2} - \frac{\varphi_m}{2}\right) \tag{9-4}$$

in which β is the angle between the soil nail wall and horizontal direction and is equal to 90 degrees in this example; φ_m is the average value of the internal friction angle of soil weighted

by soil layer thickness. η_j is calculated using the following equation:

$$\eta_j = \eta_a - (\eta_a - \eta_b)\frac{z_j}{h} \tag{9-5}$$

in which η_b is the empirical coefficient, and is herein taken as 0.85 within the recommended range from 0.6 to 1.0 in JGJ 120-2012; h is the excavation depth and is equal to 6m (see Figure 9-1); z_j is the vertical distance from the soil nail to the top surface of the wall for the soil nail in the j-th row; η_a is the calculation coefficient and is given below:

$$\eta_a = \frac{\sum_{j=1}^{n}(h - \eta_b z_j)\Delta E_{aj}}{\sum_{j=1}^{n}(h - z_j)\Delta E_{aj}} \tag{9-6}$$

in which ΔE_{aj} is the standard value of active earth pressure originating in an area with S_V and S_H as side lengths for the soil nail in the j-th row; n is the number of soil nail rows and is equal to 3 herein.

$p_{ak,j}$ is calculated as:

$$p_{ak,j} = \gamma z_j \tan\left(\frac{\pi}{2} - \frac{\varphi_m}{2}\right)^2 + q \tag{9-7}$$

in which γ is the unit weight of soil and is taken as 18kN/m^3; q is the construction traffic load and is equal to 10kPa.

$R'_{k,j}$ is calculated using the following equation:

$$R'_{k,j} = \pi d_j \sum q_{sik} l_j \tag{9-8}$$

in which d_j is the diameter of the drill hole, and is taken as 100mm herein; q_{sik} is the standard value of ultimate bond strength and is taken as 75kPa in this design; l_j is the effective length of the soil nails in j-th row, as shown in Figure 9-2.

N_j is calculated using the following equation:

$$N_j = A_s f_y = \frac{\pi}{4} d^2 f_y \tag{9-9}$$

in which A_s is the cross-sectional area of the steel bar; d is the diameter of the steel bar; f_y is the design value of the soil nail tensile capacity in the j-th row. Herein, N_j is taken as equal to F_y.

9.2.2 Soil internal friction angle

The internal friction angle φ is estimated from SPT data based on the transformation model suggested in the Geological engineering handbook (5-th edition, 2018) in China. The model is defined as:

$$\varphi = \sqrt{12N} + 20 \tag{9-10}$$

in which N is the normalized SPT-N value at vertical overburden stress of P_a = 98kPa, and can be obtained by Peck (1974):

$$N = N' 0.77 \log \frac{1960}{\sigma_v} \tag{9-11}$$

in which N' is the energy-corrected SPT-N value and is taken as the mean value of SPT-N above 8.9m for deterministic design, because the height of the wall (h = 6m) is less than 8.9m and the soil can be divided into two layers obviously as shown in Figure 9-3. σ_v is the effective overburden pressure and is taken as the value at the depth of 3m (half of h). In this problem, the above transformation model is denoted as TM 1.

The internal friction angle φ also can be estimated from SPT data based on the transformation model suggested by Mayne et al (2001). The model is defined as:

$$\varphi = \sqrt{15.4N} + 20 \tag{9-12}$$

in which N is the normalized SPT-N value at vertical overburden stress of P_a = 98kPa, and is given by:

$$N = N' / \left(\sigma_v / P_a\right)^{0.5} \tag{9-13}$$

in which N' and σ_v is the same as shown in TM 1. In this problem, the above transformation model is denoted as TM 2.

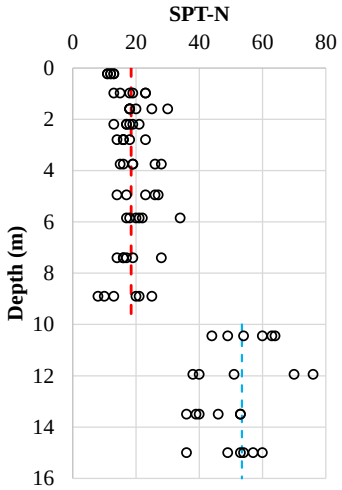

Figure 9-3 The profile of SPT-N with depth

9.2.3 Design results

In this design problem, the length of the soil nail (L) and their horizontal spacing (S_H) are required to be specified. Consider, for example, the possible value of L varying from 4m to 5m at an interval of 0.1m. There are, hence, 11 possible values 1.0, 1.1, 1.2, 1.3, 1.4, 1.5, 1.6, 1.7, 1.8, 1.9, and 2.0m of S_H, resulting in a total of 121 possible designs. For each possible design, calculate $FS_{t,j}$ for every row of the soil nails and select the minimum safety factor as the final

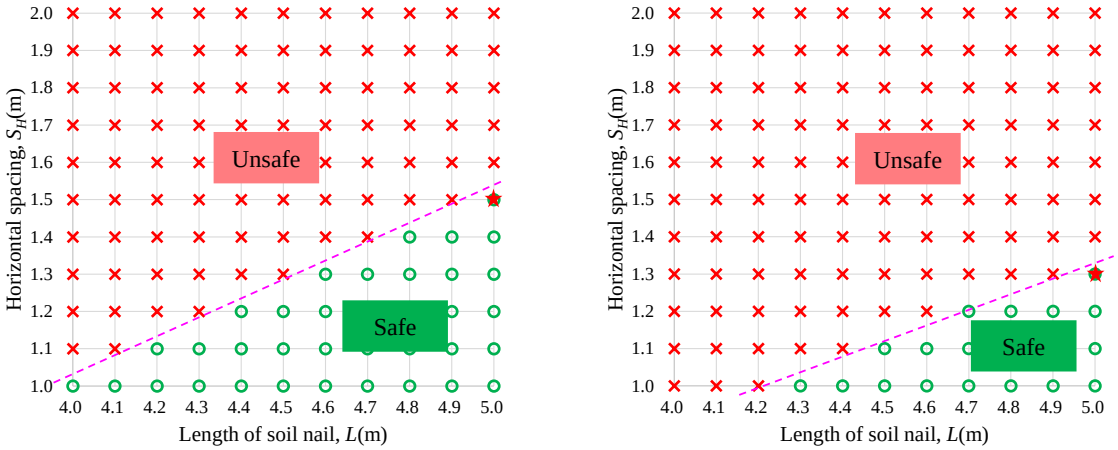

(a) $FS_T = 1.4$. (b) $FS_T = 1.6$.

Figure 9-4 Deterministic design results with different allowable safety factors FS_T. (TM 1)

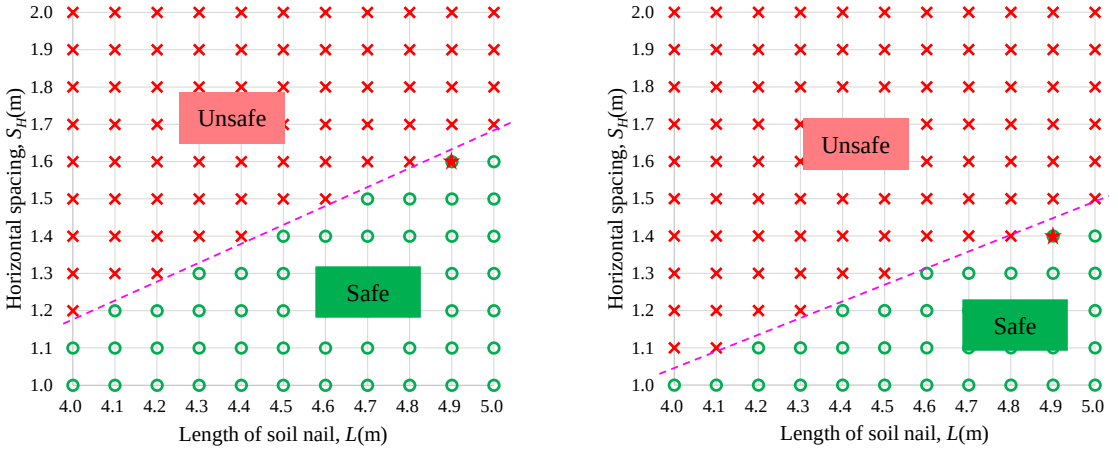

(a) $FS_T = 1.4$. (b) $FS_T = 1.6$.

Figure 9-5 Deterministic design results with different allowable safety factors FS_T. (TM 2)

safety factor FS. Then, compare FS with the allowable safety factor ($FS_T = 1.6$ and 1.4 for 2-level and 3-level wall, respectively (JGJ 120-2012, 2012)). If the FS of a possible design is greater than FS_T, the possible design is a feasible design and is located in the safe domain. If the FS of a possible design is less than FS_T, the possible design is not a satisfactory design.

Figure 9-4 shows the deterministic design results with different allowable FS_T values using TM 1. The feasible design and infeasible design are shown by circles and crosses in Figure 9-4, respectively. The safe domain is located at the low right corner, which means that the safety factor of soil nails increases as the S_H decreases and L increases. The final design can be identified form feasible designs through some optimization criteria, such as minimum construction costs (Wang and Kulhawy, 2008; Wang, 2009, 2011). Consider, for example, the equivalent construction cost L/S_H. Figure 9-4 also shows the final designs by the star. For FS_T =1.4 and 1.6m, the final designs are taken as {L = 5.0m, S_H =1.5m} and {L = 5.0m, S_H=1.3m}, respectively. Figure 9-5 shows the deterministic design results with different allowable FS_T

values using TM 2. For FS_T=1.4 and 1.6m, the final designs are taken as $\{L = 4.9\text{m}, S_H = 1.6\text{m}\}$ and $\{L = 4.9\text{m}, S_H = 1.4\text{m}\}$, respectively.

9.3 Probabilistic characterization of the soil internal friction angle

For reliability-based design, it needs to know statistics of the soil parameters (e.g., soil internal friction angle). In this problem, the statistics are obtained using BEST App, which is developed by WHU and can be downloaded at https://www.wandoujia.com/apps/7626085. Detailed algorithms implemented in BEST can be referred to Wang and Cao (2013) and Cao et al. (2016), which are not pursued here. Figure 9-6a shows the userform of BEST App for uncertainty quantification. Using the BEST App requires the soil type, design parameter, transformation model and its associated model error, sample number, prior information, and test data as input. The transformation model used in this problem is derived from Eq. (9-10):

$$\sqrt{N} = \frac{1}{\sqrt{12}}\varphi - \frac{20}{\sqrt{12}} \tag{9-14}$$

The model error is represented by a normal random variable, and its mean and standard deviation are equal to 0 and 0.33 (half of the standard deviation value of $\sqrt{N}$). The sample number is taken as 10,000. The prior information of soil internal friction angle is quantified by the uniform distributions of the mean value and standard deviation, which range from 15 to 45 and from 0.75 to 6.75, respectively. The test data are taken as the value of $\sqrt{N}$ in this problem. Figure 9-6b shows the results obtained from BEST App for the probabilistic characterization of soil internal friction angle using TM 1. The mean and standard deviation values of the soil internal friction angle are 35.88 degrees and 2.93 degrees, respectively, and that is normally distributed. In the same way, the mean and standard deviation values of the soil internal friction angle also can be characterized by BEST App using TM 2, which are 39.35 degrees and 2.47 degrees, respectively.

9.4 Reliability-based design using Monte Carlo simulation

An efficient MCS-based full probabilistic design approach, which directly makes use of Generalized Subset simulation (GSS) (Li et al, 2017) to perform RBD of geotechnical structures, is employed to solve this design problem. Detailed algorithms of GSS-based RBD can be referred to Gao et al. (2019). The design space keeps the same as that used in the deterministic design (see Section 9.2). The internal friction angle of soil is considered as an uncertain parameter, which is represented by a Gaussian random variable with a mean value of 35.88 degrees and a standard deviation of 2.93 degrees for TM 1, as discussed in Section 9.3. The target failure probability (P_{fT}) is taken as 0.0001. If the failure probability P_f of a possible design is less than P_{fT}, then it is a feasible design; otherwise the possible design is an infeasible design (Cao et al, 2019; Peng et al, 2017; Li et al, 2016; Wang and Cao, 2013; Wang et al, 2011). Figure 9-7 shows the RBD results of different rows of soil nails using TM 1 under P_{fT}=

0.0001. The feasible design and infeasible design are shown by circles and crosses, respectively. The local optimization designs of different rows, which are selected according to the minimum equivalent construction cost L/S_H, are indicated by stars in Figure 9-7. Then the final global design is taken as $\{L = 4.9\text{m}, S_H = 1.3\text{m}\}$ which is the minimum construction cost of three different local optimization designs. In the same way, Figure 9-8 shows the RBD results of 3 different rows of soil nails using TM 2, and the final global design is taken as $\{L = 4.9\text{m}, S_H = 1.3\text{m}\}$. Besides, the RBD results of soil nail wall under target failure probability P_{fT} equal to 0.001 are also calculated and presented in Table 9-1.

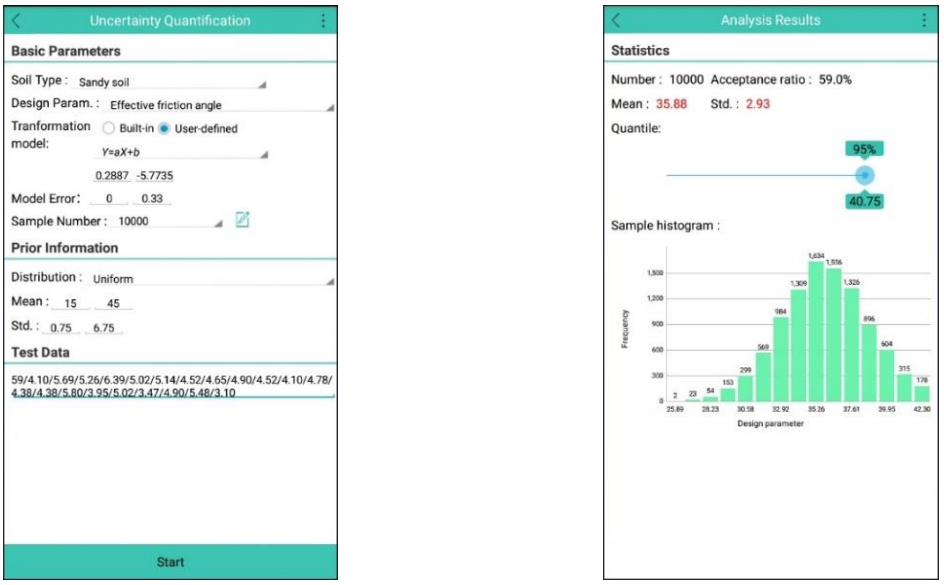

(a) Uncertainty quantification form (b) Analysis results form

Figure 9-6 Userforms of BEST App

Table 9-1 Final design of different design methods

Transformation models	Design methods	Allowable values	Design parameters	
			L(m)	S_H(m)
TM 1	Deterministic design	FS_T=1.4	5.0	1.5
		FS_T=1.6	5.0	1.3
	Reliability-based design	P_{fT} = 0.001	4.9	1.4
		P_{fT} = 0.0001	4.9	1.3
TM 2	Deterministic design	FS_T=1.4	4.9	1.6
		FS_T=1.6	4.9	1.4
	Reliability-based design	P_{fT} = 0.001	4.9	1.4
		P_{fT} = 0.0001	4.9	1.3

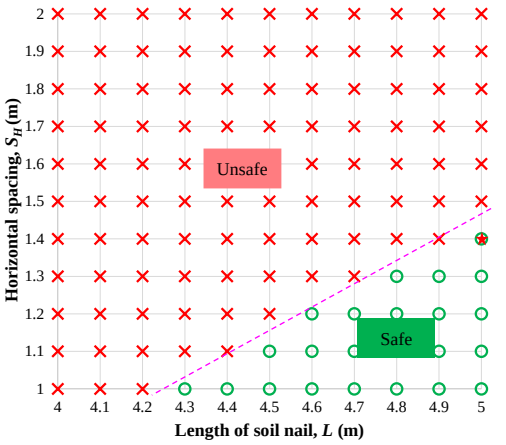

(a) Row 1

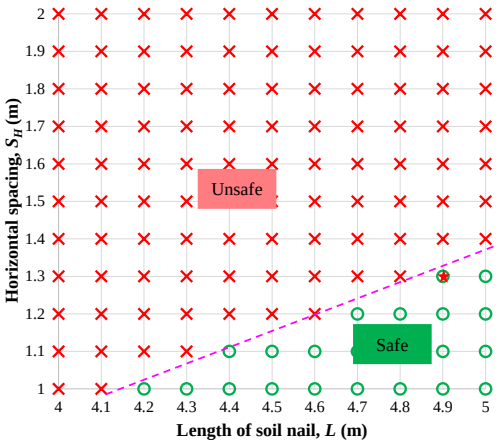

(b) Row 2

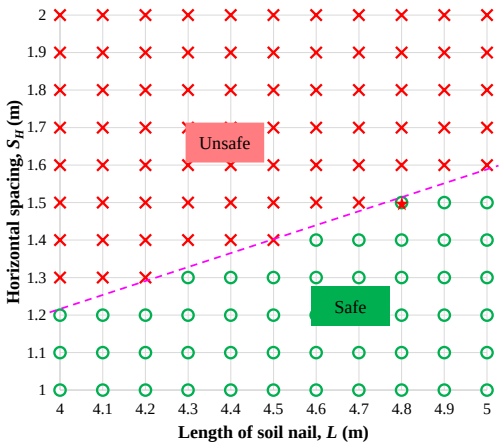

(c) Row 3

Figure 9-7 Design results obtain by GSS with different rows (TM 1)

9.5 Comparison

Table 9-1 summarizes the final design results using the deterministic design method and the RBD method. Results obtained from the deterministic design method based on JGJ 120-2012 in China and the RBD method are close in this design example. However, it shall be pointed out that this design scenario may not be a case in general. Moreover, during the design process presented in this report, only the soil nail capacity limit state is considered. In some cases, the overall stability of the soil wall may also be of concern, which is not considered in design calculations presented in this problem.

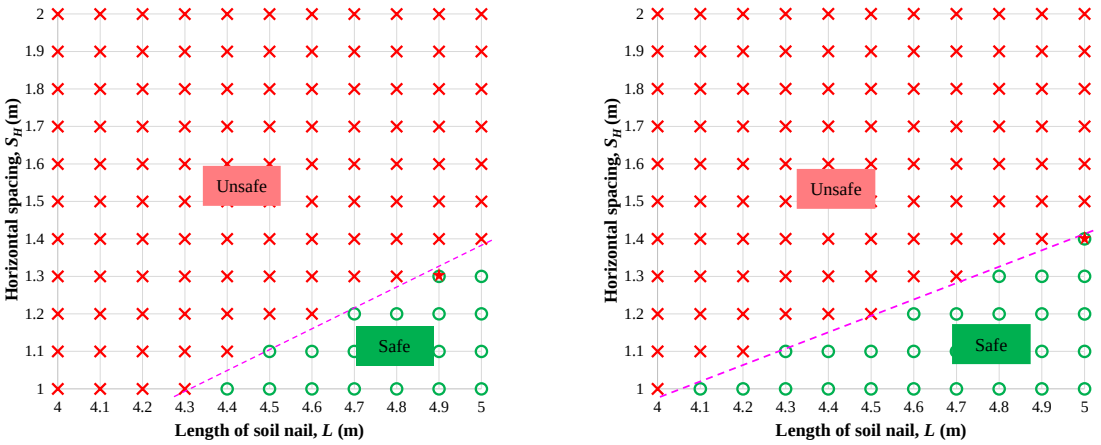

(a) Row 1

(b) Row 2

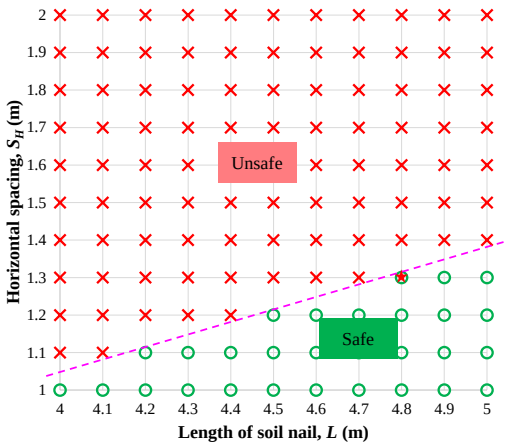

(c) Row 3

Figure 9-8 Design results obtain by GSS with different rows (TM 2)

References

Cao, Z. J., Li, D. Q., and Wang Y., (2016). Probabilistic approaches for geotechnical site characterization and slope stability analysis. Zhejiang University Press and Springer-Verlag Berlin Heidelberg 2017.

Cao, Z.J., Peng, X., Li, D.Q. and Tang, X.S., (2019). Full probabilistic geotechnical design under various design scenarios using direct Monte Carlo simulation and sample reweighting. Engineering Geology, 248, 207-219.

Gao, G. H., Li, D. Q., Cao, Z. J., Wang, Y., and Zhang, L., (2019). Full probabilistic design of earth retaining structures using generalized subset simulation. Computers and Geotechnics, 112, 159-172.

Geological Engineering Handbook Editorial Board of China, (2018). Geological engineering handbook (5-th Edition). China Building Industry Press, Beijing. (in Chinese).

Li, D.Q., Shao, K.B., Cao, Z.J., Tang, X.S. and Phoon, K.K., (2016). A generalized surrogate response aided-subset simulation approach for efficient geotechnical reliability-based

design. Computers and Geotechnics, 74, 88-101.

Li, D. Q., Yang, Z. Y., Cao, Z. J., Au, S. K., Phoon, K. K., (2017). System reliability analysis of slope stability using generalized subset simulation. Applied Mathematical Modelling. 46, 650-664.

Mayne, P. W., Christopher, B. R., and DeJong, J., (2001). Manual on Subsurface Investigations, National Highway Institute Publication No. FHWA NHI-01-031, Federal Highway Administration.

Ministry of Housing and Urban-Rural Development of the People's Republic of China, (2012). Technical specification for retaining and protection of building foundation excavations (JGJ 120-2012). China Building Industry Press, Beijing. (in Chinese).

Peck, R. B., Hansen, W. E., and Thornburn, T. H., (1974). Foundation Engineering, 2nd Ed., John Wiley & Sons Inc., New York, 514P.

Peng, X., Li, D. Q., Cao, Z. J., Gong, W., Juang, C. H., (2017). Reliability-based robust geotechnical design using Monte Carlo simulation. Bulletin of Engineering Geology and the Environment. 76(3), 1217-1227.

Wang, Y. and Cao, Z.J., (2013). Expanded reliability-based design of piles in spatially variable soil using efficient Monte Carlo simulations. Soils and Foundations, 53(6), 820–834.

Wang, Y., and Cao, Z. J., (2013). Probabilistic characterization of Young's modulus of soil using equivalent samples. Engineering Geology, 159, 106-118.

Wang, Y., (2011). Reliability-based design of spread foundations by Monte Carlo simulations. Géotechnique. 61(8), 677-685.

Wang, Y., Au, S.K. and Kulhawy, F.H., (2011). Expanded reliability-based design approach for drilled shafts. Journal of Geotechnical and Geoenvironmental Engineering, 137(2), 140-149.

Wang, Y., (2009). Reliability-based economic design optimization of spread foundations. Journal of Geotechnical and Geoenvironmental Engineering. 135(7), 954-959.

Wang, Y., Kulhawy, F. H., (2008). Economic design optimization of foundations. ASCE Journal of Geotechnical and Geoenvironmental Engineering. 134 (8), 1097-1105.